NASA CR-144776

OCEAN DATA SYSTEMS, INC.

SURFACE PROPERTIES
OF OCEAN FRONTS

Final Report

April 5, 1976

odsi

OCEAN DATA SYSTEMS, INC.
6000 EXECUTIVE BLVD., ROCKVILLE, MARYLAND 20852 • 301/881-3031

Submitted to
NATIONAL AERONAUTICS
AND SPACE ADMINISTRATION
Goddard Space Flight Center
Greenbelt, Maryland

SURFACE PROPERTIES OF OCEAN FRONTS

Final Report

April 5, 1976

Prepared under
Contract No. NAS 5-22370

Prepared by
Paul M. Wolff
William E. Hubert
OCEAN DATA SYSTEMS, INC.
Monterey, California

Foreword

This paper constitutes the final technical report on a study of Surface Properties of Ocean Fronts for the National Aeronautics and Space Administration under Contract No. NAS 5-22370. The basic report provides background information on oceanic fronts and describes the results of the several models which were developed to study the dynamics of oceanic fronts and their effects on various surface properties. The details of the four numerical models used in these studies are given in separate Appendices which contain all of the physical equations, program documentation and running instructions for the models.

The following scientists participated as consultants and scientific collaborators in this project: Professors D.F. Liepper and R.J. Renard from the U.S. Naval Postgraduate School and Dr. Taivo Laevastu and Messrs. S. Larson and K. Rabe from the U.S. Navy's Environmental Prediction Research Facility.

TABLE OF CONTENTS

1.0 DEFINITION OF OCEAN FRONTS

Although oceanic fronts, especially major ones, have been referred to in scientific literature at least as long as their atmospheric counterparts, their definition is not as precise and definite as for atmospheric fronts. This is partly due to the fact that the nature of oceanic fronts can be different in different locations and is affected by a great number of factors, both permanent and temporal ones. There has been recently a renewed interest in the study of oceanic surface fronts, partly due to their importance in naval, fisheries, and navigation problems and partly due to the fact that most oceanic fronts can be observed from satellites, either as temperature or color or sea surface roughness discontinuities.

The best definition of oceanic fronts is that of LaFond (1960), "The oceanic front is the leading edge of a border separating unlike water masses. Fronts can occur not only between water masses of different salinity but also between those differing in other properties, such as temperature". Before describing the characteristics of the front, we have to define "surface water types". The term "water masses" refers to deep water masses (below the thermocline) where temperature and salinity can be considered as conservative properties and which are defined on temperature-salinity diagrams. The term "water type" has been applied in the

past to a singular point in the temperature-salinity diagram. Temperature and salinity are not as conservative in surface layers; however, surface waters can be characterized by other properties, such as biological (e.g., plankton) content, color, turbidity, and range of annual change of temperature and salinity (Schott, 1935; Laevastu, 1963). The term "surface water type" has been introduced to designate surface waters with definite but relatively uniform characteristics.

Thus the oceanic fronts at the surface are boundaries of unlike surface water types; they form limits (boundaries) of natural regions of the oceans (Laevastu and LaFond, 1970). The fronts can be major ones, easily recognizable from relatively pronounced changes of the properties (e.g., temperature) or they can be relatively broad transition regions with gradual changes.

LaFond and LaFond (1971) found that the California Front, which can be considered as an "average" front, was characterized by strong horizontal temperature (and salinity) gradients, large vertical changes in isotherm depths, temperature inversions, and a large thermocline separation. Furthermore, measured current shear showed relative current in the upper layers to be in a southerly direction on the eastern side of the front and in a westerly direction on the western side; currents inside the boundary region exhibited diverse directions.

Fronts are usually (but not exclusively) determined by dynamic factors and are thus convergences (and/or divergences) of surface currents. They can be caused by thermohaline gradients, surface wind systems, or by coastal topography, such as coastal fronts occurring, for example, along the continental slopes.

The most common property for recognition of surface fronts is sea surface temperature gradient. Shpaykher and Moretskiy (1964) have characterized some properties of the oceanic Polar front in the following table:

TABLE 1-1: BASIC PARAMETERS OF OCEANIC FRONTS

Area		Width of frontal zone, km	Maximum horizontal gradient		Depth of frontal divide, m	Slope angle of interface
			t, °C/km	S, ‰/km		
Arctic Sea	greatest	108	0,39	0,69	125	6'00"
	smallest	2	0,01	0,01	7	0'07"
	mean	21	0,10	0,12	21	1'17"
Greenland Sea	greatest	75	0,30	0,08	1000	1°08'16"
	smallest	20	0,01	0,02	150	18'20"
	mean	46	0,11	0,04	531	32'42"
Norwegian Sea	greatest	200	0,16	-	1500	1°08'45"
	smallest	24	0,02	-	100	12'44"
	mean	80	0,07	-	745	31'19"

As there are seasonal changes in surface temperature, frontal discontinuities disappear in some seasons (see e.g., Colton, et. al., 1975). The coastal fronts are only recognizable by temperature gradients (outside upwelling areas) during summer (when coastal waters are warmer than offshore waters) and during winter (when coastal waters are colder than offshore waters). During spring and autumn, temperature gradients are frequently masked at coastal fronts. The second indicator for surface fronts is water color, caused either by different plankton content (quantity of standing crop of phytoplankton) or by the amount and type of minerogen suspended matter. Salinity discontinuities as well as current discontinuities at fronts can be recognized only by special measurements and not by remote sensing. Major oceanic fronts can be recognized also by changes of waves (surface roughness).

Contrary to the transient nature of meteorological fronts, oceanic fronts are relatively stable in respect to their mean positions. They frequently represent the time-averaged signature of atmospheric features. However, some seasonal shifts, meanderings and quasi-synoptic changes in frontal positions occur (see further Section 3).

One of the main objectives of the present study is to construct numerical models for the study of the movement as well as changes in sharpness (gradients) of the fronts as affected by surface driving forces, such as winds. One of

the practical reasons for this is that surface thermal fronts can be recognized in cloudless areas from infrared satellite observations. However, during the periods when the frontal areas under consideration are cloud covered, it might be necessary to complement the satellite observations with numerical computations on the possible changes in frontal positions and sharpness.

A further objective of this study is to model the effects of oceanic fronts on surface roughness (waves, wave patterns) so that the microwave radiometer observations from satellites could be correctly interpreted as to which surface roughness (wave pattern) changes are due to true sharp discontinuities in surface wind patterns (meteorological fronts) and which are due to major oceanic fronts with large current shears.

2.0 APPLICATIONS

Oceanic thermal fronts often coincide with the boundaries of commercially important fish species. There may also be an aggregation of fish near or at the oceanic thermal fronts (see e.g., Lee, 1952; Hela and Laevastu, 1962). Thus it is of economic importance to fisheries to analyze and predict oceanic fronts.

As the currents of major oceanic fronts, such as the Gulf Stream front, can be strong and opposite in direction, use can be made of the currents in navigation for time and fuel saving in shipping.

The vertical thermal and salinity structure (the temperature and salinity) change with depth on different sides of the oceanic fronts. Thus, the propagation patterns of sound will be different on different sides of oceanic fronts and the fronts will greatly affect sonar ranges through them (Laevastu, Wolff, and LaFond, 1970). LaFond and LaFond (1971) for example, found that temperature inversions at the California Front (which is a "medium intensity" front) produce sound channels above the level of increased temperature. Some further effects of oceanic fronts (Polar Front in the Denmark Strait) on the propagation of sound have been described by Nunn (1968). Consequently, the knowledge of the positions

of oceanic fronts is of utility to the Navy, for submarine as well as anti-submarine warfare.

Finally, a large part of the energy for the atmosphere originates from the oceans (sensible and latent heat exchange). This feedback is largest where the difference between the properties of the sea surface (temperature and water vapor pressure) and the surface air are large. Large differences of these properties occur where the temperature gradients of sea surface temperature are sharp (i.e., at oceanic fronts), (Laevastu and Hamilton, 1972). Cyclogenesis often occurs in the vicinity of major oceanic fronts, and the climatological mean position of Arctic and Polar atmospheric fronts over the oceans coincides closely with the corresponding major oceanic fronts.

3.0 SYNOPTIC AND SEASONAL BEHAVIOR

Although general knowledge indicates that oceanic fronts are relatively stationary over synoptic time periods (up to 3 days), no detailed synoptic study on the dynamics of offshore oceanic fronts has been carried out. Available studies of offshore oceanic fronts using multiple ship traverses show that the major fronts are relatively stationary, but include relatively large-scale meanders, whereas the minor fronts (e.g., Sargasso Sea fronts) show relatively irregular and small scale meandering and considerable changes of position and intensity.

Colton, et al, 1975, found that surface temperature fronts in the Sargasso Sea divide it into a cooler, more productive northern part and warmer, less productive southern part. They also found a sharp faunal change across this front. This surface thermal front in the Sargasso Sea, however, cannot be found during the warm season from July to September. One of the main objectives of this study is to model and investigate the possible changes of offshore oceanic fronts as affected by surface driving forces (mainly surface winds).

Recent studies of coastal fronts (oceanic fronts near continental slopes) show that these fronts are greatly bound to bathymetric features (continental slope), but that changes

(small meanderings and mixing) at these fronts occur in a tidal rhythm as well as through the action of surface wind.

Seasonal migrations of major surface fronts have been studied by Laevastu and LaFond (1970) and others. Stefanson (1969) found that the near-shore end of a frontal zone southeast of Iceland appears to move north-south with the season, and that it might be displaced as much as 50 nautical miles. Some minor fronts in low latitudes can migrate in some seasons as much as 230 miles with an average speed of 7 miles per day (Hela and Laevastu, 1962). Rossov and Kislyakov (1969) found that seasonal and year-to-year changes of the position of the Polar Front in the Atlantic can reach 200 nautical miles.

Voronina (1962) found that the Antarctic front is largely determined by surface winds and that it can change from a convergence to a divergence if surface winds change in the same sense. Besides changes in position, some seasonal changes of sharpness (gradients) of the fronts also occur. It can be assumed that changes of current in the surface layers plus changes in surface wind regimes and heat exchange processes are responsible for these seasonal changes. Considerable seasonal change can occur in the color and turbidity of different water types due to seasonal cycles in phytoplankton production.

It is known from empirical observations as well as from theoretical considerations that there is considerable

variation in the thermocline in frontal zones. These changes are largely determined by the dynamics of the upper layers of the ocean. No detailed studies, nor numerical modeling, of the thermocline changes at frontal regions are available at present. The models (HN models) programmed within this project will contribute to our knowledge in this area.

It is well known to seamen that currents strongly affect wave characteristics. If the current runs against the sea, waves are steeper, the length appears shorter and the seas are very choppy. Again, if the current runs with the sea, the seas are smoother and the waves rounder and longer. Those effects can easily be observed in narrows where strong tidal currents occur and in channels between islands. Quantitative observations at sea are scarce on the effects of currents on wave shape, length and height. Groen and Dorrestein (1958) have constructed graphs which give the ratios of wave length, speed, height and steepness of waves in currents with different speeds to the same elements in non-flowing water.

There is a mass transport (wave current) connected with waves. Therefore, a long swell (which is causing a "wave current") affects also the shorter superimposed waves (sea) the same way as currents do. Any swell trains which run nearly in opposite direction to the sea can be expected to cause steeper, shorter waves and a swell running in the same direction as the sea should cause the sea (wind waves) to be less steep, round and longer. This effect has been treated

theoretically by Longuet-Higgins and Stewart (1960, 1961). These effects could be expected to occur at oceanic frontal regions. Another set of models (spectro-angular wave model and wave refraction model) programmed and/or adapted within this project will help to evaluate these effects quantitatively.

4.0 NUMERICAL STUDY OF FRONTAL DYNAMICS

This study is a preliminary demonstration of the applicability of a hydrodynamical-numerical model to the simulation of oceanic frontogensis. As the model has been described elsewhere in this report, this section is devoted to a description of three initial test (simulation) runs and a final test run for a case with unusually strong initial thermal gradient and convergent winds.

In all cases a two layer ocean was simulated in which the lower layer was initially at rest. In each case a current field, initially specified in the top layer, developed in both the top and bottom layers in response to an imposed wind field and to the initial imbalance in the mass and velocity fields. As the initial state of the pressure (depth) and density structure needed to balance the specified motion fields are not known, the model must be run for a sufficient number of real-time hours to establish proper dynamic balance between mass and motion fields. In all four test cases described here, run times were extended to the point where balance was achieved. This problem and the way in which balance is finally realized within the model itself is common to all Primitive Equation models (including those used for routine atmospheric prediction).

In order to demonstrate the use of the HN model for routine conditions of initial current structure and surface wind stress, three different simulation runs were conducted in an initial test series. These consisted of a twelve-hour simulation of a current shear front (Case I), an eighteen-hour simulation of a surface wind convergence front (Case II), and a twleve-hour simulation of a cyclonic wind field moving across a current shear front (Case III). The several important physical constraints which differed in the simulation runs are listed in Table 4-1.

In Case I the initial current and steady state wind field, uniform in the east-west direction, are shown in Figure 4-1. The initial current was zonal, non-divergent and had linear shear in the northern and southern portions of the grid. The wind field, also specified as a shear flow, was divergent south of the front and convergent north of it. It should be noted that at the front the initial current and wind field were set to zero.

In Case II the initial current field was prescribed as uniformly flowing to the west at 2.5 cm sec^{-1}. The wind field, shown in Figure 4-2, simulated a convergent wind stress front. North of the front, the winds were divergent and south of the front, they were convergent. In Case II, as in Case I, the wind field varied only in the north-south direction.

TABLE 4-1: PARAMETER SPECIFICATIONS

PARAMETER	CASE I	CASE II; III
TOTAL DEPTH	300 m.	300 m.
GRID MESH	10 km.	10 km.
TIME STEP	60 sec.	60 sec.
THICKNESS OF SURFACE LAYER	50 m.	75 m.
DENSITY OF SURFACE LAYER	1.026 g cm^{-3}	1.025 g cm^{-3}
DENSITY OF BOTTOM LAYER	1.029 g cm^{-3}	1.027 g cm^{-3}
LATITUDE OF CORIOLIS FORCE	30° N	45° N
SURFACE LAYER SMOOTHER(1)	.998	.998
BOTTOM LAYER SMOOTHER	.920	.920
EDDY DIFFUSION COEFFICIENT(2)	$5x10^4$	$5x10^4$

(1) These parameters simulate eddy viscosity by considering the velocities at surrounding grid points.

(2) The value of this parameter in Case III was $5x10^3$.

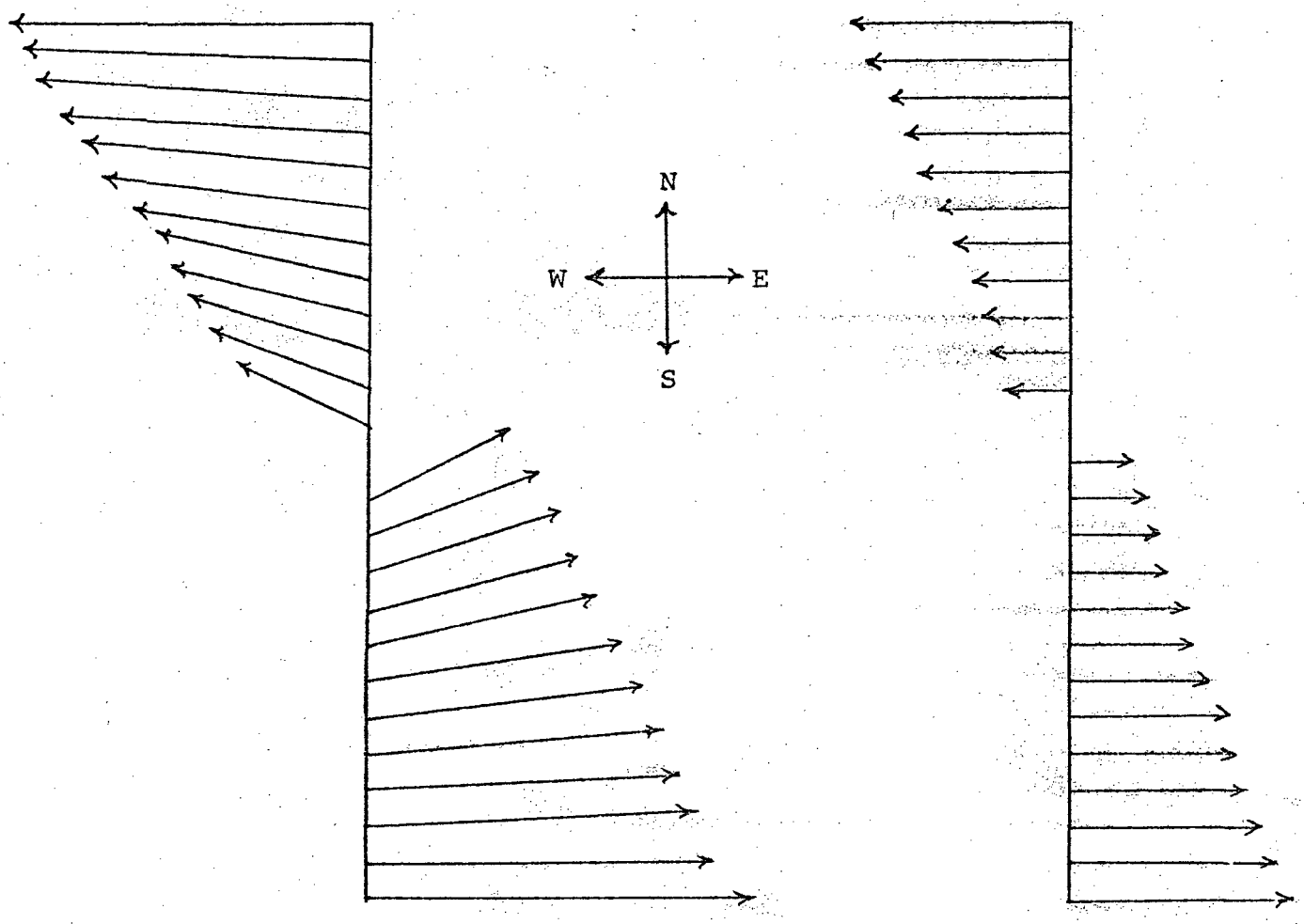

FIGURE 4-1: WIND AND CURRENT FIELDS FOR CASE I

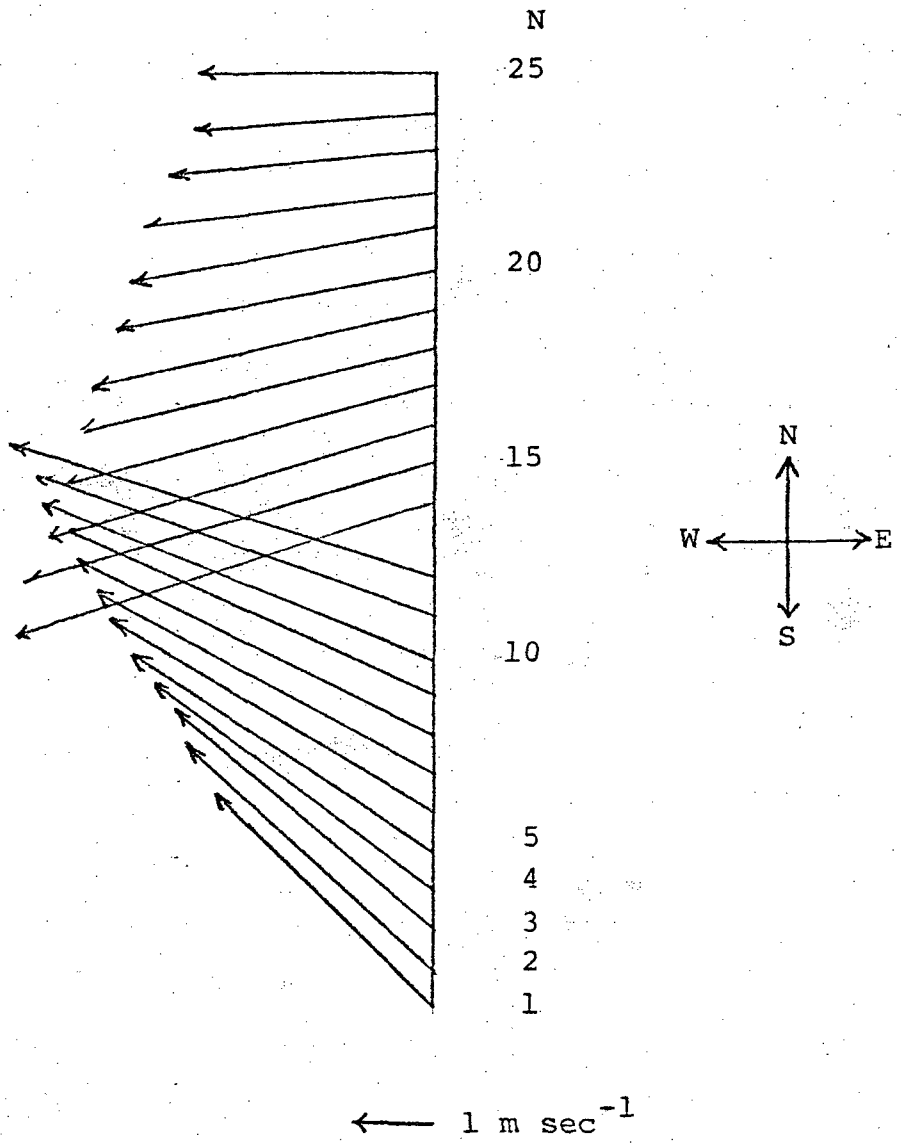

FIGURE 4-2: WIND FIELD FOR CASE II

In Case III the initial current field was that used in Case I. An initial uniform wind field of 5.4 m sec^{-1} from 112° (south of east) was prescribed over the grid. As the simulation proceeded this wind field was modified by a cyclonic disturbance. This disturbance was of a radius of 60 nautical miles and moved from the southern boundary to the Northwest.

The discussion of the results of these inital cases is limited to a description of the dynamic behavior of the two layer ocean. In Case I a shear front in both the wind field and current field was prescribed. The front, as defined by the slope of the interface between the top and bottom layers, is shown in Figure 4-3. The top layer deepens under the influence of the convergent wind north of the front and shoals under the divergent regime south of the front. The initial trough in the interface occurring at the location of zero velocity in the wind and current fields becomes less pronounced by the end of the twelve hour simulation run.

The currents in the surface layer in Case I at locations north and south of the front are shown in Figure 4-4 in the form of progressive vector diagrams. From this figure, it can be seen that the primary mode of the response of the simulated ocean to the initial conditions and the steady-state wind field is that of a rotary current.

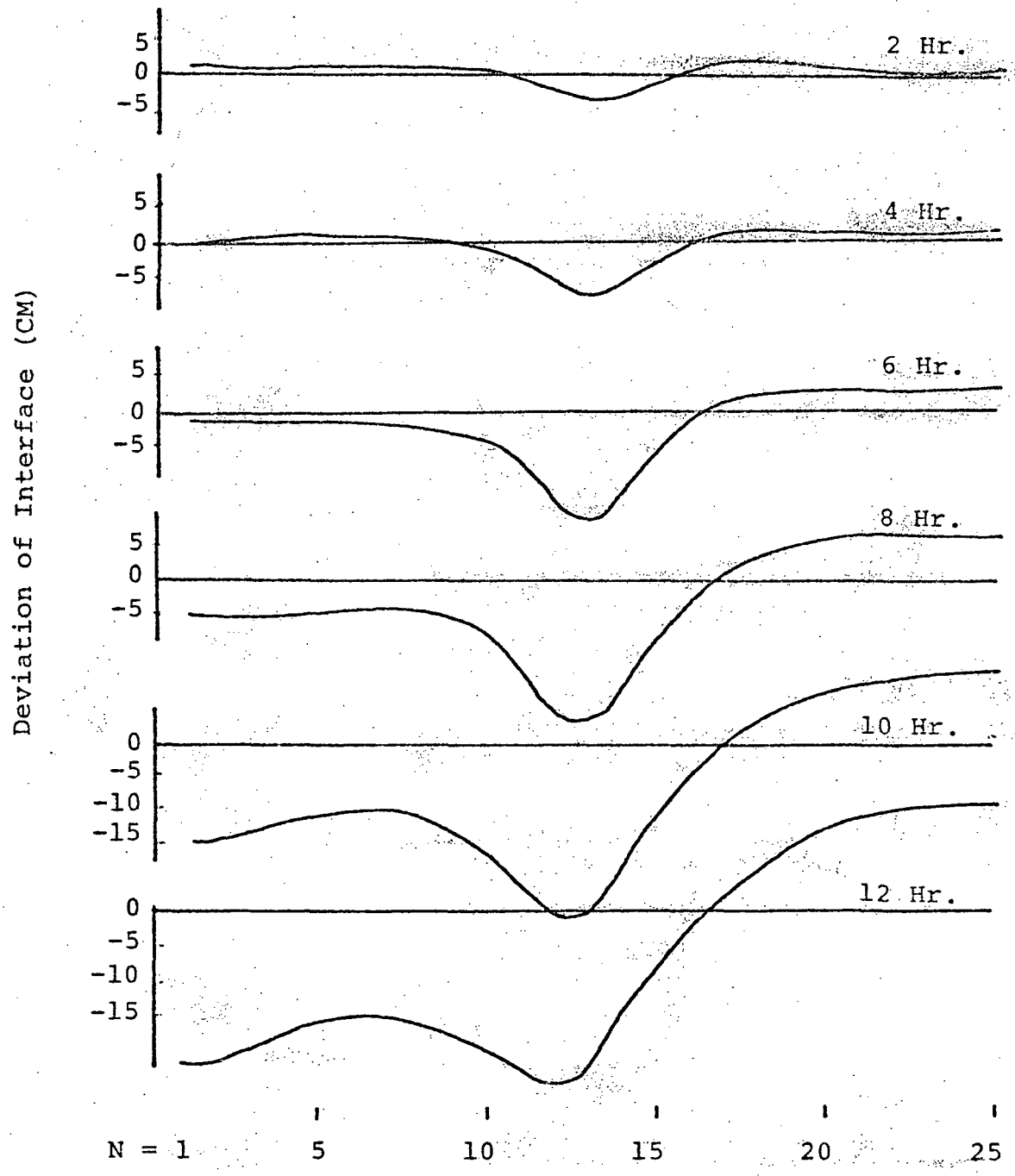

FIGURE 4-3: DEVIATION OF INTERFACE FROM INITIAL POSITION ALONG M = 15 CASE I

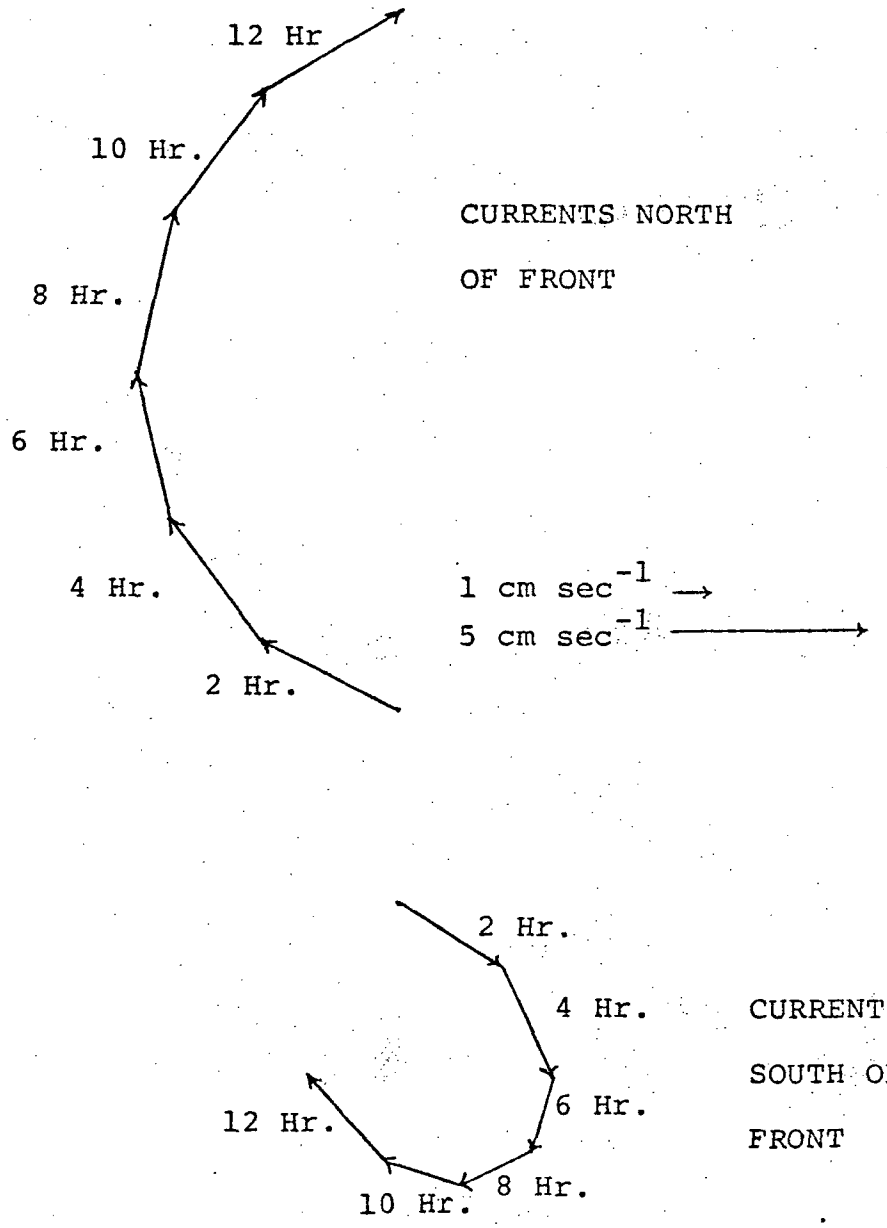

FIGURE 4-4: CURRENTS IN TOP LAYER - CASE I.

Case II simulated a convergence front, the development of which is shown in Figure 4-5. In this run the front develops without a trough in the interface as happened in Case I. This fact can be attributed to the lack of a null current line in the initial current field in Case II. After twelve hours the slope of the interface in this run was about 50% of that in Case I. Also, it appears that the top of the front is eroding northward from its initial position resulting in a gradually decreasing frontal slope.

The currents north and south of the front in Case II are again depicted by progressive vector diagrams and are shown in Figure 4-6. While the rotary current response is the same as seen in Case I, there is not the initial change in direction across the front in Case II due to the uniform initial currents in this case. Again no change was found in the initial temperature distribution in Case II.

Case III simulated the interaction of a time dependent windfield and an initial shear current. The development of the front is seen in Figure 4-7. In this case the front develops through the first four hours as in Case I. At six hours however, the topography of the interface becomes distinctly different from that of Case I. This interface topography continues to evolve differently through the remaining six hours of the run. The general form of the front is similar to that of Case I in which the interface deepens in the north and shoals to the south.

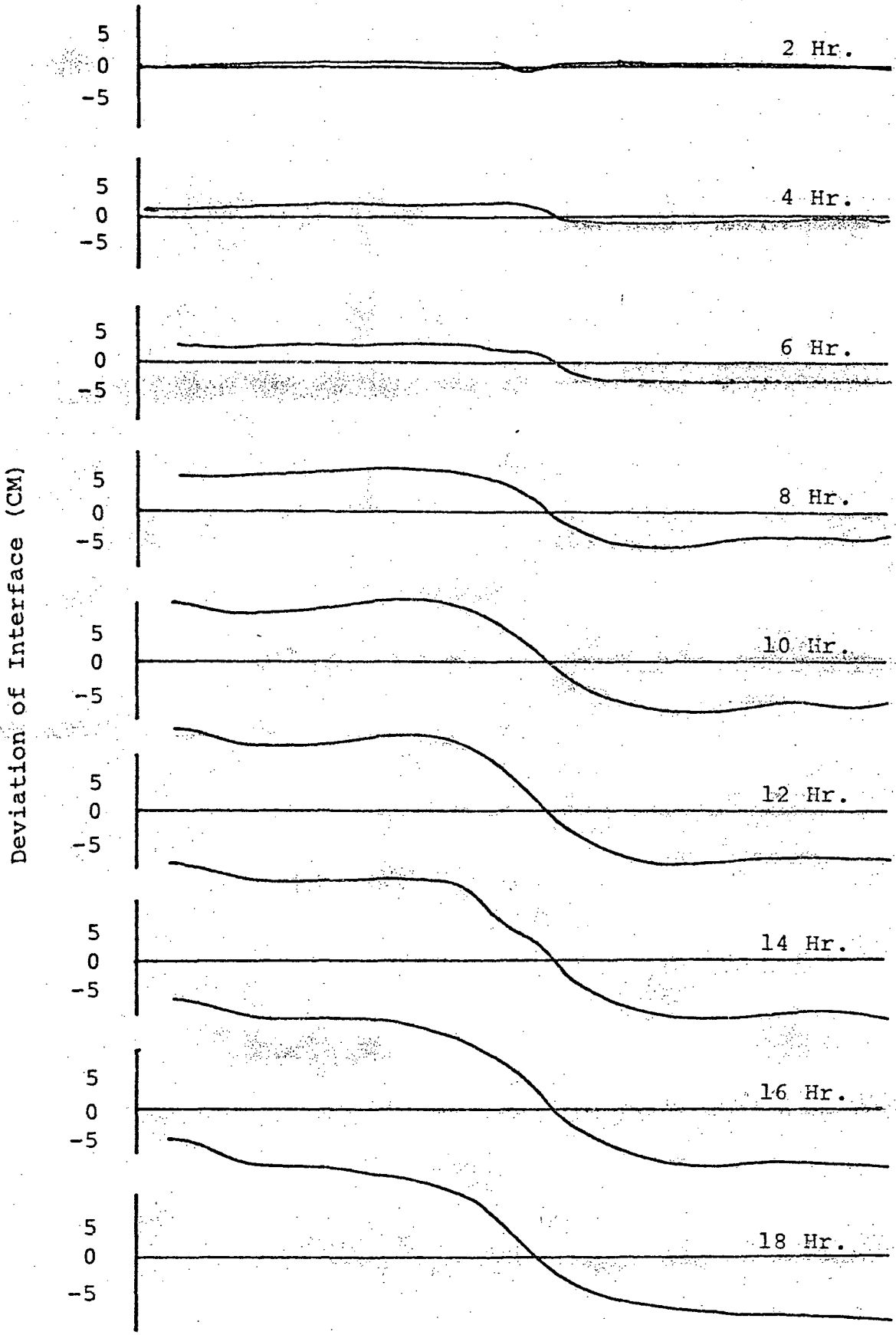

FIGURE 4-5: DEVIATION OF INTERFACE FROM INITIAL POSITION ALONG M = 15 CASE II

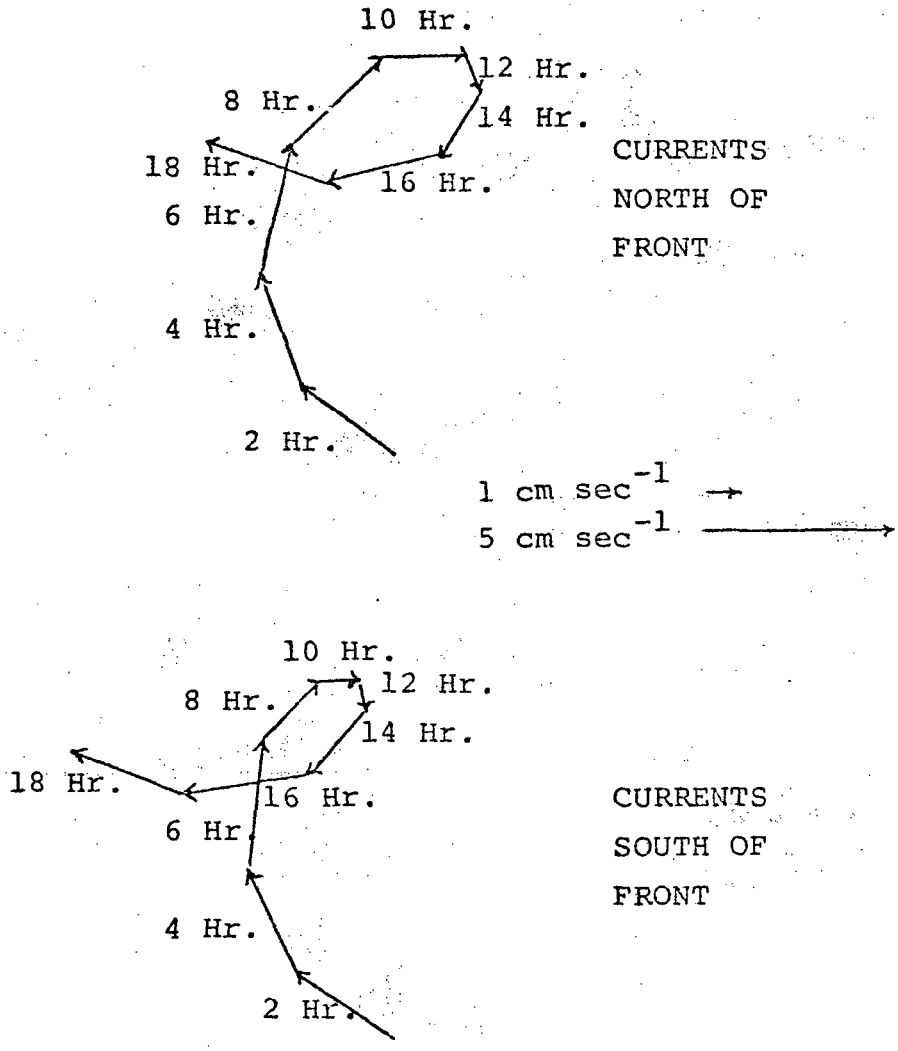

FIGURE 4-6: CURRENTS IN TOP LAYER
CASE II

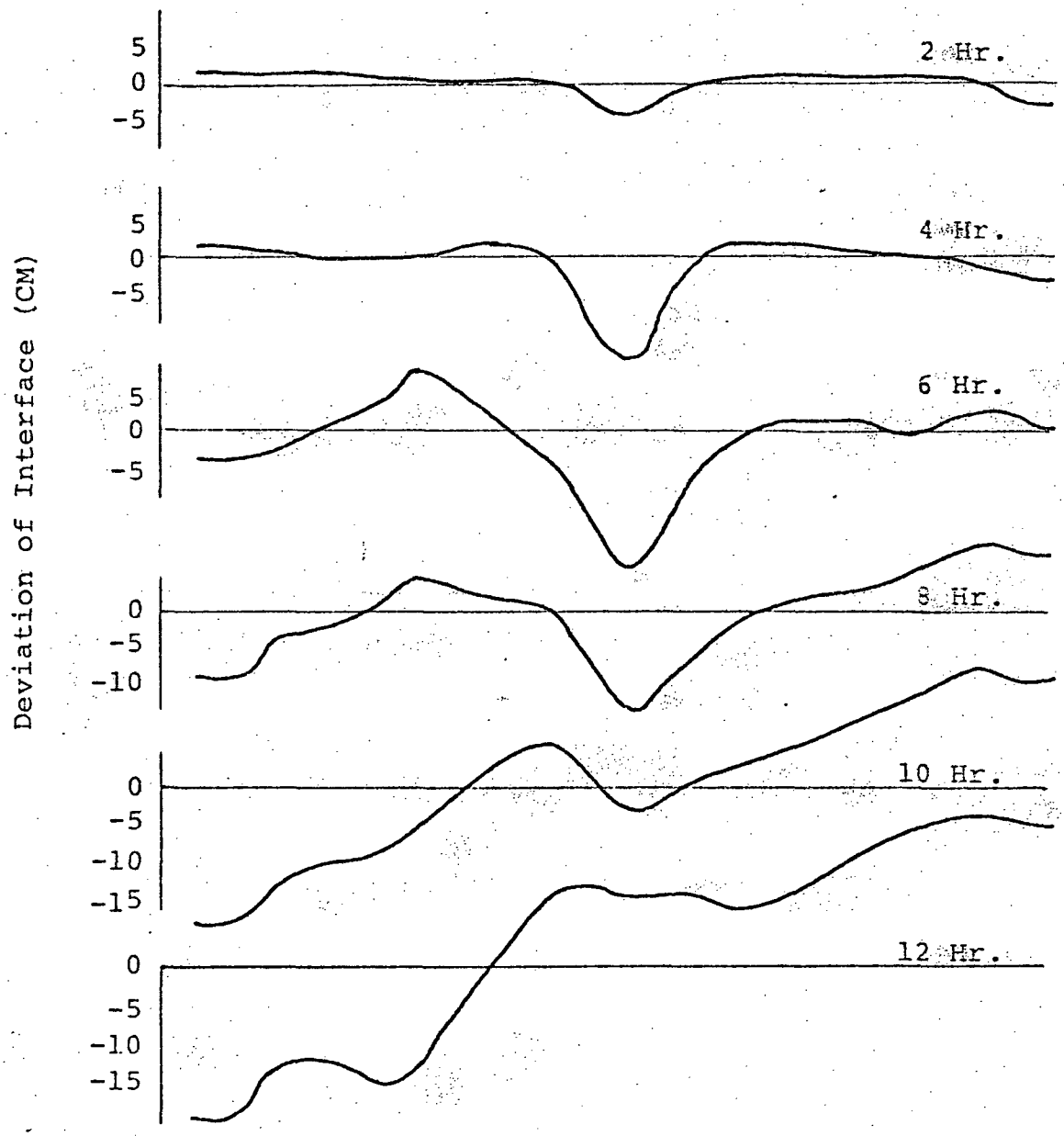

FIGURE 4-7: DEVIATION OF INTERFACE FROM INITIAL POSITION ALONG M=15 CASE III.

The currents in the surface layer in the northern and southern regions are shown in Figure 4-8. Because in Case III the wind field is not uniform in the east-west direction, the currents are not as representative of the region concerned as they are for Cases I and II. By comparing Figures 4-4 and 4-8, the impact of the different wind regimes can be seen. In the northern region the rotary current is rather strongly deformed compared to Case I due to the differing wind regimes.

Since the initial test runs did not show appreciable changes in temperature structure in the upper layer (because of the weak initial thermal gradient and comparatively short run time), an additional test case was formulated to demonstrate that temperature changes would occur. In this case, a strong front was specified initially and current/wind forces were specified which should cause a gradual weakening of the frontal intensity -- especially in the frontal fringes.

Figure 4-9 shows the initial north-south temperature profile (homogeneous cold and warm water masses with a sharp gradient in between) and the change in surface layer temperature which occurred after 120 hours of run time. Notice that some blurring can be seen at the cold edge but the largest changes (almost 0.6°C) occurred at the warm edge of the front. This non-symetrical pattern is due to the way the initial winds and currents were defined. Figures 4-10 and 4-11 show the initial and final temperature values.

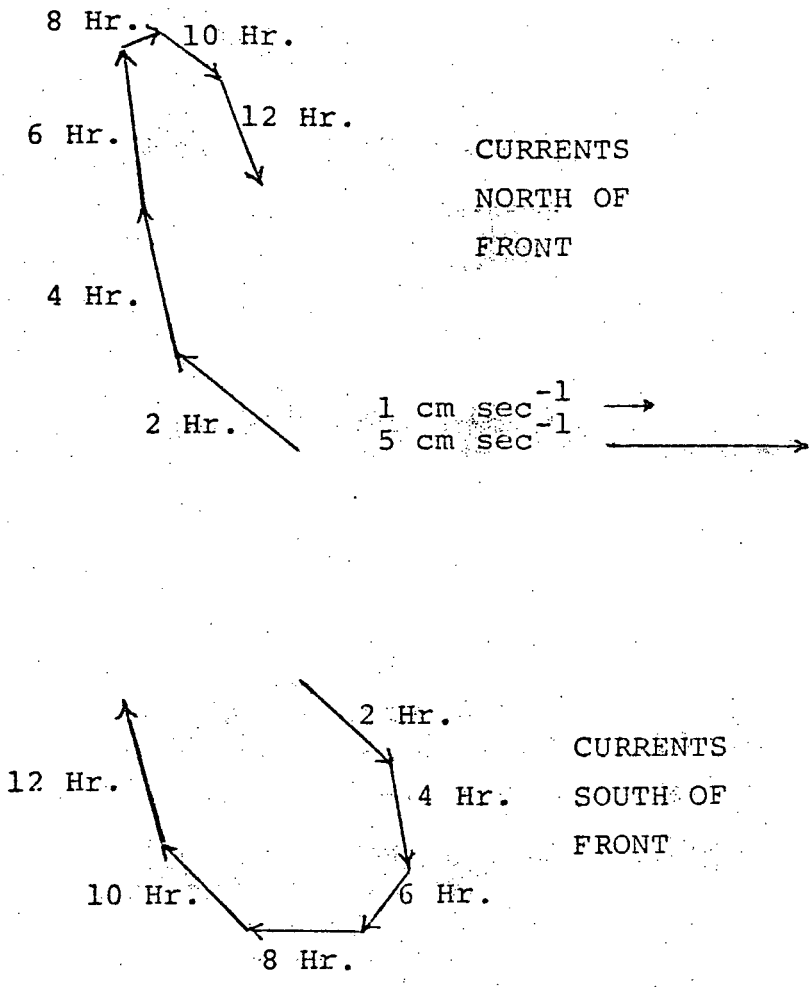

FIGURE 4-8: CURRENT IN TOP LAYER
CASE III

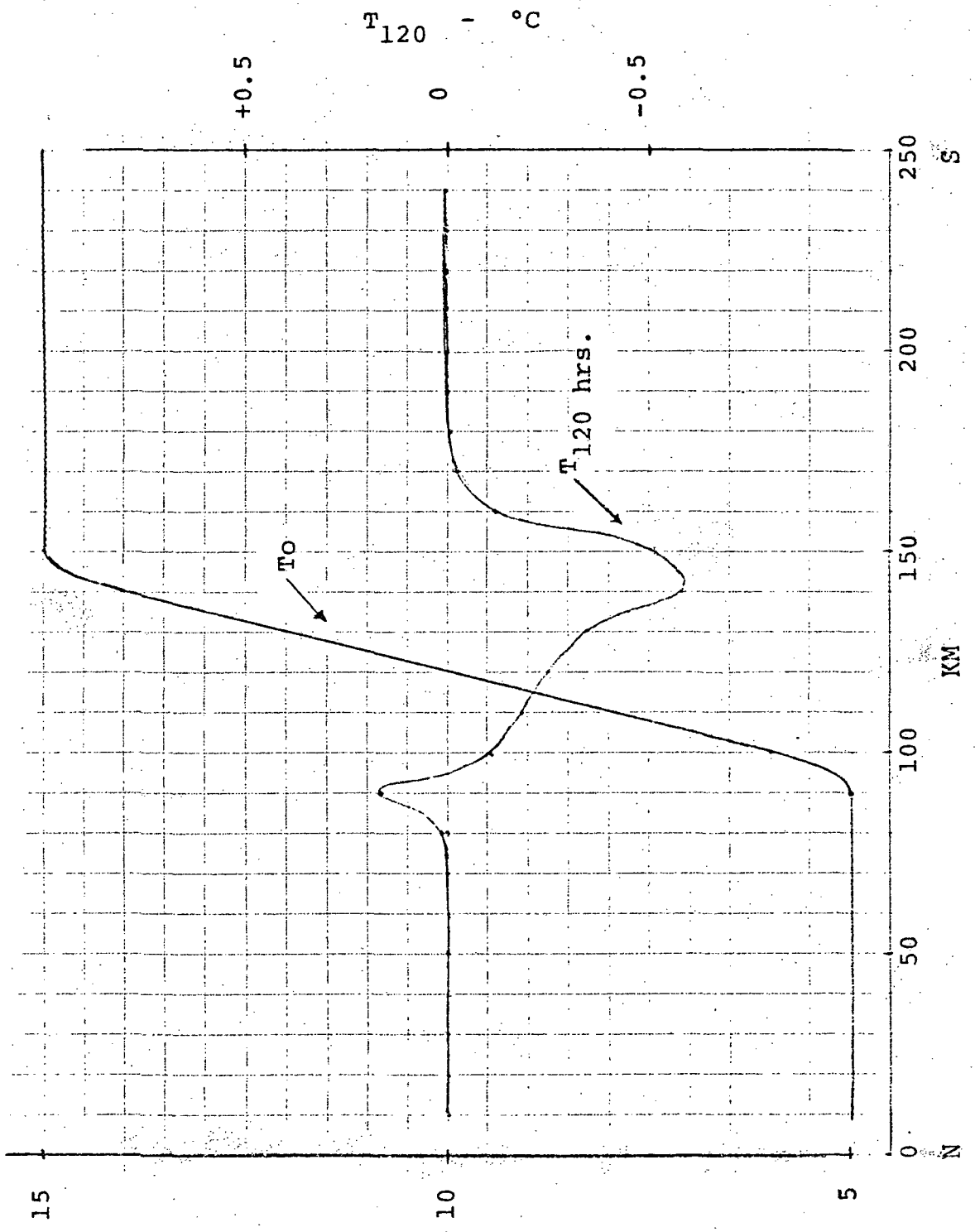

FIGURE 4-9: ORIGINAL TEMPERATURE PROFILE AND TEMPERATURE CHANGE AFTER 120 HRS. CASE IV.

TEMPERATURE FIELD*****

5.00000	5.00000	5.00000	5.00000	5.00000	5.00000	5.00000	5.00000	5.00000	5.00000
5.00000	5.00000	5.00000	5.00000	5.00000	5.00000	5.00000	5.00000	5.00000	5.00000
5.00000	5.00000	5.00000	5.00000	5.00000	5.00000	5.00000	5.00000	5.00000	5.00000
5.00000	5.00000	5.00000	5.00000	5.00000	5.00000	5.00000	5.00000	5.00000	5.00000
5.00000	5.00000	5.00000	5.00000	5.00000	5.00000	5.00000	5.00000	5.00000	5.00000
5.00000	5.00000	5.00000	5.00000	5.00000	5.00000	5.00000	5.00000	5.00000	5.00000
5.00000	5.00000	5.00000	5.00000	5.00000	5.00000	5.00000	5.00000	5.00000	5.00000
5.00000	5.00000	5.00000	5.00000	5.00000	5.00000	5.00000	5.00000	5.00000	5.00000
5.00000	5.00000	5.00000	5.00000	5.00000	5.00000	5.00000	5.00000	5.00000	5.00000
6.00000	6.00000	6.00000	6.00000	6.00000	6.00000	6.00000	6.00000	6.00000	6.00000
8.00000	8.00000	8.00000	8.00000	8.00000	8.00000	8.00000	8.00000	8.00000	8.00000
10.00000	10.00000	10.00000	10.00000	10.00000	10.00000	10.00000	10.00000	10.00000	10.00000
12.00000	12.00000	12.00000	12.00000	12.00000	12.00000	12.00000	12.00000	12.00000	12.00000
14.00000	14.00000	14.00000	14.00000	14.00000	14.00000	14.00000	14.00000	14.00000	14.00000
15.00000	15.00000	15.00000	15.00000	15.00000	15.00000	15.00000	15.00000	15.00000	15.00000
15.00000	15.00000	15.00000	15.00000	15.00000	15.00000	15.00000	15.00000	15.00000	15.00000
15.00000	15.00000	15.00000	15.00000	15.00000	15.00000	15.00000	15.00000	15.00000	15.00000
15.00000	15.00000	15.00000	15.00000	15.00000	15.00000	15.00000	15.00000	15.00000	15.00000
15.00000	15.00000	15.00000	15.00000	15.00000	15.00000	15.00000	15.00000	15.00000	15.00000
15.00000	15.00000	15.00000	15.00000	15.00000	15.00000	15.00000	15.00000	15.00000	15.00000
15.00000	15.00000	15.00000	15.00000	15.00000	15.00000	15.00000	15.00000	15.00000	15.00000
15.00000	15.00000	15.00000	15.00000	15.00000	15.00000	15.00000	15.00000	15.00000	15.00000
15.00000	15.00000	15.00000	15.00000	15.00000	15.00000	15.00000	15.00000	15.00000	15.00000

FIGURE 4-10. INITIAL TEMPERATURE FIELD

TEMPERATURE OF SURFACE LAYER (DEGREES) AFTER T = 432000.

1	2	3	4	5	6	7	8	9	10	11	12	13	14	15
4.997	4.997	4.997	4.997	4.997	4.997	4.997	4.997	4.997	4.997	4.997	4.997	4.997	4.997	4.997
4.997	4.997	4.997	4.997	4.997	4.997	4.997	4.997	4.997	4.997	4.997	4.997	4.997	4.997	4.997
4.997	4.997	4.997	4.997	4.997	4.997	4.997	4.997	4.997	4.997	4.997	4.997	4.997	4.997	4.997
4.997	4.997	4.997	4.997	4.997	4.997	4.997	4.997	4.997	4.997	4.997	4.997	4.997	4.997	4.997
4.997	4.997	4.997	4.997	4.997	4.997	4.997	4.997	4.997	4.997	4.997	4.997	4.997	4.997	4.997
4.997	4.997	4.997	4.997	4.997	4.997	4.997	4.997	4.997	4.997	4.997	4.997	4.997	4.997	4.997
4.997	4.997	4.997	4.997	4.997	4.997	4.997	4.997	4.997	4.997	4.997	4.997	4.997	4.997	4.997
4.998	4.998	4.998	4.998	4.998	4.998	4.997	4.997	4.997	4.997	4.997	4.997	4.997	4.997	4.997
5.018	5.018	5.018	5.018	5.018	5.018	5.018	5.017	5.017	5.017	5.017	5.017	5.017	5.017	5.017
5.173	5.173	5.172	5.171	5.170	5.169	5.168	5.167	5.166	5.165	5.165	5.165	5.165	5.165	5.165
5.907	5.907	5.904	5.902	5.899	5.897	5.895	5.893	5.891	5.890	5.888	5.887	5.887	5.887	5.887
7.834	7.834	7.831	7.828	7.824	7.821	7.819	7.816	7.814	7.812	7.810	7.809	7.809	7.809	7.809
9.783	9.783	9.780	9.776	9.773	9.770	9.766	9.764	9.761	9.759	9.758	9.756	9.756	9.756	9.755
11.683	11.683	11.679	11.675	11.671	11.668	11.664	11.662	11.659	11.657	11.655	11.654	11.654	11.654	11.654
13.440	13.440	13.436	13.432	13.429	13.425	13.422	13.420	13.417	13.415	13.414	13.413	13.413	13.413	13.413
14.513	14.513	14.511	14.508	14.506	14.504	14.502	14.500	14.499	14.498	14.497	14.497	14.497	14.497	14.497
14.889	14.889	14.888	14.887	14.886	14.886	14.885	14.885	14.885	14.884	14.884	14.884	14.884	14.884	14.884
14.978	14.978	14.977	14.977	14.977	14.977	14.977	14.977	14.977	14.977	14.977	14.977	14.977	14.977	14.977
14.993	14.993	14.993	14.993	14.993	14.993	14.993	14.993	14.993	14.993	14.993	14.993	14.993	14.993	14.993
14.995	14.995	14.995	14.995	14.995	14.995	14.995	14.995	14.995	14.995	14.995	14.995	14.995	14.995	14.995
14.996	14.996	14.996	14.996	14.996	14.996	14.996	14.996	14.996	14.996	14.996	14.996	14.996	14.996	14.996
14.996	14.996	14.996	14.996	14.996	14.996	14.996	14.996	14.996	14.996	14.996	14.996	14.996	14.996	14.996
14.996	14.996	14.996	14.996	14.996	14.996	14.996	14.996	14.996	14.996	14.995	14.996	14.995	14.996	14.996
14.997	14.997	14.997	14.997	14.997	14.997	14.997	14.997	14.997	14.997	14.997	14.997	14.997	14.997	14.997
14.997	14.997	14.997	14.997	14.997	14.997	14.997	14.997	14.997	14.997	14.997	14.997	14.997	14.997	14.997

16	17	18	19	20	21	22	23	24	25	26	27	28	29	30
4.997	4.997	4.997	4.997	4.997	4.997	4.997	4.997	4.997	4.997	4.997	4.997	4.997	4.997	4.997
4.997	4.997	4.997	4.997	4.997	4.997	4.997	4.997	4.997	4.997	4.997	4.997	4.997	4.997	4.997
4.997	4.997	4.997	4.997	4.997	4.997	4.997	4.997	4.997	4.997	4.997	4.997	4.997	4.997	4.997
4.997	4.997	4.997	4.997	4.997	4.997	4.997	4.997	4.997	4.997	4.997	4.997	4.997	4.997	4.997
4.997	4.997	4.997	4.997	4.997	4.997	4.997	4.997	4.997	4.997	4.997	4.997	4.997	4.997	4.997
4.997	4.997	4.997	4.997	4.997	4.997	4.997	4.997	4.997	4.997	4.997	4.997	4.997	4.997	4.997
4.997	4.997	4.997	4.997	4.997	4.997	4.997	4.997	4.997	4.997	4.997	4.997	4.997	4.997	4.997
5.017	5.017	5.017	5.017	5.017	5.017	5.017	5.017	5.017	5.017	5.017	5.017	5.017	5.017	5.017
5.165	5.165	5.165	5.165	5.165	5.165	5.165	5.166	5.166	5.166	5.167	5.167	5.167	5.167	5.167
5.887	5.887	5.888	5.888	5.889	5.889	5.890	5.891	5.892	5.893	5.894	5.895	5.895	5.895	5.895
7.809	7.810	7.810	7.811	7.813	7.814	7.816	7.817	7.819	7.821	7.823	7.824	7.825	7.824	7.824
9.756	9.757	9.758	9.759	9.760	9.761	9.763	9.765	9.767	9.769	9.771	9.773	9.774	9.773	9.773
11.654	11.655	11.655	11.656	11.658	11.660	11.662	11.664	11.666	11.668	11.670	11.672	11.673	11.672	11.672
13.413	13.414	13.414	13.415	13.417	13.418	13.420	13.422	13.423	13.425	13.427	13.429	13.430	13.430	13.430
14.497	14.497	14.498	14.499	14.499	14.500	14.501	14.502	14.504	14.505	14.506	14.507	14.508	14.508	14.508
14.884	14.884	14.885	14.885	14.885	14.885	14.886	14.886	14.887	14.887	14.888	14.888	14.888	14.888	14.888
14.977	14.977	14.977	14.977	14.977	14.977	14.977	14.977	14.977	14.977	14.977	14.978	14.978	14.978	14.978
14.993	14.993	14.993	14.993	14.993	14.993	14.993	14.993	14.993	14.993	14.993	14.993	14.993	14.993	14.993
14.995	14.995	14.995	14.995	14.995	14.995	14.995	14.995	14.995	14.995	14.995	14.995	14.995	14.995	14.995
14.996	14.996	14.996	14.996	14.996	14.996	14.996	14.996	14.996	14.996	14.996	14.996	14.996	14.996	14.996
14.996	14.996	14.996	14.996	14.996	14.996	14.996	14.996	14.996	14.996	14.996	14.996	14.996	14.996	14.996
14.996	14.996	14.996	14.996	14.996	14.996	14.996	14.996	14.996	14.996	14.996	14.996	14.996	14.996	14.996
14.997	14.997	14.997	14.997	14.997	14.997	14.997	14.997	14.997	14.997	14.997	14.997	14.997	14.997	14.997
14.997	14.997	14.997	14.997	14.997	14.997	14.997	14.997	14.997	14.997	14.997	14.997	14.997	14.997	14.997

FIGURE 4-11. TEMPERATURE FIELD AFTER 120 HOURS

5.0 NUMERICAL STUDIES OF SEA STATE CHANGES

One basic objective of this overall study was to determine the influence of oceanic fronts upon sea state - especially the effect of fronts on wave energy distributions and/or variations in wave steepness which might be detected by satellites. Two approaches to this problem were utilized: (a) a spectral wave model (see App. B) was used to study sea-state energy distributions around an atmospheric convergence zone which would support/amplify an oceanic front and (b) a model described by Johnson (1947) was used to study wave changes caused by intersection with a current boundary, i.e., a numerical wave refraction model was used as described in App. C.

5.1 Wind Wave Changes Across Oceanic Fronts

a. Experiment Design

The French D.S.A. V spectroangular wave model was used to generate typical wind wave fields resulting from an atmospheric convergence situation and, also, the passage of a tropical cyclone. The description of this numerical model is found in App. B of this report. To reproduce the wind fields, the 29 row x 33 column grid was used, a wind speed of 20 kts from the ESE occurring at row 14 and above and a wind speed of 10 kts from the ESE at row 15 and below. For

the tropical cyclone experiment, a cyclone of radius 200 nmi and maximum wind speeds of 60 kts, at the wall of the eye was prescribed. The wind speed profile was based on:

$$V_D = V_{max} + \frac{V_{max} - V_{Back}}{\ln(R_{eye}/R_{circ})} \times \ln(D/R_{eye})$$

where:

V_D is the velocity at distance D

V_{Back} is the velocity of the background flow

R_{eye} is the radius at the eye

R_{circ} is the radius of the storm

V_{max} is the maximum wind velocity

In both experiments the grid mesh length was set at 40 nmi. The time step between introduction of wind fields was 3 hr. The program was run out through 40 hours of computations in both instances.

b. Case 1: Convergent Wind Field Results

Figures 5-1, 5-2 and 5-3 depict a subsegment across the front of the fields for $H_{1/10}$, direction of maximum energy, and period of maximum energy, after 33 hours of computation. Higher wave heights are evident on the northern side of the front as well as longer periods. The fact that the heights decrease, 10 ft. to 7 ft., and the periods shorten, 8 sec. to 6 sec., as the convergence is approached is due to

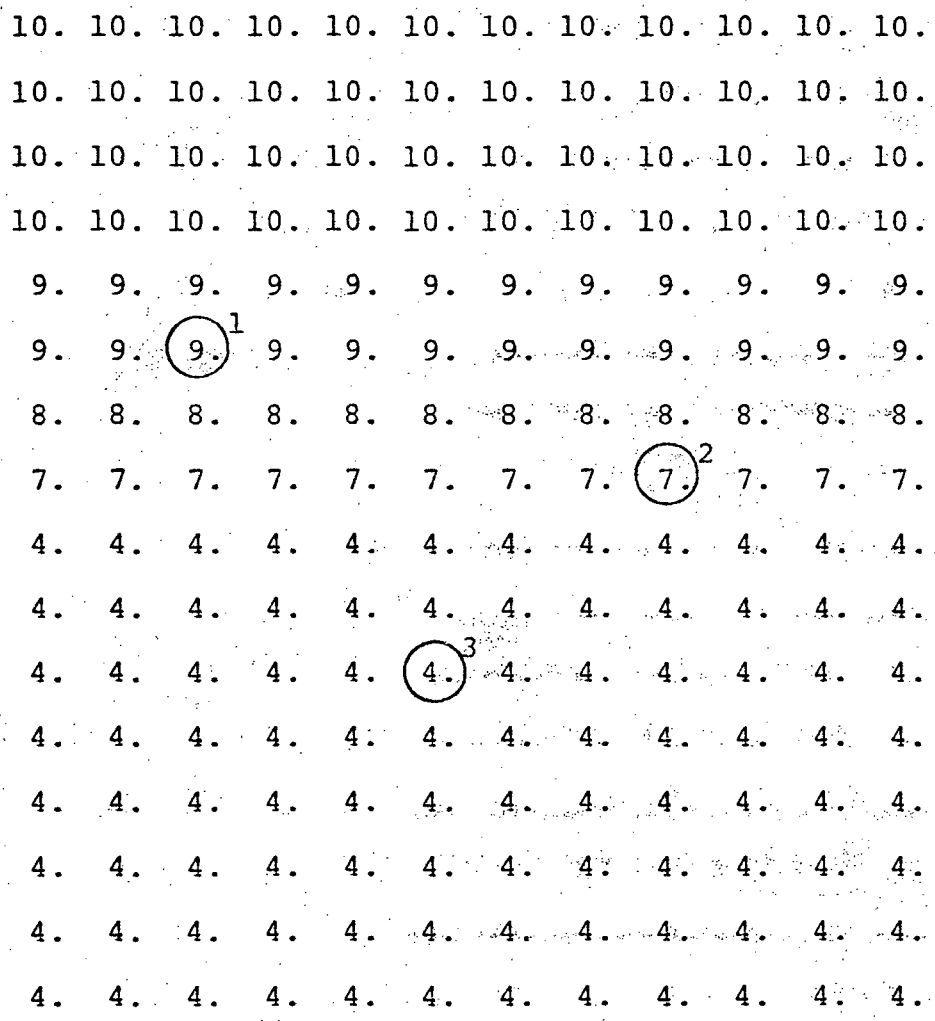

FIGURE 5-1

$H_{1/10}$ Wave Height (ft) at
Hour 33 of Convergent Case

67	67	67	67	67	67	67	67	67	67	67	67
67	67	67	67	67	67	67	67	67	67	67	67
67	67	67	67	67	67	67	67	67	67	67	67
67	67	67	67	67	67	67	67	67	67	67	67
45	45	45	45	45	45	45	45	45	45	45	45
67	67	(67)[1]	67	67	67	67	67	67	67	67	67
67	67	67	67	67	67	67	67	67	67	67	67
45	45	45	45	45	45	45	45	(45)[2]	45	45	45
112	112	112	112	112	112	112	112	112	112	112	112
112	112	112	112	112	112	112	112	112	112	112	112
112	112	112	112	112	(112)[3]	112	112	112	112	112	112
112	112	112	112	112	112	112	112	112	112	112	112
112	112	112	112	112	112	112	112	112	112	112	112
112	112	112	112	112	112	112	112	112	112	112	112
112	112	112	112	112	112	112	112	112	112	112	112
112	112	112	112	112	112	112	112	112	112	112	112

FIGURE 5-2

Wave Direction of Maximum Energy at
Hour 33 of Convergent Case

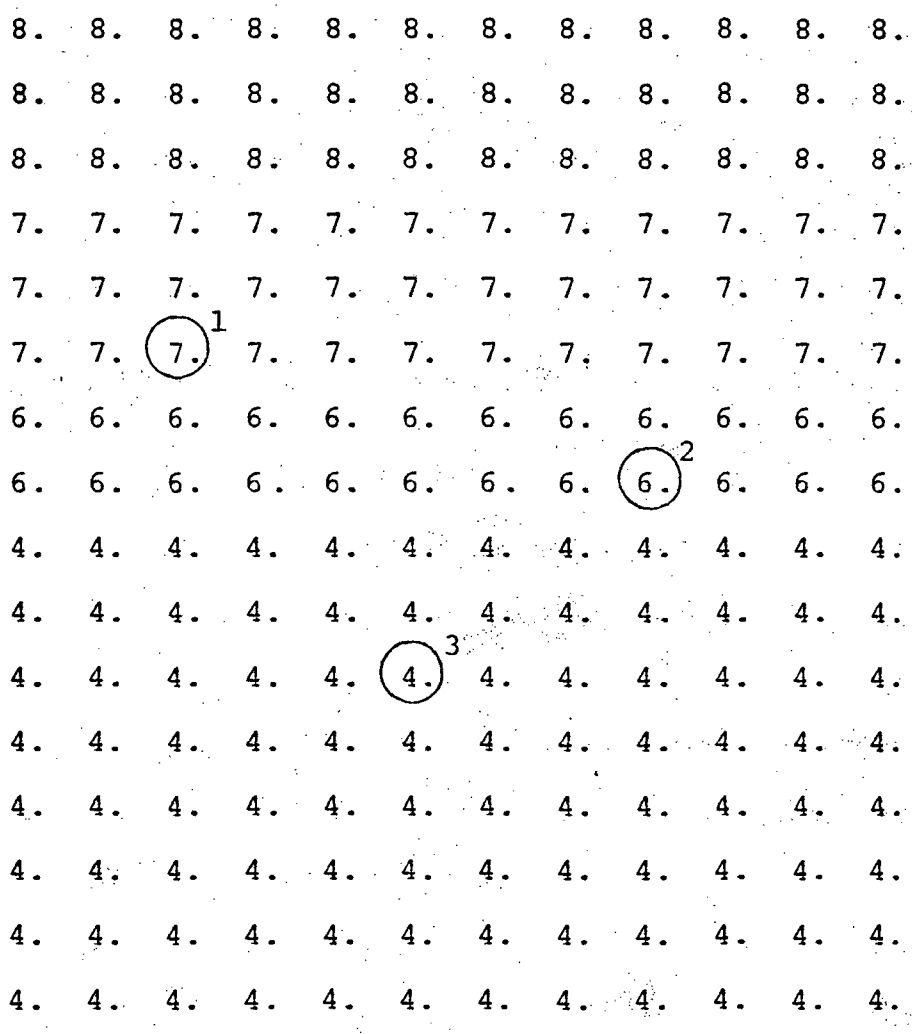

FIGURE 5-3

Period of Maximum Energy (sec) at
Hour 33 of Convergent Case

the combined effects of increased wave-interference and dampening. On the southern side, the lighter wind speeds result in a comparatively flat $H_{1/10}$ field of 4 ft. with a period of maximum energy of 4 sec.

The direction field shows two bands of anomalous directions of maximum energy. These are clarified when the spectral information at the three special points are inspected on Figure 5-4. As can be seen, the direction of maximum energy, when moving from points 1 to 3, undergoes a dampening of ENE components, while the NE components remain large enough to become the direction of maximum energy. The overall pattern shows a decrease in energy when crossing the front accompanied by a corresponding shift in the direction. Likewise, the period of maximum energy shortens once the energy decreases while propagating southward across the front.

c. Case 2: Tropical Cyclone Results

For this experiment results for three different times are presented (21, 27 and 33 hours of computation). These times correspond to the passage of the storm across the convergent front described in the previous section. In this case, the storm was initiated at t=0 and allowed to travel across the wave field produced by the convergent wind fields.

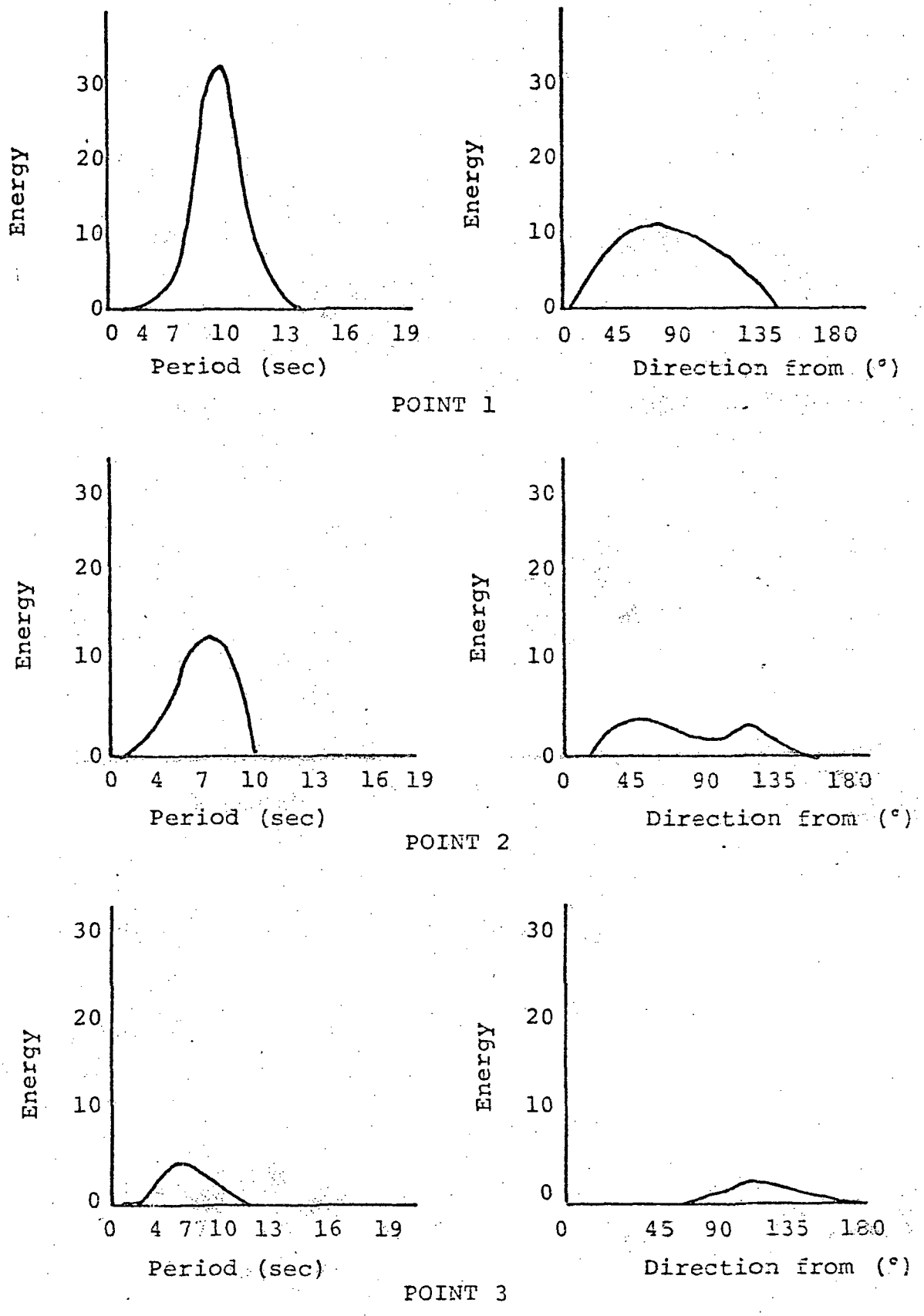

FIGURE 5-4: SPECTRAL COMPONENTS OF SPECIAL POINTS AT HOUR 33 OF CONVERGENT CASE

Figures 5-5 through 5-7 depict the surface wave parameter fields generated by the wind field shown in Figure 5-8. As can be seen, much higher values of $H_{1/10}$ occur around the storm and to its right where the storm velocity and background flow coincide. The directions of maximum energy take on a cyclonic appearance. (Values of "382°" mean that no single direction has a predominance of energy.) The same pattern is evident in the wave period field, with higher periods occuring to the right and ahead of the storm. Here, points of no predominant period of maximum energy are left blank.

Much the same results are evident from the results at 27 hours, Figures 5-9 through 5-12. At this time the storm is in the process of crossing the convergence zone. From Figure 5-9, it can be seen that the values of $H_{1/10}$ have spread across the zone. The directional field still has a cyclonic nature and has almost totally obscured the convergent initial pattern. In the wave period field the high periods are evident moving ahead of the storm path. An interesting aspect is the spread of 11 sec. periods along both sides of the convergent zone.

Figures 5-13 through 5-16 depict the results after 33 hours of computation. At this time the storm is largely across the convergent zone and moving away. As can be seen, the wave height field has decreased substantially, reverting to the original state. The directional field,

10.	10.	10.	10.	10.	10.	10.	10.	10.	10.	10.	10.
10.	10.	10.	10.	10.	10.	10.	10.	10.	10.	10.	10.
10.	10.	10.	10.	10.	10.	10.	10.	10.	10.	11.	11.
10.	10.	10.	10.	10.	10.	10.	11.	11.	11.	11.	11.
9.	10.	10.	10.	11.	11.	11.	11.	11.	11.	11.	11.
9.	9.	10. (1)	10.	10.	11.	11.	11.	11.	11.	11.	11.
8.	9.	10.	10.	11.	11.	11.	11.	11.	11.	11.	11.
7.	8.	9.	11.	11.	11.	11.	11.	11. (2)	11.	10.	9.
7.	9.	11.	13.	14.	13.	12.	12.	12.	11.	10.	10.
8.	11.	14.	16.	16.	14.	13.	12.	12.	12.	11.	10.
10.	13.	17.	21.	20.	18. (3)	14.	12.	13.	11.	12.	10.
10.	13.	15.	17.	21.	18.	17.	13.	12.	12.	11.	11.
9.	9.	11.	13.	15.	19.	17.	14.	11.	10.	10.	10.
6.	6.	6.	9.	12.	15.	17.	13.	10.	9.	9.	9.
5.	4.	4.	6.	8.	12.	13.	10.	8.	8.	8.	8.
4.	4.	4.	5.	7.	10.	8.	7.	6.	7.	7.	7.

FIGURE 5-5

$H_{1/10}$ Wave Height Field (ft) at
Hour 21 of Tropical Storm Case

67	67	67	67	67	67	67	67	67	90	90	90
67	67	67	67	67	67	67	67	90	90	90	90
67	67	67	67	67	67	67	67	90	90	90	90
67	67	67	67	67	67	67	90	90	90	90	90
67	67	67	67	67	67	90	90	90	90	90	90
67	67	(67)[1]	67	67	67	90	90	90	90	90	112
45	67	67	67	67	90	90	90	382	382	112	112
67	382	382	67	90	90	90	112	(112)[2]	112	112	112
67	67	67	90	90	112	112	112	112	112	135	112
45	67	67	90	90	112	112	112	112	135	135	135
45	67	90	90	112	(112)[3]	135	135	135	135	135	135
67	67	90	112	135	112	135	135	157	135	135	135
45	90	90	112	112	135	157	135	157	157	157	157
90	90	90	90	135	157	157	157	157	157	157	157
90	112	90	90	180	157	180	157	157	157	157	180
112	112	135	180	180	180	180	157	157	180	180	180

FIGURE 5-6

Direction of Maximum Energy (° from) at
Hour 21 of Tropical Storm Case

8.	8.	8.	8.	8.	8.	8.	8.	8.	8.	8.	8.
8.	8.	8.	8.	8.	8.	8.	8.	8.	8.	8.	8.
8.	8.	8.	8.	8.	8.	8.	8.	8.	8.	8.	8.
7.	8.	8.	8.	8.	8.	8.	8.	8.	8.	8.	8.
7.	8.	8.	8.	8.	8.	8.	8.	8.	8.	8.	8.
7.	8.	(8.)[1]	8.	8.	8.	8.	8.	8.	8.	8.	8.
8.	8.	8.	8.	8.	8.	12.	12.	.	.	10.	10.
7.	.	.	13.	13.	13.	13.	13.	(13.)[2]	11.	11.	11.
11.	11.	11.	13.	13.	11.	11.	11.	11.	11.	11.	11.
10.	10.	10.	11.	11.	11.	11.	11.	11.	11.	11.	11.
8.	10.	10.	11.	11.	(11.)[3]	11.	11.	11.	11.	11.	11.
8.	8.	10.	10.	10.	11.	11.	11.	11.	11.	11.	11.
8.	7.	8.	8.	8.	10.	10.	10.	11.	11.	11.	11.
6.	6.	6.	8.	8.	8.	10.	10.	10.	10.	10.	10.
4.	4.	4.	6.	7.	8.	8.	8.	8.	9.	9.	10.
4.	4.	4.	4.	7.	8.	8.	8.	8.	8.	9.	8.

FIGURE 5-7

Period of Maximum Energy (sec) at
Hour 21 of Tropical Storm Case

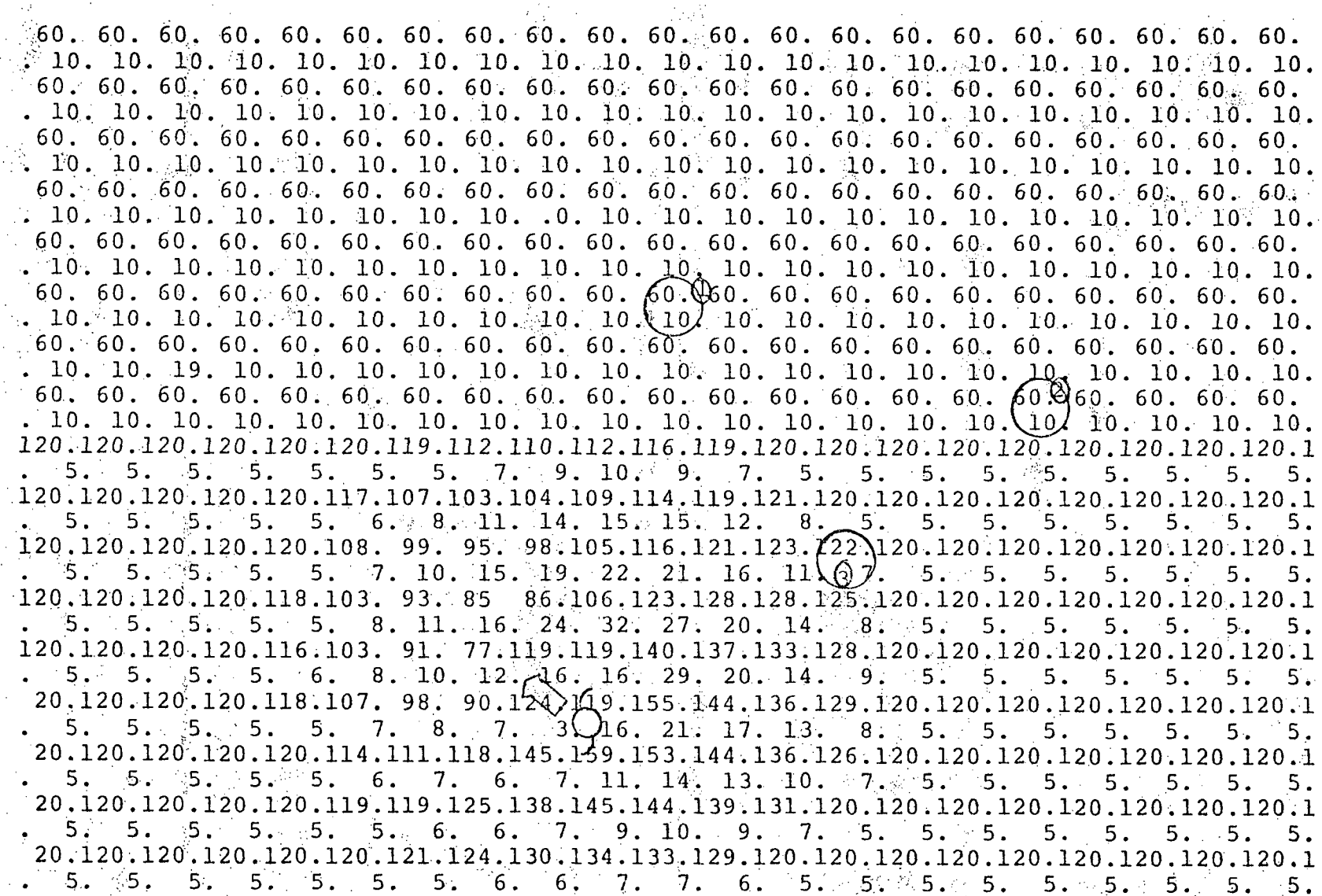

FIGURE 5-8 Wind Speed (m sec^{-1}) and Direction (° from) for Hour 21 of Tropical Storm Case

10.	10.	10.	10.	11.	11.	11.	11.	11.	11.	11.	11.
10.	10.	10.	11.	11.	11.	11.	11.	11.	11.	11.	11.
10.	10.	11.	11.	11.	11.	11.	11.	11.	11.	11.	11.
11.	11.	11.	11.	12.	12.	12.	11.	11.	11.	11.	11.
11.	12.	12.	12.	12.	12.	12.	11.	11.	11.	11.	11.
13.	14.	(14.)[1]	14.	13.	13.	12.	12.	11.	11.	11.	10.
15.	15.	15.	14.	14.	12.	12.	11.	11.	11.	10.	10.
16.	16.	15.	14.	12.	12.	11.	11.	(10)[2]	9.	9.	8.
19.	18.	16.	14.	13.	10.	11.	10.	9.	9.	8.	8.
16.	20.	17.	13.	11.	11.	10.	9.	10.	8.	8.	7.
14.	20.	17.	13.	10.	(9.)[3]	9.	9.	8.	8.	7.	7.
10.	15.	14.	11.	9.	8.	8.	8.	8.	7.	7.	7.
10.	12.	10.	9.	7.	8.	8.	8.	7.	6.	7.	7.
8.	9.	7.	6.	6.	6.	7.	7.	6.	6.	6.	7.
5.	6.	5.	5.	5.	5.	6.	6.	6.	5.	6.	6.
4.	4.	4.	4.	5.	5.	5.	5.	5.	5.	5.	5.

FIGURE 5-9

$H_{1/10}$ Wave Height Field (H) at
Hour 27 of Tropical Storm Case

67	67	67	67	67	90	90	90	90	90	90	112
67	67	67	67	90	90	90	90	90	112	112	112
67	67	90	90	90	90	90	90	112	112	112	112
67	90	90	90	90	90	90	112	112	112	112	112
67	90	90	90	90	112	112	112	112	112	112	112
90	90	(90)[1]	90	112	112	112	112	112	112	135	135
90	90	112	112	112	112	112	112	135	135	135	135
112	112	112	112	112	135	135	135	(135)[2]	135	135	135
90	112	112	135	135	135	135	135	135	135	135	135
90	135	135	135	135	135	135	135	157	157	135	135
112	135	157	157	135	(135)[3]	135	157	157	157	157	157
135	157	157	180	157	157	157	157	157	157	157	157
180	180	180	180	157	157	157	180	180	157	157	157
225	180	180	157	157	180	180	180	180	180	180	180
157	202	202	135	180	180	180	180	180	180	180	180
135	135	112	112	202	202	180	180	180	180	180	180

FIGURE 5-10

Direction of Maximum Energy (° from) at
Hour 27 of Tropical Storm Case

8.	8.	8.	8.	8.	8.	8.	8.	8.	8.	8.	8.
8.	8.	8.	8.	8.	8.	8.	8.	8.	8.	8.	8.
8.	8.	8.	8.	8.	8.	8.	8.	8.	8.	8.	8.
8.	8.	8.	8.	10.	10.	8.	8.	8.	8.	8.	8.
8.	10.	10.	10.	10.	10.	10.	10.	10.	10.	10.	8.
10.	10.	(10.)[1]	10.	12.	12.	10.	10.	10.	10.	10.	10.
11.	11.	11.	13.	13.	10.	10.	10.	10.	10.	10.	10.
11.	11.	11.	11.	11.	11.	11.	11.	(11.)[2]	11.	11.	11.
10.	11.	11.	11.	11.	11.	11.	11.	11.	11.	11.	11.
10.	10.	11.	11.	11.	11.	11.	11.	11.	11.	11.	11.
8.	10.	10.	10.	9.	(9.)[3]	9.	11.	11.	11.	11.	11.
8.	9.	9.	8.	9.	9.	10.	10.	10.	9.	9.	10.
8.	8.	8.	8.	8.	9.	10.	10.	10.	9.	9.	9.
8.	8.	8.	8.	8.	8.	10.	8.	8.	8.	9.	10.
6.	7.	7.	6.	7.	8.	8.	9.	7.	7.	8.	10.
4.	4.	4.	4.	6.	7.	7.	6.	6.	7.	7.	7.

FIGURE 5-11

Period of Maximum Energy (sec) at
Hour 27 of Tropical Storm Case

```
 60. 60. 60. 60. 60. 60. 60. 60. 60. 60. 60. 60. 60. 60. 60. 60. 60. 60. 60. 60. 60. 60. 60.
. 10. 10. 10. 10. 10. 10. 10. 10. 10. 10. 10. 10. 10. 10. 10. 10. 10. 10. 10. 10. 10. 10. 10.
 60. 60. 60. 60. 60. 60. 60. 60. 60. 60. 60. 60. 60. 60. 60. 60. 60. 60. 60. 60. 60. 60. 60.
. 10. 10. 10. 10. 10. 10. 10. 10. 10. 10. 10. 10. 10. 10. 10. 10. 10. 10. 10. 10. 10. 10. 10.
 60. 60. 60. 60. 60. 60. 60. 60. 60. 60. 60. 60. 60. 60. 60. 60. 60. 60. 60. 60. 60. 60. 60.
. 10. 10. 10. 10. 10. 10. 10. 10. 10. 10. 10. 10. 10. 10. 10. 10. 10. 10. 10. 10. 10. 10. 10.
 60. 60. 60. 60. 60. 60. 60. 60. 60. 60. 60. 60. 60. 60. 60. 60. 60. 60. 60. 60. 60. 60. 60.
. 10. 10. 10. 10. 10. 10. 10. 10. 10. 10. 10. 10. 10. 10. 10. 10. 10. 10. 10. 10. 10. 10. 10.
 60. 60. 60. 60. 60. 60. 60. 60. 60. 60. 60. 60. 60. 60. 60. 60. 60. 60. 60. 60. 60. 60. 60.
. 10. 10. 10. 10. 10. 10. 10. 10. 10. 10. 10. 10. 10. 10. 10. 10. 10. 10. 10. 10. 10. 10. 10.
 60. 60. 60. 60. 60. 60. 60. 60. 60. 60. 60. 60. 60. 60. 60. 60. 60. 60. 60. 60. 60. 60. 60.
. 10. 10. 10. 10. 10. 10. 10. 10. 10. 10. 10. 10. 10. 10. 10. 10. 10. 10. 10. 10. 10. 10. 10.
 60. 60. 60. 60. 60. 60. 60. 60. 60. 60. 60. 60. 60. 60. 60. 60. 60. 60. 60. 60. 60. 60. 60.
. 10. 10. 10. 10. 10. 10. 10. 10. 10. 10. 10. 10. 10. 10. 10. 10. 10. 10. 10. 10. 10. 10. 10.
 60. 60. 60. 60. 62. 63. 60. 60. 60. 60. 60. 60. 60. 60. 60. 60. 60. 60. 60. 60. 60. 60. 60.
. 10. 10. 10. 10. 11. 11. 10. 10. 10. 10. 10. 10. 10. 10. 10. 10. 10. 10. 10. 10. 10. 10. 10.
 60. 60. 63. 69. 73. 76. 76. 71. 60. 60. 60. 60. 60. 60. 60. 60. 60. 60. 60. 60. 60. 60. 60.
. 10. 10. 12. 14. 15. 15. 14. 12. 10. 10. 10. 10. 10. 10. 10. 10. 10. 10. 10. 10. 10. 10. 10.
 60. 63. 68. 72. 78. 84. 87. 85. 75. 60. 60. 60. 60. 60. 60. 60. 60. 60. 60. 60. 60. 60. 60.
. 10. 11. 14. 18. 20. 21. 19. 16. 12. 10. 10. 10. 10. 10. 10. 10. 10. 10. 10. 10. 10. 10. 10.
20.106. 97. 93. 96.107.118.123.125.123.120.120.120.120.120.120.120.120.120.120.120.120.120.1
  5.  8. 11. 16. 21. 24. 22. 17. 12.  7.  5.  5.  5.  5.  5.  5.  5.  5.  5.  5.  5.  5.  5.
16.102. 91. 82. 82.119.127.130.129.126.120.120.120.120.120.120.120.120.120.120.120.120.120.1
  6.  8. 11. 16. 25. 16. 28. 20. 14.  8.  5.  5.  5.  5.  5.  5.  5.  5.  5.  5.  5.  5.  5.
16.103. 91. 76.119.119.145.139.134.128.120.120.120.120.120.120.120.120.120.120.120.120.120.120.1
  6.  7.  9. 11. 16. 16. 27. 19. 14.  8.  5.  5.  5.  5.  5.  5.  5.  5.  5.  5.  5.  5.  5.
18.108.101. 99.150.172.154.144.136.128.120.120.120.120.120.120.120.120.120.120.120.120.120.120.1
  5.  7.  7.  6.  5. 15. 18. 16. 12.  7.  5.  5.  5.  5.  5.  5.  5.  5.  5.  5.  5.  5.  5.
20.115.114.122.145.155.151.143.135.124.120.120.120.120.120.120.120.120.120.120.120.120.120.1
  5.  6.  6.  6.  7. 11. 13. 12.  9.  6.  5.  5.  5.  5.  5.  5.  5.  5.  5.  5.  5.  5.  5.
20.120.120.126.136.142.141.136.128.120.120.120.120.120.120.120.120.120.120.120.120.120.120.1
  5.  5.  6.  6.  7.  8.  9.  8.  6.  5.  5.  5.  5.  5.  5.  5.  5.  5.  5.  5.  5.  5.  5.
20.120.120.123.128.131.130.124.120.120.120.120.120.120.120.120.120.120.120.120.120.120.120.1
  5.  5.  5.  6.  6.  7.  6.  6.  5.  5.  5.  5.  5.  5.  5.  5.  5.  5.  5.  5.  5.  5.  5.
20.120.120.120.120.120.120.120.120.120.120.120.120.120.120.120.120.120.120.120.120.120.120.1
  5.  5.  5.  5.  5.  5.  5.  5.  5.  5.  5.  5.  5.  5.  5.  5.  5.  5.  5.  5.  5.  5.  5.
20.120.120.120.120.120.120.120.120.120.120.120.120.120.120.120.120.120.120.120.120.120.120.1
  5.  5.  5.  5.  5.  5.  5.  5.  5.  5.  5.  5.  5.  5.  5.  5.  5.  5.  5.  5.  5.  5.  5.
20.120.120.120.120.120.120.120.120.120.120.120.120.120.120.120.120.120.120.120.120.120.120.1
  5.  5.  5.  5.  5.  5.  5.  5.  5.  5.  5.  5.  5.  5.  5.  5.  5.  5.  5.  5.  5.  5.  5.
```

FIGURE 5-12 Wind Speed (m sec^{-1}) and Direction (° from) for Hour 27 of the Tropical Storm Case

11.	11.	11.	11.	11.	11.	11.	11.	11.	11.	11.	11.
12.	12.	12.	11.	11.	11.	11.	11.	11.	11.	11.	11.
12.	12.	12.	12.	11.	11.	11.	11.	11.	11.	11.	10.
13.	12.	12.	11.	11.	11.	11.	11.	11.	11.	10.	11.
13.	13.	12.	11.	11.	11.	11.	10.	11.	10.	10.	10.
13.	12.	(12.)[1]	11.	11.	11.	10.	10.	10.	10.	10.	10.
12.	12.	11.	11.	10.	10.	101	10.	10.	10.	9.	9.
12.	11.	10.	11.	10.	9.	9.	9.	(9.)[2]	8.	8.	8.
10.	10.	9.	9.	8.	7.	7.	7.	7.	7.	6.	6.
8.	9.	9.	8.	8.	7.	7.	7.	6.	6.	6.	6.
7.	8.	8.	7.	7.	(7.)[3]	7.	6.	6.	6.	6.	6.
6.	7.	7.	6.	6.	6.	6.	6.	6.	6.	6.	6.
6.	6.	6.	5.	6.	6.	6.	6.	5.	5.	5.	6.
5.	5.	5.	6.	5.	5.	5.	5.	5.	5.	5.	5.
4.	4.	5.	5.	5.	5.	5.	5.	5.	5.	5.	5.
4.	4.	5.	4.	5.	5.	5.	5.	5.	4.	5.	5.

FIGURE 5-13

$H_{1/10}$ Wave Height Field (ft) at
Hour 33 of Tropical Storm Case

90	90	90	90	112	112	112	112	112	112	112	112
90	90	90	112	112	112	112	112	112	112	112	112
112	112	112	112	112	122	112	112	112	112	135	135
112	112	112	112	112	112	112	135	135	135	135	135
112	112	112	112	135	135	135	135	135	135	135	135
112	112	135 (1)	135	135	135	135	135	135	135	135	135
135	135	135	135	135	135	135	135	135	135	135	135
135	135	135	157	157	135	157	157	157 (2)	157	157	157
135	135	157	157	157	157	157	157	157	157	157	157
135	157	157	157	157	157	157	157	157	157	157	157
180	180	180	180	180	180 (3)	180	157	157	157	157	157
180	180	180	180	180	180	180	180	180	180	180	157
180	180	180	180	180	180	180	180	180	180	180	180
202	202	202	202	180	180	180	180	180	180	180	180
112	112	112	202	202	180	212	180	180	180	180	180
112	112	112	112	112	112	202	202	112	112	180	180

FIGURE 5-14

Direction of Maximum Energy (° from) at
Hour 33 of Tropical Storm Case

8.	10.	10.	10.	10.	10.	10.	10.	10.	8.	8.	8.
10.	10.	10.	10.	10.	10.	10.	10.	10.	8.	8.	8.
10.	10.	10.	10.	10.	10.	10.	10.	10.	8.	8.	8.
10.	10.	10.	10.	10.	10.	9.	8.	8.	8.	8.	8.
10.	10.	10.	10.	10.	9.	9.	8.	8.	8.	8.	8.
10.	10.	10.	10.	10.	10.	8.	8.	8.	8.	8.	8.
10.	10.	10.	10.	10.	10.	10.	10.	8.	8.	8.	8.
10.	10.	12.	10.	10.	10.	10.	10.	10.	10.	9.	8.
10.	10.	10.	10.	10.	11.	11.	11.	11.	11.	9.	11.
9.	9.	10.	10.	10.	10.	10.	10.	10.	9.	9.	9.
8.	9.	9.	8.	8.	8.	9.	10.	10.	10.	9.	9.
8.	8.	8.	8.	8.	8.	9.	8.	8.	7.	7.	9.
7.	7.	7.	7.	7.	7.	7.	7.	7.	7.	7.	7.
6.	7.	7.	7.	7.	7.	7.	7.	7.	7.	7.	7.
4.	4.	4.	6.	6.	7.	4.	7.	7.	7.	7.	7.
4.	4.	4.	4.	4.	4.	4.	4.	4.	4.	4.	4.

FIGURE 5-15

Period of Maximum Energy (sec) at

Hour 33 of Tropical Storm Case

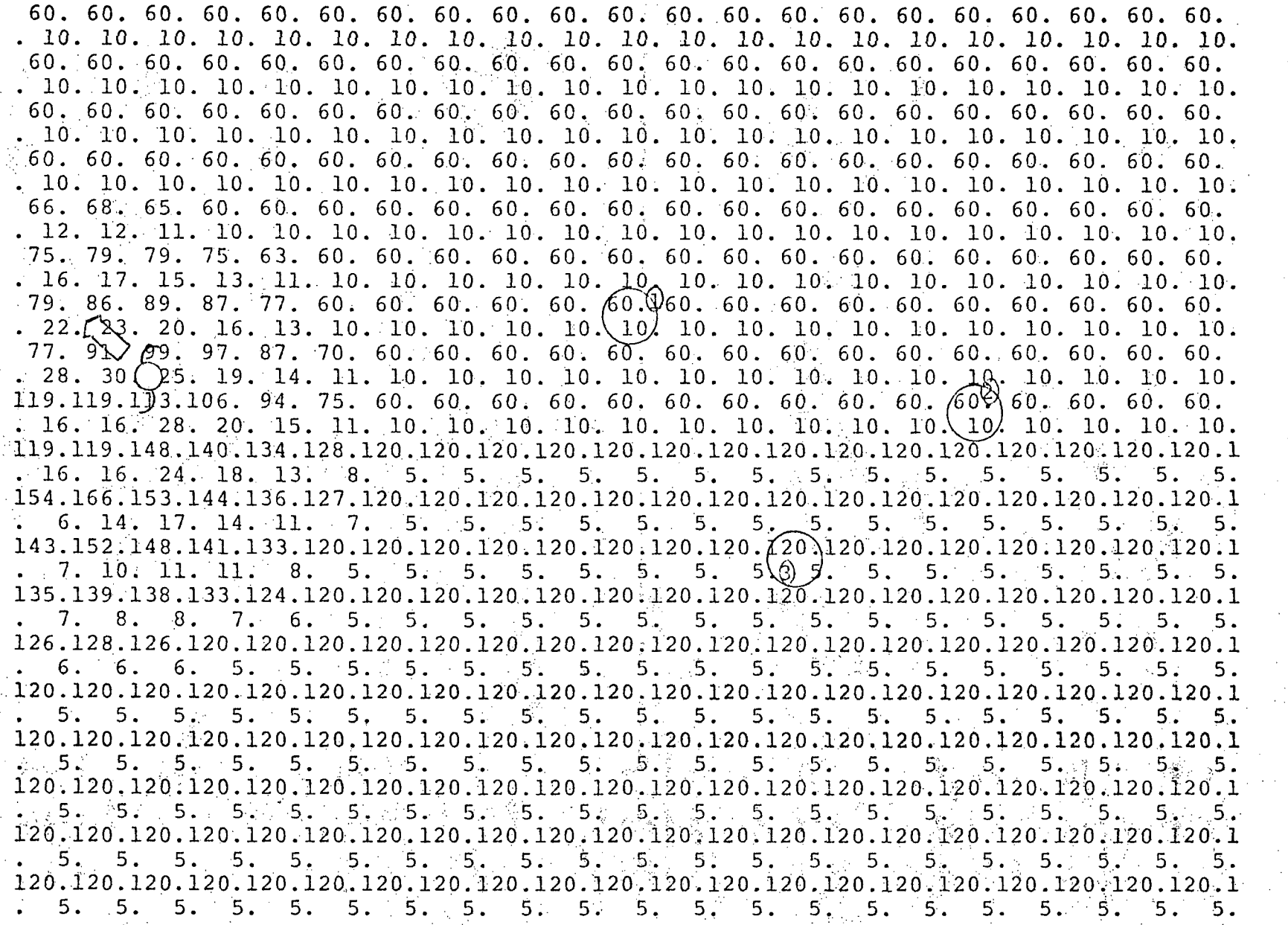

FIGURE 5-16 Wind Speed (m sec^{-1}) and Direction (^{o} from) for Hour 33 of the Tropical Storm Case

however, is still quite extensively altered due to the passage of the storm. The periods of maximum energy have begun to revert to their original state with the longer periods occuring at the convergence zone.

Figures 5-17 thorough 5-19 depict the directional and periodic energy spectra for the three special points as functions of time. Despite their locations which account for initial energy differences, all three show the same overall patterns in the energy versus direction spectra. A shift in direction to the southeast is evident in all three and, except for the northern-most point, all experience a decrease in energy. In the case of period of maximum energy, Point 1 experiences an increase to longer periods, Points 2 and 3 a decrease. Only Point 1 experiences an increase in energy in either spectra.

5.2 The Effects of Oceanic Fronts on Wave Refraction.

The theory presented in this section is based upon Johnson's (1947) methods for calculating the effects at oceanic velocity fronts on the refraction of waves. The basic equations are presented in a following section (App. C) in which the full computer program is described. This section will deal only with the results of Johnson's theoretical study and the numerical results based upon his work.

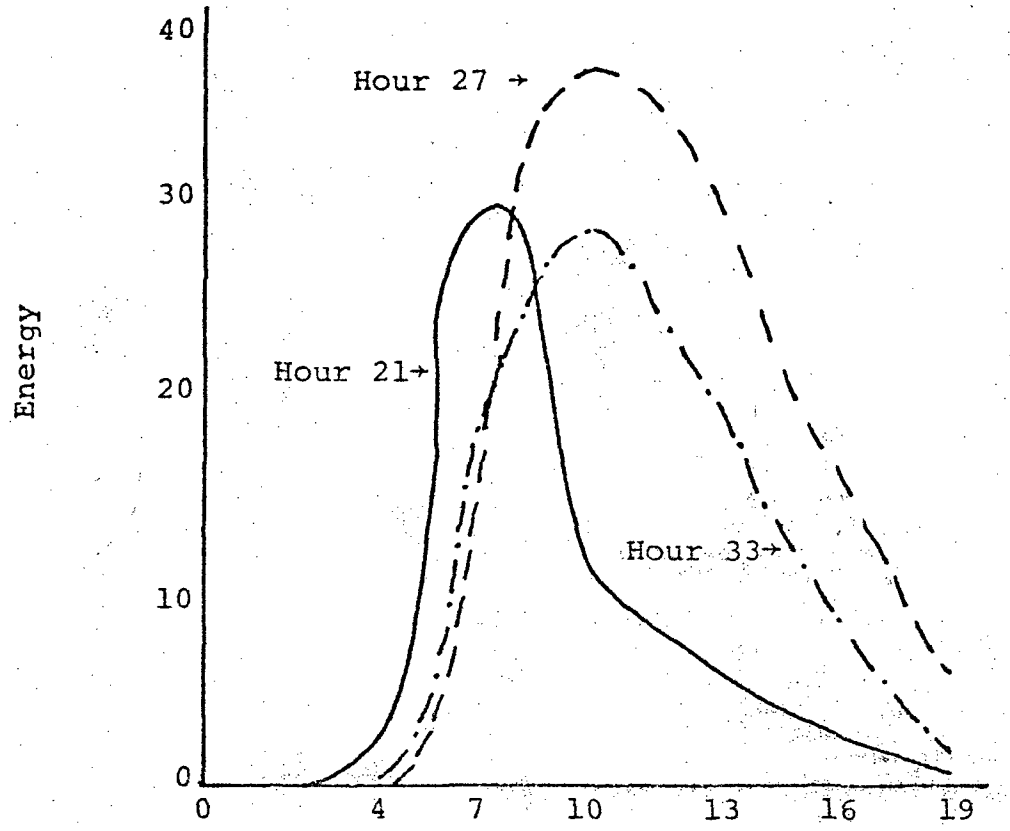

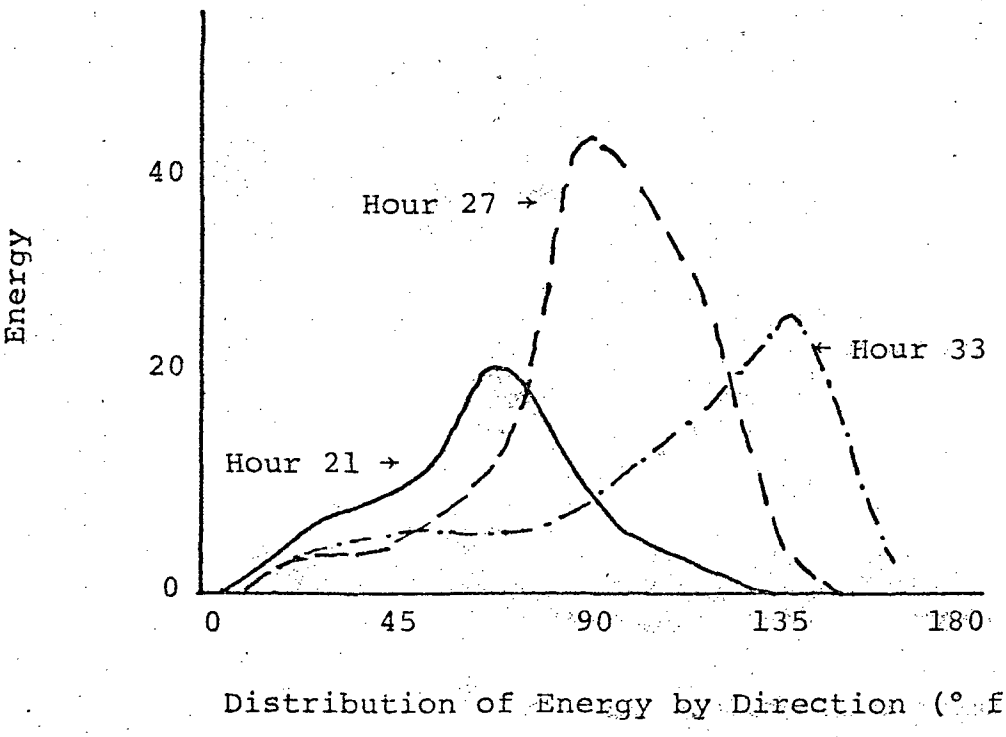

FIGURE 5-17: DISTRIBUTION OF SPECTRAL ENERGY BY TIME FOR SPECIAL POINT 1

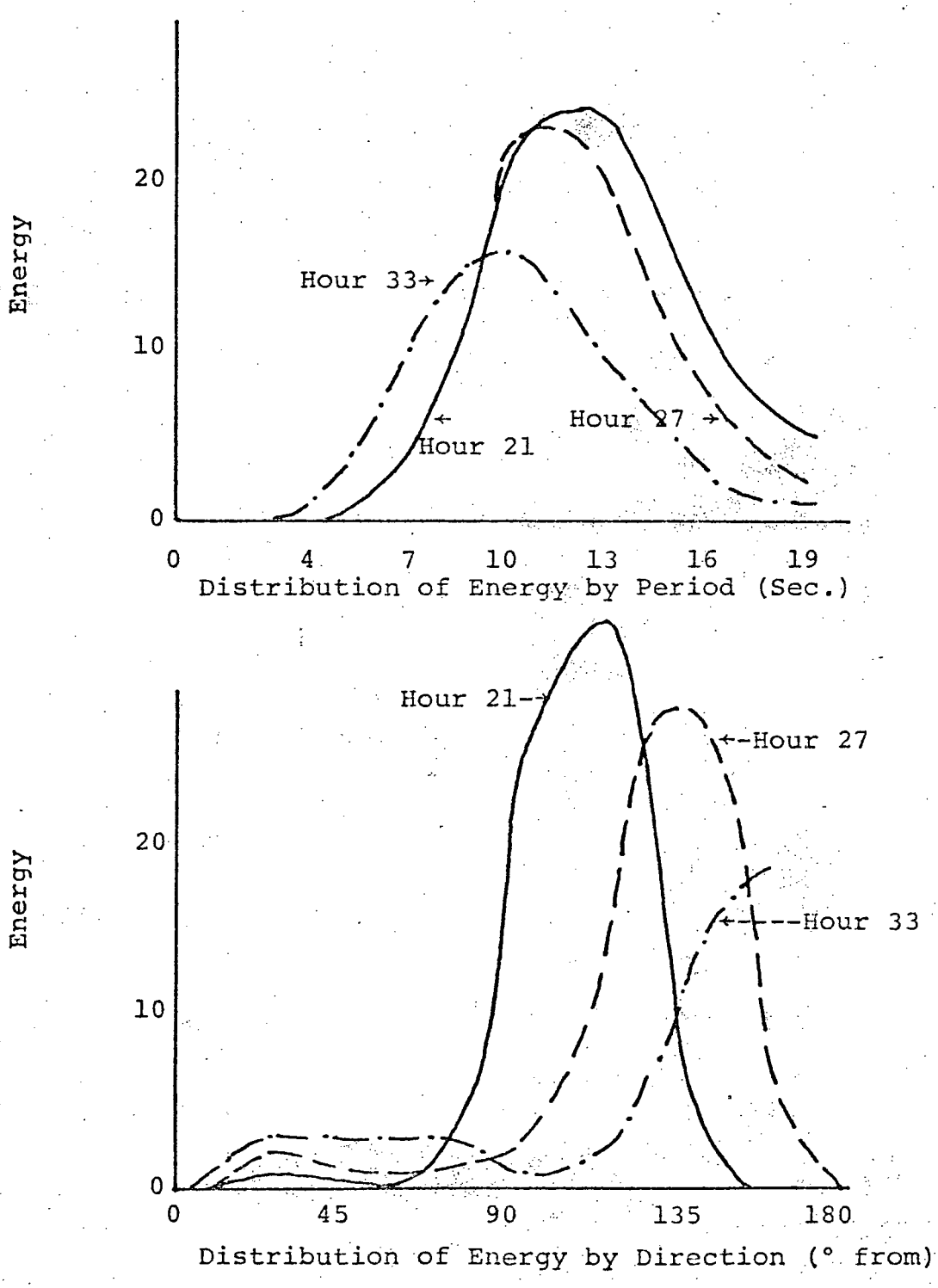

FIGURE 5-18: DISTRIBUTION OF SPECTRAL ENERGY WITH TIME FOR SPECIAL POINT 2.

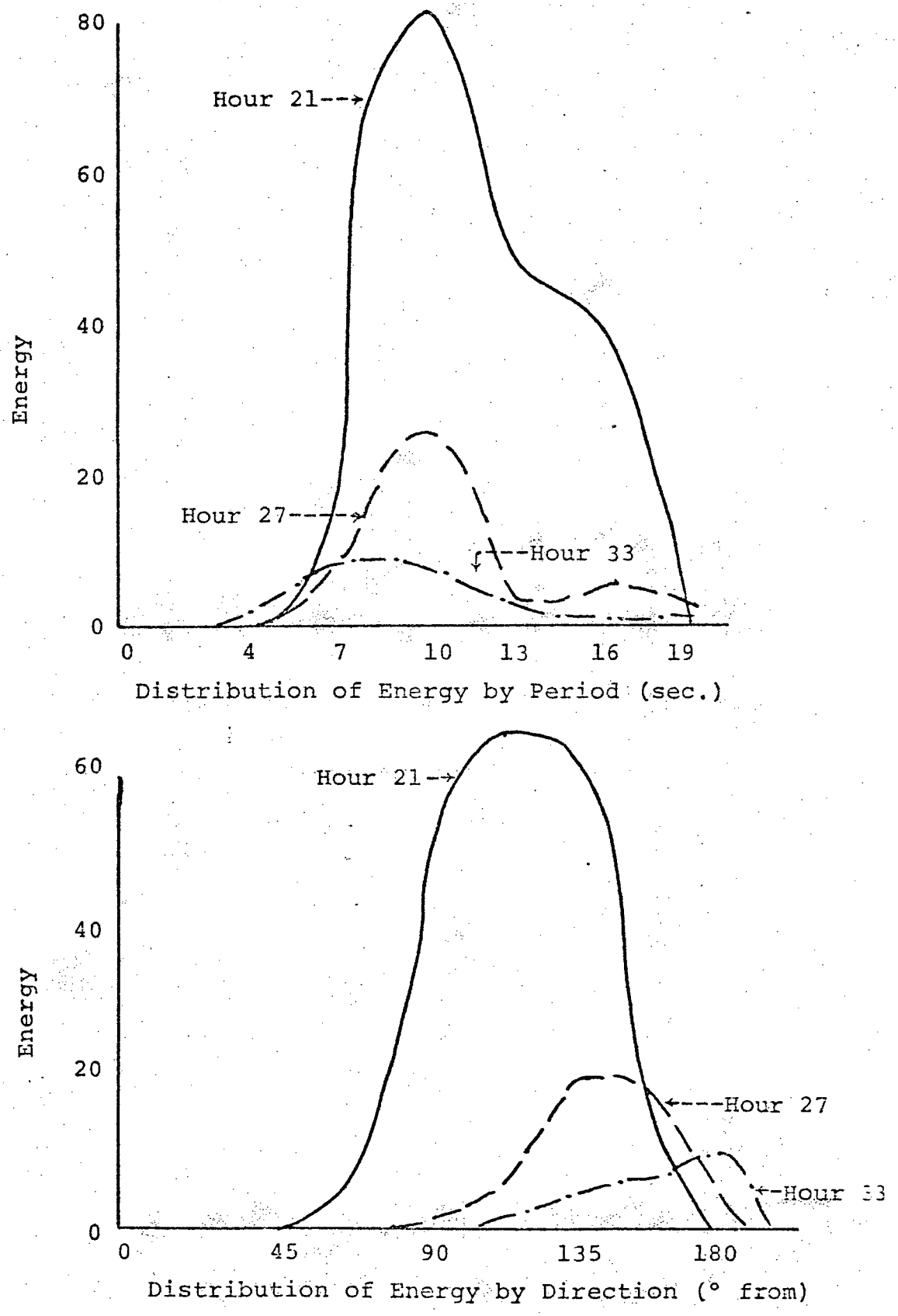

FIGURE 5-19: DISTRIBUTION OF SPECTRAL ENERGY WITH TIME AT SPECIAL POINT 3.

The core of Johnson's results are summarized by Figures 5-20 through 5-22. Given m, the ratio of current velocity over the wave ray speed, Figure 5-20 shows that the incident angle, α, is transformed into angle β dependent upon this ratio. The largest alterations occuring in cases where the two are of equal magnitude, with the current either opposing (negative on) or conciding (positive on) with the ray direction.

Figure 5-21 shows the effect of the currents upon the steepness of the waves. Here the largest effects are found at m=-1. This value is relatively uncommon in deep water cases but can easily be encountered in near-coastal areas such as river outlets. As can be seen from Figure 5-22, the maximum effect upon the wavelength occurred at m=+1, m=-1 resulting in a shortening of the wavelength. From the above results, it is clear that wave height is increased with negative values of m and median values of α.

Two examples of the results of the numerical model are shown in Figures 5-23 and 5-24. Table 5-1 summarizes the results of all computer runs. From this it can be seen that the maximum height change occurred at α=30, m=-.064. The maximum directional shift was -9° at α=60, m=-.064. The maximum steepness occurred at α=45, m=-.064. It can then be concluded that the most severe alterations at wave fronts occur when large opposing currents are encountered.

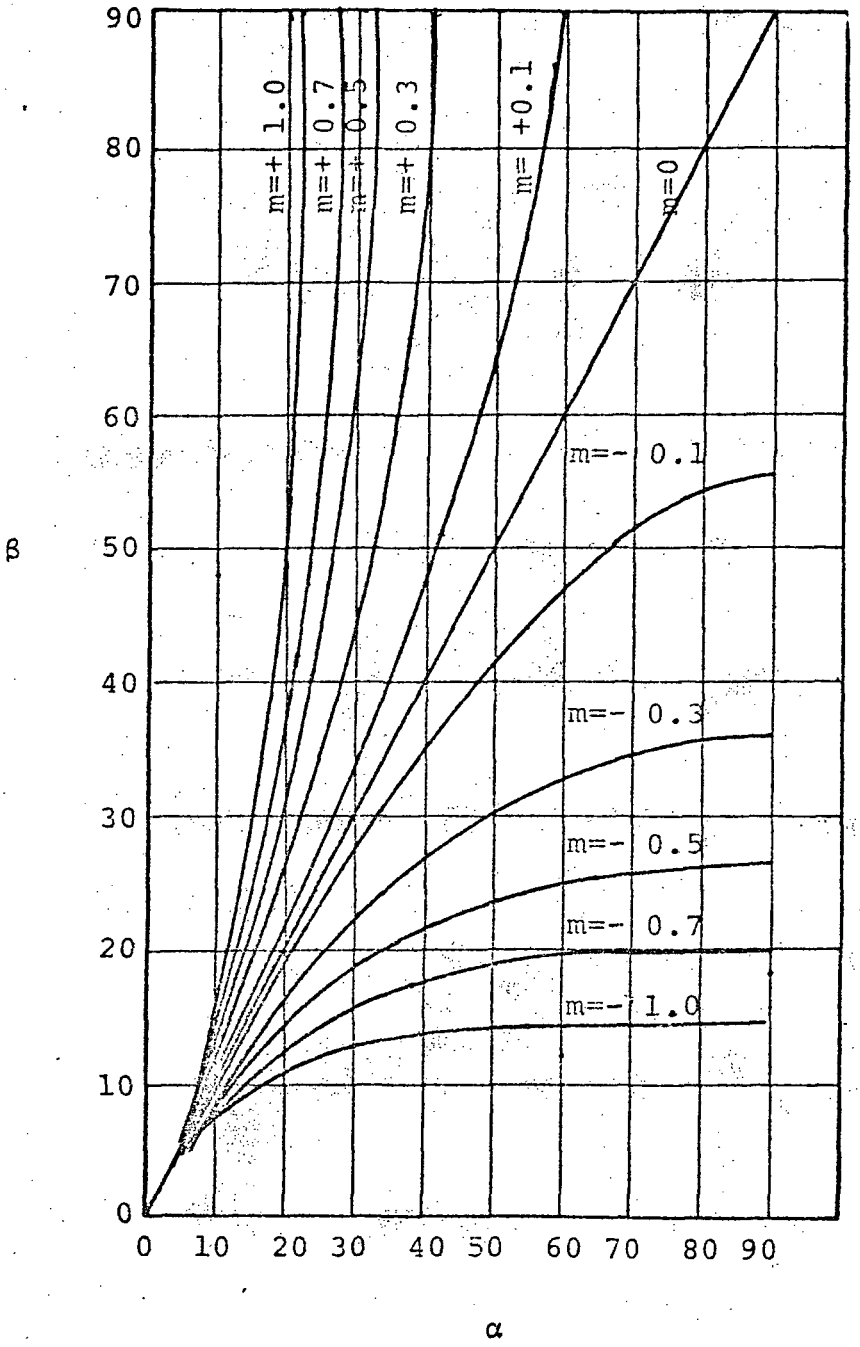

FIGURE 5-20: THE EFFECT OF WAVE DIRECTION ON THE REFRACTION OF WAVES BY CURRENTS

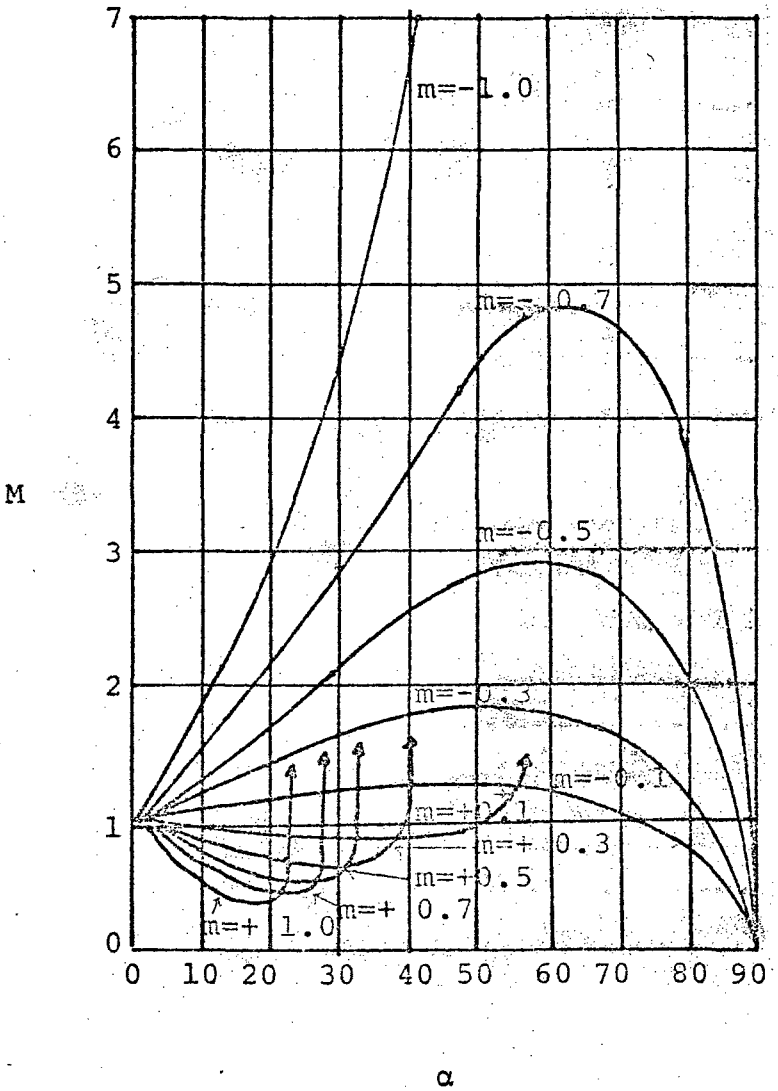

FIGURE 5-21: STEEPNESS FACTOR IN REFRACTION OF WAVES BY CURRENTS

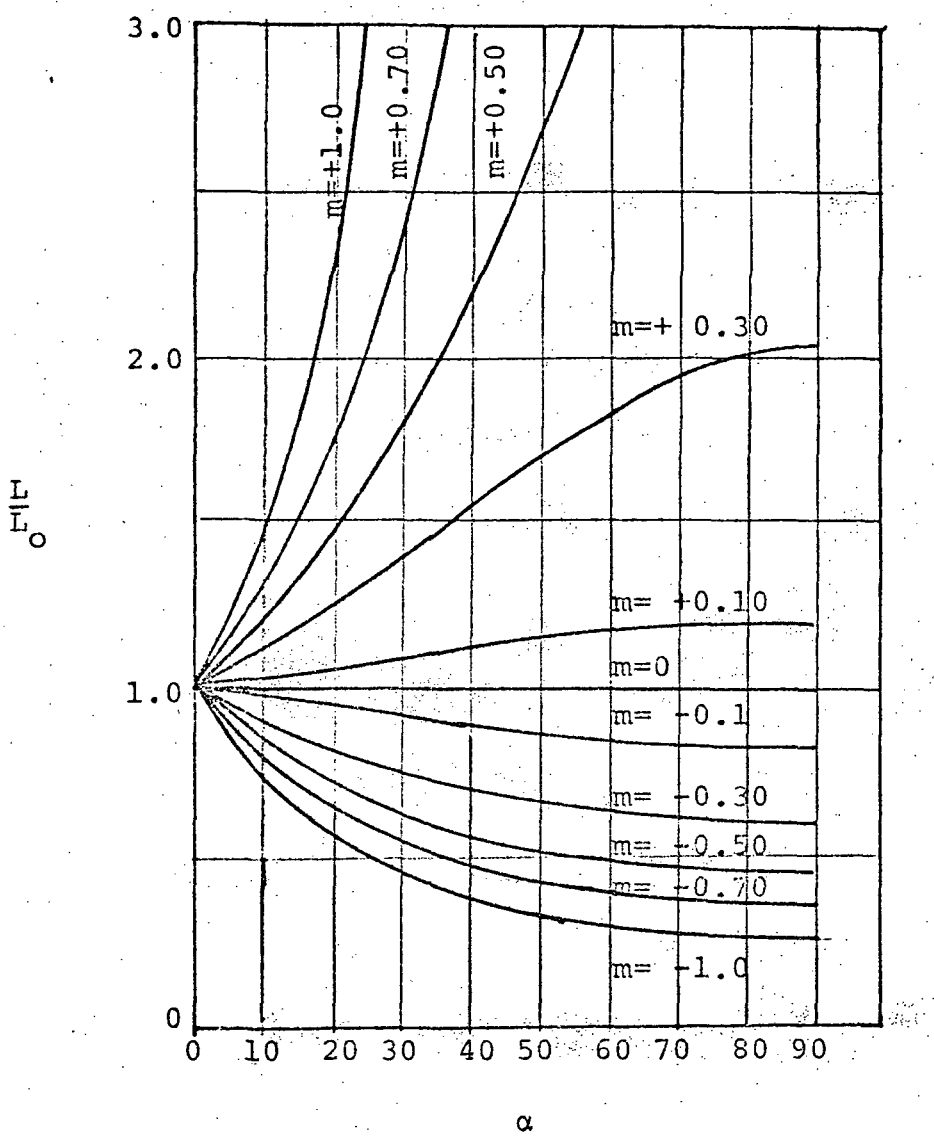

FIGURE 5-22: WAVE LENGTH CHANGES DUE TO REFRACTION OF WAVES BY CURRENTS

TEST CASE 1
SET NO. 1. PERIOD = 10.00 SECS.. RAY NO. 2. TIME STEP = 7.0119SECS./

POINT	X	Y	ANGLE	DEPTH	MAX DIF	FIT	LENGTH	SPEED	HEIGHT	KR	KS	NEWH
1	15.0	3.0	135.0				512.04	51.20	1.00			
2	14.9	3.1	135.0	1000.00	.00	.00	512.04	51.20	1.00	1.0000	1.0000	.00
3	14.7	3.3	135.0	1000.00	.00	.00	512.04	51.20	1.00	1.0000	1.0000	.00
4	14.6	3.4	135.0	1000.00	.00	.00	512.04	51.20	1.00	1.0000	1.0000	.00
5	14.4	3.6	135.0	1000.00	.00	.00	512.04	51.20	1.00	1.0000	1.0000	.00
6	14.3	3.7	135.0	1000.00	.00	.00	512.04	51.20	1.00	1.0000	1.0000	.00
7	14.2	3.8	135.0	1000.00	.00	.00	512.04	51.20	1.00	1.0000	1.0000	.00
8	14.0	4.0	135.0	1000.00	.00	.00	512.04	51.20	1.00	1.0000	1.0000	.00
9	13.9	4.1	135.0	1000.00	.00	.00	512.04	51.20	1.00	1.0000	1.0000	.00
10	13.7	4.3	135.0	1000.00	.00	.00	512.04	51.20	1.00	1.0000	1.0000	.00
11	13.6	4.4	135.0	1000.00	.00	.00	512.04	51.20	1.00	1.0000	1.0000	.00
12	13.4	4.6	135.0	1000.00	.00	.00	512.04	51.20	1.00	1.0000	1.0000	.00
13	13.3	4.7	135.0	1000.00	.00	.00	512.04	51.20	1.00	1.0000	1.0000	.00
14	13.2	4.8	135.0	1000.00	.00	.00	512.04	51.20	1.00	1.0000	1.0000	.00
15	13.0	5.0	135.0	1000.00	.00	.00	512.04	51.20	1.00	1.0000	1.0000	.00
16	12.9	5.1	135.0	1000.00	.00	.00	512.04	51.20	1.00	1.0000	1.0000	.00
17	12.7	5.3	135.0	1000.00	.00	.00	512.04	51.20	1.00	1.0000	1.0000	.00
18	12.6	5.4	135.0	1000.00	.00	.00	512.04	51.20	1.00	1.0000	1.0000	.00
19	12.5	5.5	135.0	1000.00	.00	.00	512.04	51.20	1.00	1.0000	1.0000	.00
20	12.3	5.7	135.0	1000.00	.00	.00	512.04	51.20	1.00	1.0000	1.0000	.00
21	12.2	5.8	135.0	1000.00	.00	.00	512.04	51.20	1.00	1.0000	1.0000	.00
22	12.0	6.0	135.0	1000.00	.00	.00	512.04	51.20	1.00	1.0000	1.0000	.00
23	11.9	6.1	135.0	1000.00	.00	.00	512.04	51.20	1.00	1.0000	1.0000	.00
24	11.7	6.3	135.0	1000.00	.00	.00	512.04	51.20	1.00	1.0000	1.0000	.00
25	11.6	6.4	135.0	1000.00	.00	.00	512.04	51.20	1.00	1.0000	1.0000	.00
26	11.5	6.6	135.0	1000.00	.00	.00	512.04	51.20	1.00	1.0000	1.0000	.00
27	11.3	6.7	135.0	1000.00	.00	.00	512.04	51.20	1.00	1.0000	1.0000	.00
28	11.2	6.8	135.0	1000.00	.00	.00	512.04	51.20	1.00	1.0000	1.0000	.00
29	11.0	7.0	135.0	1000.00	.00	.00	512.04	51.20	1.00	1.0000	1.0000	.00
30	10.9	7.1	135.0	1000.00	.00	.00	512.04	51.20	1.00	1.0000	1.0000	.00
31	10.8	7.2	135.0	1000.00	.00	.00	512.04	51.20	1.00	1.0000	1.0000	.00
32	10.6	7.4	135.0	1000.00	.00	.00	512.04	51.20	1.00	1.0000	1.0000	.00
33	10.5	7.5	135.0	1000.00	.00	.00	512.04	51.20	1.00	1.0000	1.0000	.00
34	10.3	7.7	135.0	1000.00	.00	.00	512.04	51.20	1.00	1.0000	1.0000	.00
35	10.2	7.8	135.0	1000.00	.00	.00	512.04	51.20	1.00	1.0000	1.0000	.00
36	10.0	8.0	135.0	1000.00	.00	.00	512.04	51.20	1.00	1.0000	1.0000	.00
37	9.9	8.1	135.0	1000.00	.00	.00	512.04	51.20	1.00	1.0000	1.0000	.00
38	9.8	8.2	135.0	1000.00	.00	.00	512.04	51.20	1.00	1.0000	1.0000	.00
39	9.6	8.4	135.0	1000.00	.00	.00	512.04	51.20	1.00	1.0000	1.0000	.00
40	9.5	8.5	135.0	1000.00	.00	.00	512.04	51.20	1.00	1.0000	1.0000	.00
41	9.3	8.7	135.0	1000.00	.00	.00	512.04	51.20	1.00	1.0000	1.0000	.00
42	9.2	8.8	135.0	1000.00	.00	.00	512.04	51.20	1.00	1.0000	1.0000	.00
43	9.1	8.9	135.0	1000.00	.00	.00	512.04	51.20	1.00	1.0000	1.0000	.00
44	8.9	9.1	135.0	1000.00	.00	.00	512.04	51.20	1.00	1.0000	1.0000	.00
45	8.8	9.2	135.0	1000.00	.00	.00	512.04	51.20	1.00	1.0000	1.0000	.00
46	8.6	9.4	135.0	1000.00	.00	.00	512.04	51.20	1.00	1.0000	1.0000	.00
47	8.5	9.5	135.0	1000.00	.00	.00	512.04	51.20	1.00	1.0000	1.0000	.00
48	8.3	9.7	135.0	1000.00	.00	.00	512.04	51.20	1.00	1.0000	1.0000	.00
49	8.2	9.8	135.0	1000.00	.00	.00	512.04	51.20	1.00	1.0000	1.0000	.00
50	8.1	9.9	135.0	1000.00	.00	.00	512.04	51.20	1.00	1.0000	1.0000	.00
	.75540	2.3[illegible]	.70711									
	.75540	28.47970	.67613									
	.75540	.74200	.67613									
	2.31333	.70711	.70711									
	2.31333	-.67613	.73678									
51	7.[illegible]	10.1	134.3	1000.00	.00	.00	489.61	51.23	1.01	1.0000	1.0000	.00
52	7.4	10.2	134.3	1000.00	.00	.00	489.61	51.23	1.01	1.0000	1.0000	.00
53	7.2	10.4	134.3	1000.00	.00	.00	489.61	51.23	1.01	1.0000	1.0000	.00
54	7.1	10.5	134.3	1000.00	.00	.00	489.61	51.23	1.01	1.0000	1.0000	.00
55	7.0	10.7	134.3	1000.00	.00	.00	489.61	51.23	1.01	1.0000	1.0000	.00

FIGURE 5-23: EXAMPLE OF COMPUTER OUTPUT, α=45°, C=-50 cm/sec

TEST CASE 1
SET NO. 1, PERIOD = 10.00 SECS., RAY NO. 3, TIME STEP = 7.8119SECS./

POINT	X	Y	ANGLE	DEPTH	MAX DIF	FIT	LENGTH	SPEED	HEIGHT	KR	KS	NEWH
1	15.0	3.0	135.0				512.04	51.20	1.00			
2	14.9	3.1	135.0	1000.00	.00	.00	512.04	51.20	1.00	1.0000	1.0000	.00
3	14.7	3.3	135.0	1000.00	.00	.00	512.04	51.20	1.00	1.0000	1.0000	.00
4	14.6	3.4	135.0	1000.00	.00	.00	512.04	51.20	1.00	1.0000	1.0000	.00
5	14.4	3.6	135.0	1000.00	.00	.00	512.04	51.20	1.00	1.0000	1.0000	.00
6	14.3	3.7	135.0	1000.00	.00	.00	512.04	51.20	1.00	1.0000	1.0000	.00
7	14.2	3.8	135.0	1000.00	.00	.00	512.04	51.20	1.00	1.0000	1.0000	.00
8	14.0	4.0	135.0	1000.00	.00	.00	512.04	51.20	1.00	1.0000	1.0000	.00
9	13.9	4.1	135.0	1000.00	.00	.00	512.04	51.20	1.00	1.0000	1.0000	.00
10	13.7	4.3	135.0	1000.00	.00	.00	512.04	51.20	1.00	1.0000	1.0000	.00
11	13.6	4.4	135.0	1000.00	.00	.00	512.04	51.20	1.00	1.0000	1.0000	.00
12	13.4	4.6	135.0	1000.00	.00	.00	512.04	51.20	1.00	1.0000	1.0000	.00
13	13.3	4.7	135.0	1000.00	.00	.00	512.04	51.20	1.00	1.0000	1.0000	.00
14	13.2	4.8	135.0	1000.00	.00	.00	512.04	51.20	1.00	1.0000	1.0000	.00
15	13.0	5.0	135.0	1000.00	.00	.00	512.04	51.20	1.00	1.0000	1.0000	.00
16	12.9	5.1	135.0	1000.00	.00	.00	512.04	51.20	1.00	1.0000	1.0000	.00
17	12.7	5.3	135.0	1000.00	.00	.00	512.04	51.20	1.00	1.0000	1.0000	.00
18	12.6	5.4	135.0	1000.00	.00	.00	512.04	51.20	1.00	1.0000	1.0000	.00
19	12.5	5.5	135.0	1000.00	.00	.00	512.04	51.20	1.00	1.0000	1.0000	.00
20	12.3	5.7	135.0	1000.00	.00	.00	512.04	51.20	1.00	1.0000	1.0000	.00
21	12.2	5.8	135.0	1000.00	.00	.00	512.04	51.20	1.00	1.0000	1.0000	.00
22	12.0	6.0	135.0	1000.00	.00	.00	512.04	51.20	1.00	1.0000	1.0000	.00
23	11.9	6.1	135.0	1000.00	.00	.00	512.04	51.20	1.00	1.0000	1.0000	.00
24	11.7	6.3	135.0	1000.00	.00	.00	512.04	51.20	1.00	1.0000	1.0000	.00
25	11.6	6.4	135.0	1000.00	.00	.00	512.04	51.20	1.00	1.0000	1.0000	.00
26	11.5	6.5	135.0	1000.00	.00	.00	512.04	51.20	1.00	1.0000	1.0000	.00
27	11.3	6.7	135.0	1000.00	.00	.00	512.04	51.20	1.00	1.0000	1.0000	.00
28	11.2	6.8	135.0	1000.00	.00	.00	512.04	51.20	1.00	1.0000	1.0000	.00
29	11.0	7.0	135.0	1000.00	.00	.00	512.04	51.20	1.00	1.0000	1.0000	.00
30	10.9	7.1	135.0	1000.00	.00	.00	512.04	51.20	1.00	1.0000	1.0000	.00
31	10.8	7.2	135.0	1000.00	.00	.00	512.04	51.20	1.00	1.0000	1.0000	.00
32	10.6	7.4	135.0	1000.00	.00	.00	512.04	51.20	1.00	1.0000	1.0000	.00
33	10.5	7.5	135.0	1000.00	.00	.00	512.04	51.20	1.00	1.0000	1.0000	.00
34	10.3	7.7	135.0	1000.00	.00	.00	512.04	51.20	1.00	1.0000	1.0000	.00
35	10.2	7.8	135.0	1000.00	.00	.00	512.04	51.20	1.00	1.0000	1.0000	.00
36	10.0	8.0	135.0	1000.00	.00	.00	512.04	51.20	1.00	1.0000	1.0000	.00
37	9.9	8.1	135.0	1000.00	.00	.00	512.04	51.20	1.00	1.0000	1.0000	.00
38	9.8	8.2	135.0	1000.00	.00	.00	512.04	51.20	1.00	1.0000	1.0000	.00
39	9.6	8.4	135.0	1000.00	.00	.00	512.04	51.20	1.00	1.0000	1.0000	.00
40	9.5	8.5	135.0	1000.00	.00	.00	512.04	51.20	1.00	1.0000	1.0000	.00
41	9.3	8.7	135.0	1000.00	.00	.00	512.04	51.20	1.00	1.0000	1.0000	.00
42	9.2	8.8	135.0	1000.00	.00	.00	512.04	51.20	1.00	1.0000	1.0000	.00
43	9.1	8.9	135.0	1000.00	.00	.00	512.04	51.20	1.00	1.0000	1.0000	.00
44	8.9	9.1	135.0	1000.00	.00	.00	512.04	51.20	1.00	1.0000	1.0000	.00
45	8.8	9.2	135.0	1000.00	.00	.00	512.04	51.20	1.00	1.0000	1.0000	.00
46	8.6	9.4	135.0	1000.00	.00	.00	512.04	51.20	1.00	1.0000	1.0000	.00
47	8.5	9.5	135.0	1000.00	.00	.00	512.04	51.20	1.00	1.0000	1.0000	.00
48	8.3	9.7	135.0	1000.00	.00	.00	512.04	51.20	1.00	1.0000	1.0000	.00
49	8.2	9.8	135.0	1000.00	.00	.00	512.04	51.20	1.00	1.0000	1.0000	.00
50	8.1	9.9	135.0	1000.00	.00	.00	512.04	51.20	1.00	1.0000	1.0000	.00
	.78540	2.35619	.70711									
	.78540	31.09158	.74026									
	.78540	.83345	.74026									
	2.40425	.70711	.70711									
	2.40425	-.74026	.67232									
51	7.9	10.1	137.8	1000.00	.00	.00	536.05	51.23	.99	1.0000	1.0000	.00
52	7.8	10.2	137.8	1000.00	.00	.00	536.05	51.23	.99	1.0000	1.0000	.00
53	7.6	10.3	137.8	1000.00	.00	.00	536.05	51.23	.99	1.0000	1.0000	.00
54	7.5	10.5	137.8	1000.00	.00	.00	536.05	51.23	.99	1.0000	1.0000	.00
55	7.3	10.6	137.8	1000.00	.00	.00	536.05	51.23	.99	1.0000	1.0000	.00

FIGURE 5-24: EXAMPLE OF COMPUTER OUTPUT, α=45°, C=-50 cm/sec

TABLE 5-1: SUMMARY OF WAVE REFRACTION COMPUTER RUNS.

U (cm sec^{-1})	T (sec)	M	α	C_o ($ft\ sec^{-1}$)	H_o (ft)	L_o (ft)	$\frac{H}{L}_o$	β	C ($ft\ sec^{-1}$)	M (ft)	L (ft)	$\frac{M}{L}$
-20	10	-.012	30	51.2	1	512	.00195	29.6	51.21	1.01	505.5	.00199
-20	10	-.012	45	51.2	1	512	.00195	44.0	51.21	1.00	502.9	.00198
-20	10	-.012	60	51.2	1	512	.00195	57.9	51.21	.99	500.9	.00197
-50	10	-.032	30	51.2	1	512	.00195	29.0	51.23	1.02	496.0	.00205
-50	10	-.032	45	51.2	1	512	.00195	42.5	51.23	1.01	489.6	.00206
-50	10	-.032	60	51.2	1	512	.00195	55.1	51.23	.97	484.8	.00200
-100	10	-.064	30	51.2	1	512	.00195	28.0	51.31	1.04	480.7	.00216
-100	10	-.064	45	51.2	1	512	.00195	40.3	51.31	1.03	468.6	.00219
-100	10	-.064	60	51.2	1	512	.00195	51.0	51.31	.97	459.6	.00211
20	10	.012	20	51.2	1	512	.00195	20.2	51.21	.99	516.7	.00191
20	10	.012	30	51.2	1	512	.00195	30.4	51.21	.99	518.7	.00190
20	10	.012	45	51.2	1	512	.00195	46.1	51.21	1.00	521.5	.00191
50	10	.032	20	51.2	1	512	.00195	20.5	51.23	.99	523.5	.00189
50	10	.032	30	51.2	1	512	.00195	31.1	51.23	.98	528.8	.00185
50	10	.032	45	51.2	1	512	.00195	47.8	51.23	.99	536.0	.00184
100	10	.064	20	51.2	1	512	.00195	20.9	51.31	.97	535.2	.00181
100	10	.064	30	51.2	1	512	.00195	32.3	51.31	.96	546.5	.00175
100	10	.064	45	51.2	1	512	.00195	50.9	51.31	.99	561.8	.00176

6.0 THE EFFECTS OF OCEANIC FRONTS ON AIR/SEA EXCHANGE PROCESSES

It is known that the ocean-atmosphere heat and moisture exchange (feedback) is different on opposite sides of oceanic (and atmospheric) fronts (e.g., Laevastu and Hamilton, 1972). This relatively abrupt spatial exchange of heat and moisture (evaporation) might affect various observations and sensings by satellites of the near-surface atmosphere as well as the sea surface.

In order to study and demonstrate quantitatively the feedback of energy from the oceans to the atmosphere, the best exchange formulas, verified in various past research, were programmed into an integrated computer program (App. D of this report). In this program, sea surface temperature (T_w) and winds (V) were prescribed; all other parameters were computed. The results of a 24-hour "steady state" computation are shown in Figure 6-1.

The heat and moisture feedback from the ocean depends greatly on the removal of these quantities through turbulent transfer, which is a function of surface wind speed. Furthermore, the quantitative turbulent transfer is also dependent on the difference between the sea surface temperature and water vapor pressure and the corresponding properties of the near-surface air, ($T_w - T_a$ and $e_w - e_a$).

The properties of the surface air (temperature and water vapor pressure) adjust relatively rapidly to the corresponding properties of the sea surface, so that an "equilibrium difference" is established within five to six hours. The adjustment of the properties of surface air to the corresponding properties of the sea surface, and the resulting "equilibrium difference" is dependent on the rate of change of sea surface temperature under the trajectory of surface air $(V_r \frac{\partial T_w}{\partial r})$. Thus, the surface wind speed and its direction in relation to the sea surface isotherms determines the heat and moisture exchange (see Figure 6-1); the sea surface temperature gradient influences this exchange to a lesser degree.

Consequently, if the change of surface winds (both with respect to speed and direction) closely coincides with the oceanic front, a relatively sharp gradient of latent (Q_e) and sensible (Q_h) heat exchange occurs at the front (Figure 6-1). However, a comparable gradient of Q_e and Q_h can also be found at atmospheric fronts which do not coincide with oceanic fronts.

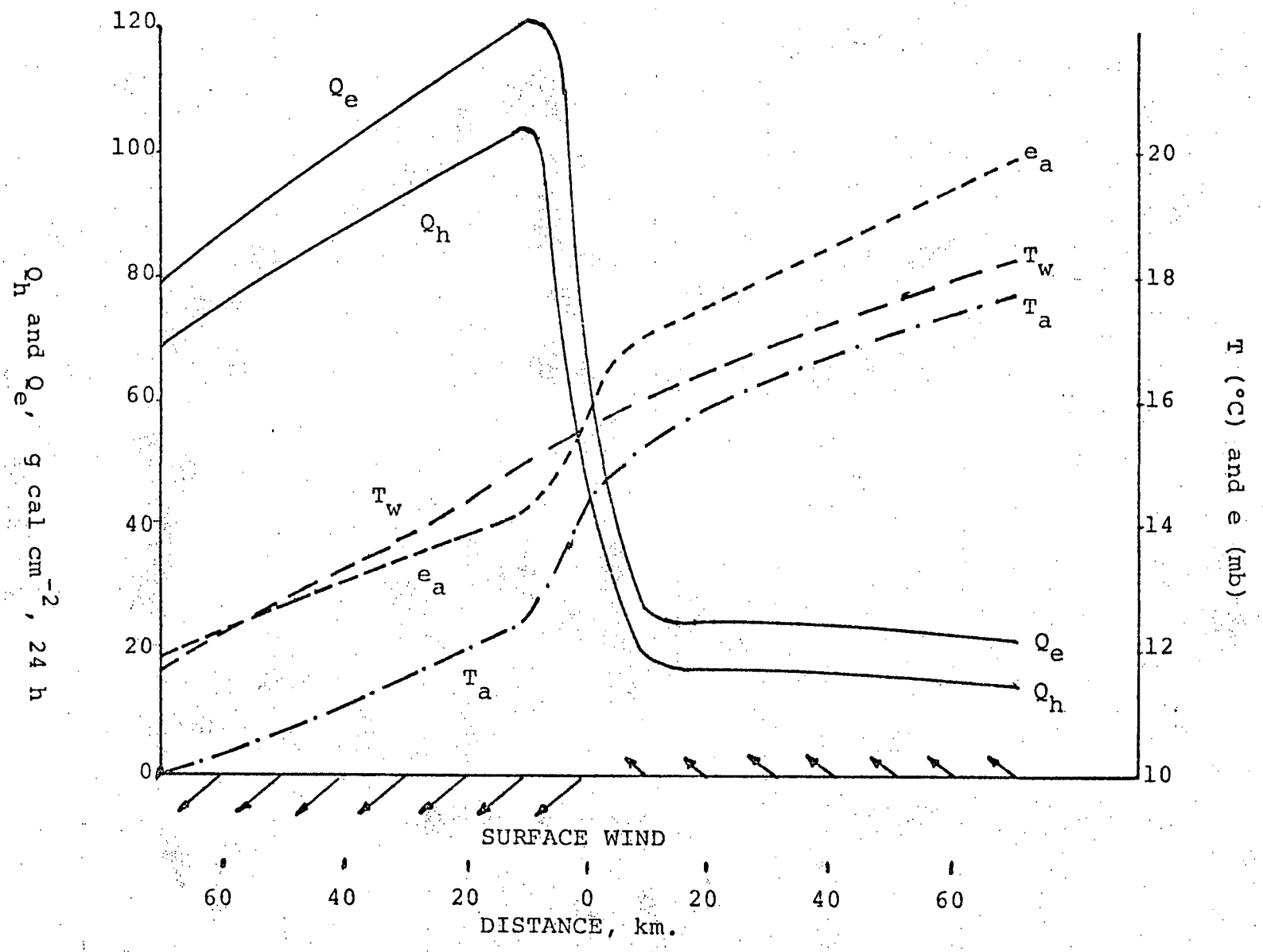

Figure 6-1: Sea surface temperature (T_w), surface winds, air temperature (T_a), water vapor pressure of the air (e_a), sensible (Q_h) and latent (Q_e) heat exchange near an oceanic front with different winds on different sides of the front.

7.0 SUMMARY

A two-layer Hydrodynamic Numerical (HN) model of the Hansen (primitive equation) type was used to show how ocean temperature structure and near-surface currents are influenced by surface wind stresses in a case where a convergent wind field coincided with an ocean front. The French Spectro-angular Wave Model was used to show differences in spectral wave energy across an ocean front being (a) maintained by surface wind convergence, and (b) disturbed by a moving cyclone. The studies of Johnson (1947) on wave refraction due to currents were programmed to demonstrate changes which can be expected in wave direction, height, and steepness due to intersection with a strong current stream (front). Finally, a computer program was developed to show changes in transport of latent and sensible heat due to air/sea temperature differences across an ocean front.

These studies indicate that surface properties vary sufficiently in the vicinity of major fronts to permit detection by satellite.

8.0 REFERENCES

COLTON, J.B., D.E. Smith and J.W. Fossi, 1975. Further Observations on a Thermal Front in the Sargasso Sea. Deep Sea Res. 22(6): 433-440.

GROEN, P. and R. Dorrestein, 1958. Zeegolven Kon. Nederl. Met. Inst., Opst. op. oceanogr. en marit. Met. Geb. 11:84 pp.

HELA, I. and T. Laevastu, 1962. Fisheries Hydrography. Fishery News (Books) Ltd., London, 137 pp.

JOHNSON, J.W., 1947. The Refraction of Surface Waves by Currents. Trans. Amer. Geophys. Union, Vol. 28, No. 6, Dec. 1947.

LAFOND, E.C., 1960. Oceanography and Food. Naval Res. Rev. Nov. 61, 9-13.

LAFOND, E.C. and K.G. LaFond, 1971. Thermal Structure through the California Front. Nav. Unders. Center, Techn. Paper 224.

LAEVASTU, T., 1963. Surface Water Types of the North Sea and their Characteristics. Am. Geogr. Soc., Ser. Atlas of the Marine Environment, Folio 4.

LAEVASTU, T. and G.D. Hamilton, 1972. The Effects of Oceanic Fronts on Properties of the Atmospheric Boundary Layers. Env. Pred. Res. Fac. Techn. Paper 2-72.

LAEVASTU, T. and E.C. LaFond, 1970. Oceanic Fronts and their Seasonal Positions on the Surface. Nav. Unders. Center Techn. Paper 204, 16 pp.

LAEVASTU, T., P.M. Wolff, and E.C. LaFond, 1970. The Effects of Oceanic Fronts on Sound Propagation (U) Nav. Unders. Center Techn. Paper (Confidential).

LEE, A.J., 1952. The Influence of Hydrography on the Bear Island Cod Fishery. Rapp. Proc. - Verb. ICES. 131, 74-102.

LONGUET-HIGGINS, M.S., and R.W. Stewart, 1961. The Changes in Amplitude of Short Gravity Waves on Steady Non-Uniform Currents. J. Fluid Mech. 10(4): 429-549.

LONGUET-HIGGINS, M.S., and R.W. Stewart, 1960. Changes in the Form of Short Gravity Waves on Long Waves and Tidal Currents. J. Fluid Mech. 8(4): 565-583.

NUNN, S.O., 1968. Study of the Oceanic Polar Front in the Denmark Strait. Naval Postgrad. School, Thesis.

ROSSOV, V.V. and A.G. Kislyakov, 1969. The Polar Front in the North Atlantic, According to Data Collected by R/V "Atlantida". ICES Symp. on Physical Variability in the North Atlantic, Paper 29.

SCHOTT, G. 1935. Geographie des Indischen und Stillen Ozeans. Boysen, Hamburg. 413 + Figures.

SHPAYKHER, A.O. and V.N. Moretskiy, 1964. The Polar Hydrological Front in the Greenland and Norwegian Seas. Okeanologia 4(2): 267-276.

STEFANSSON, U., 1969. Nearshore Fluctuations of the Frontal Zone Southeast of Iceland ICES Symp. on Physical Variability in the North Atlantic, Paper 2.

VORONINA, N.M., 1962. On the Dependence of the Character of the Boundary between Antarctic and Sub-Antarctic Pelagic Zones on the Meteorological Conditions. Geophys. Monogr. 7: 160-161.

9.0 SPECIAL BIBLIOGRAPHY

Selected from bibliography prepared at the Rosentiel School of Marine and Atmospheric Science at the University of Miami in November 1974.

A. Observational Field Studies

BANG, N.D., 1970. Major Eddies and Frontal Structures in the Agulhas Current Retroflexion Area in March 1969. Sympos. Paper, Oceanography in South Africa - 1970. (Durban, August 4-6, 1970), 13 pp.

BANG, N.D., 1973. Characteristics of an Intense Ocean Frontal System in the Upwell Regime West of Cape Town. Tellus, 25(3): 256-265.

BARANOV, E.I., 1966. Short Period Fluctuations of the Gulf Stream Front During the Winter-spring Season of 1963. Oceanology, 6(2): 228-233.

BARANOV, E.I., 1967. Study of Eddies in the Frontal Zones in the Gulf Stream. Oceanology, 7(1): 61-65.

BARANOV, E.I., and M.A. SHMATKO, 1966. An Investigation of Thermal Structure in the Frontal Zone of the Gulf Stream. Oceanology, 6(5): 630-634.

BLANTON, J.O. and J.G. PATTULLO, 1969. The subsurface Front Beneath the Subtropical Convergence in the Northeast Pacific Ocean. Trans., Amer. Geophys. Union, 50(4): 194 pp.

BOGDANOV, M.A., S.G. ORADOVSKIY, Y.V, SOLYANKIN, and N.V. KHVATSKIY, 1969. On the Frontal Zone of the Scotia Sea. Oceanology, 9(6): 777-783.

BULGAKOV, N.P., 1971. Thermohaline Structure of the Sub-Arctic Front in the Northwest Pacific Ocean. Oceanology, 11(3): 380-389.

BRISCOE, M.G., O.M. JOHANNESSEN, S. VINCENZI, and G. FURNESS, 1972. The Maltese Oceanic Front: A Surface Description by Ship and Aircraft. SACLANTCEN Conf., Proc. 7: 153-175.

BUZDALIN, Y.I., 1963. Hydrological Conditions in the Newfoundland Banks and Labrador Areas in 1960. Soviet Fisheries. Investigations in the Northwest Atlantic, Marti, Y.Y. (ed.): 152-168. (Israeli trans. to English).

CARSON, R.B., 1950. The Gulf Stream Front: A cause of Stratus on the Lower Atlantic Coast. Monthly Weather Review, 78(6): 91-101.

CLARKE, L.C. and T. Laevastu, 1966. Numerical Methods for Synoptic Computation of Oceanic Fronts and Water Type Boundaries and Their Significance in Applied Oceanography. U.S. Naval Postgrad. School, Fleet Num. Weather Facility, Monterey, Calif., Tech. Note No. 20, 39 pp.

CLARKE, L.C. and T. LAEVASTU, 1967. Numerical Methods for Synoptic Computation of Oceanic Fronts and Water Type Boundaries. Inter. J. of Oceanology and Limnol., 28-45.

CRAIG, H., Y. CHUNG, and M. FIADEIRO, 1972. A Benthic Front in the South Pacific. Earth and Planetary Sci. Letts., 16(1): 50-65.

CROMWELL, T. and J.L. REID, 1956. A Study of Oceanic Fronts. Tellus, 8(1): 94-101.

GRUZINOV, V.M., 1964. The Vertical Circulation and the Status of Frontal Zones in the Central Part of the North Atlantic. Oceanology, 3#: 408-411.

HOUTMAN, T.J., 1967. Water Masses and Fronts in the Southern Ocean South of New Zealand. 24 Stations. N.Z. Dept. of Sci. and Indus. Res. Bull. No. 174: 1-40.

JOHANNESSEN, O.M., F. DESTROBEL, and C. GEHIN, 1971. Observations of an Oceanic Frontal System East of Malta in May 1971. U.S. Nat'l Tech. Inf. Service, Government Rep. Announcement, 71(22): 86 pp.

KATZ, E.J., 1969. Further Study of a Front in the Sargasso Sea. Tellus, 21: 259-269.

KNAUSS, J.A., 1957. An Observation of an Oceanic Front. Tellus, 9(2): 234-237.

LAFOND, E.C., and E.L. SMITH, 1970. Temperature and Current in and near the Kuroshio. Proc. of the CSK Symps., Honolulu, May 1968. Also in: An Oceanogr. Data Rept. for CSK and adjacent regions, Marine Environ. Div. NUWC, May, 1968: 1-22.

LEVINE, E.R. and W.B. WHITE, 1972. Thermal Frontal Zones in the Eastern Mediterranean Sea. J. Geophys. Res., 77: 1081-1086.

MCLEISH, W., 1968. Small Scale Structures in Ocean Fronts. Trans., Amer. Geophys. Union, 49(1): 199.

NEWTON, C.W., 1959. Synoptic Comparisons of Jet Stream and Gulf Stream Systems. In: The Atmos. and Sea in Motion, B. Bolin (ed.), New York Rockefeller Inst. Press & Oxford Univ. Press: 288-304.

RAO, G.V. and W.S. MURTY, 1973. Some Case Studies of Vertical Circulations Associated with Oceanic Fronts. J. Geophys. Research, 78(3): 549-557.

RENARD, R.J. and L.C. CLARKE, 1965. Experiments in Numerical Objective Frontal Analysis. Monthly Weather Review, 93(9): 547-556,

RODEN, G.I., 1972. Temperature and Salinity Fronts at the Boundaries of the Subarctic-Subtropical Transition Zone in the Western Pacific. J. Geophys. Res., 77(36): 7175-7187.

RODEN, G., 1974. Thermohaline Structure, Fronts, and Sea-Air Energy Exchange of the Trade Wind Region East of Hawaii. J. Phys. Oceanogr., 4(2): 168-182.

U.S. NAVAL OCEANOGRAPHIC OFFICE, 1969. Montly Charts of Mean, Minimum and Maximum Sea Surface Temperatures of The North Pacific Ocean. SP-123, Navaoceano., Washington, D.C.

VON ARX, W.S., D.F. BUMPUS, and W.S. RICHARDSON, 1955. On the Fine Structure of the Gulf Stream Front. Deep Sea Res., 3: 46-65.

VOORHIS, A.D., 1969. The Horizontal Extent and Persistence of Thermal Fronts in the Sargasso Sea. Deep Sea Res., Suppl., 16: 331-337.

VOORHIS, A.D. and J.B. HERSEY, 1964. Oceanic Thermal Fronts in the Sargasso Sea. J. Geophys. Res., 69(18): 3809-3814.

WOODS, J.D., 1972. The Structure of Fronts in the Seasonal Thermocline. SACLANTCEN Conf. Proc., 7: 144-151.

WOOSTER, W.S., 1969. Equatorial Front Between Peru and Galapagos. Deep Sea Res., 16 (suppl): 407-419.

YASUI, M., 1961. Internal Waves in the Open Ocean (an Example of Internal Waves Progressing Along the Oceanic Frontal Zone). The Oceanogr. Mag., 12(2): 157-182.

B. Theoretical Studies

GARVINE, R.W., 1974. Dynamics of Small-scale Oceanic Fronts. J. Phys. Oceanogr., 4(4): 557-569.

GUTMAN, L.N. and L.N. MAL'KO, 1961. On the Theory of Fronts. Proc. (Dokl.) Acad. Sci. USSR, 138(3).

KALAZHOKOV, K.K. and L.N. GUTMAN, 1964. On the Dynamical Structure of Fronts. Geophys. Bull., Acad. Sciences USSR, January, 1964: 74-79.

MILLER, J.E., 1948. On the Concept of Frontogenesis. J. Met., 5: 169-171.

NEWTON, C.W., 1954. Frontogenesis and Frontolysis as a Three-dimensional Process. J. Met., 11: 449-461.

SMITH, E.L., 1967. A Predictive Horizontal-temperature-gradient Model of the Upper 750 Feet of the Ocean. Navy Elec. Lab. Tech. Rept. 1445, March, 1967.

TURNER, J.S., 1965. The Coupled Turbulent Transports of Salt and Heat across a Sharp Density Interface. Int. J. Heat Mass Transfer, 8: 759-767.

TURNER, J.S., 1968. The Influence of Molecular Diffusivity on Turbulent Entrainment across a Density Interface. J. Fluid Mech., 33: 639-656.

WELANDER, P. 1963. Steady Plane Fronts in a Rotating Fluid. Tellus, 15(1): 33-43.

APPENDIX A

HYDRODYNAMICAL-NUMERICAL (HN) MODEL FOR THE STUDY OF OCEANIC FRONTS

CONTENTS

1. Basic Hydrodynamical Equations and Their Finite Difference Forms

A two-layer Hydrodynamical-Numerical (HN) model of Walter Hansen's type was used in the present study. The individual layers are vertically integrated. The basic equations are as follows:

$$\dot{\zeta}_1 - \dot{\zeta}_2 + H_{u1}(U1_x) + H_{v1}(V1_y) = 0$$

$$\dot{\zeta}_2 + H_{u2}(U2_x) + H_{v2}(V2_y) = 0$$

$$\dot{U1} + \frac{r\sqrt{U1^2 + V1^2}}{H_{u1}} U1 - fV1 - g\,\zeta_{1x} = K^{(x)}$$

$$\dot{U2} + \frac{r\sqrt{U2^2 + V2^2}}{H_{u2}} U2 - fV2 - g\,\frac{\rho 1}{\rho 2}\,\zeta_{1x} - g\left(1-\frac{\rho 1}{\rho 2}\right)\zeta_{2x} = 0$$

$$\dot{V1} + \frac{r\sqrt{U1^2 + V1^2}}{H_{v1}} V1 + fU1 - g\,\zeta_{1y} = K^{(y)}$$

$$\dot{V2} + \frac{r\sqrt{U2^2 + V2^2}}{H_{v2}} V2 + fU2 - g\,\frac{\rho 1}{\rho 2}\,\zeta_{1y} - g\left(1-\frac{\rho 1}{\rho 2}\right)\zeta_{2y} = 0$$

where:

ζ_1 - surface elevation;
ζ_2 - deviation of MLD (mixed layer depth) from mean
U1,V1 - u,v components in upper layer
U2,V2 - u,v components in lower layer
r - friction coefficient
f - Coriolis parameter
g - acceleration of gravity
H - depth
ρ_1, ρ_2 - densities
$K^{(x)}$, $K^{(y)}$ - external forces

There are two inter-dependent continuity equations, one for each layer. These compute the change of sea level, the change of depth and thickness of the layers.

The equations of motion for each layer are vertically integrated through this given layer. The lower layer is driven by internal friction and by pressure gradients.

The finite difference forms used for computation are:

$$\zeta^{t+\tau}_{(n,m,1)} - \bar{\zeta}^{t-\tau}_{(n,m,1)} - \frac{\tau}{\ell}\{H^{t}_{u(n,m,1)}\ U^{t}_{(n,m,1)} - H^{t}_{u(n,m-1,1)}\ U^{t}_{(n,m-1,1)} + H^{t}_{v(n-1,m,1)}\ V^{t}_{(n-1,m,1)} - H^{t}_{v(n,m,1)}\ V^{t}_{(n,m,1)}\} - \frac{\tau}{\ell}\{H^{t}_{u(n,m,2)}\ U^{t}_{(n,m,2)} - H^{t}_{u(n,m-1,2)}\ U^{t}_{(n,m-1,2)} + H^{t}_{v(n-1,m,2)}\ V^{t}_{(n-1,m,2)} - H^{t}_{v(n,m,2)}\ V^{t}_{(n,m,2)}\}$$

$$\zeta^{t+\tau}_{(n,m,1)} = \bar{\zeta}^{t-\tau}_{(n,m,2)} - \frac{\tau}{\ell}\{H^{t}_{u(n,m,2)}\ U^{t}_{(n,m,2)} - H^{t}_{u(n,m-1,2)}\ U^{t}_{(n,m-1,2)} + H^{t}_{v(n-1,m,2)} + V^{t}_{(n-1,m,2)} - H^{t}_{v(n,m,2)}\ V^{t}_{(n,m,2)}\}$$

$$U^{t+2\tau}_{(n,m,1)} = \{1-[2\tau r/H^{t+2\tau}_{u(n,m,1)}]\sqrt{\bar{U}^{t}_{(n,m,1)}{}^{2} + V^{*t}_{(n,m,1)}{}^{2}}\}\ \bar{U}^{t}_{(n,m,1)} + 2\ f\tau V^{*t}_{(n,m,1)} - \frac{\tau g}{\ell}\{\zeta^{t+\tau}_{(n,m+1,1)} - \zeta^{t+\tau}_{(n,m,1)}\} + 2\tau X^{t+2\tau}_{(n,m)}$$

$$U^{t+2\tau}_{(n,m,2)} = \{1-[2\tau r/H^{t+2\tau}_{u(n,m,2)}] \sqrt{U^{t}_{(n,m,2)}{}^{2} + V^{*t}_{(n,m,2)}{}^{2}}\}$$

$$\bar{U}^{t}_{(n,m,2)} + 2\tau f\, V^{*t}_{(n,m,2)} - \frac{\tau g}{\ell}\{\frac{\rho 1}{\rho 2}[\zeta^{t+\tau}_{(n,m+1,1)}$$

$$- \zeta^{t+\tau}_{(n,m,1)}]\} - \frac{\tau g}{\ell}\{[1 - \frac{\rho 1}{\rho 2}][\zeta^{t+\tau}_{(n,m+1,2)}$$

$$- \zeta^{t+\tau}_{(n,m,2)}]\}$$

$$V^{t+2\tau}_{(n,m,1)} = \{1-[2\tau r/H^{t+2\tau}_{v(n,m,1)}] \sqrt{\bar{V}^{t}_{(n,m,1)}{}^{2} + U^{*t}_{(n,m,1)}{}^{2}}\}$$

$$-2\tau f\, U^{*t}_{(n,m,1)} - \frac{\tau g}{\ell}\{\zeta^{t+\tau}_{(n,m,1)} - \zeta^{t+\tau}_{(n+1,m,1)}\}$$

$$+2\tau Y^{t+2\tau}_{(n,m)}$$

$$V^{t+2\tau}_{(n,m,2)} = \{1-[2\tau r/H^{t+2\tau}_{v(n,m,2)}] \sqrt{\bar{V}^{t}_{(n,m,2)}{}^{2} + U^{*t}_{(n,m,2)}{}^{2}}\}$$

$$-2\tau f\, U^{*t}_{(n,m,2)} - \frac{\tau g}{\ell}\{\frac{\rho 1}{\rho 2}[\zeta^{t+\tau}_{(n,m,1)} - \zeta^{t+\tau}_{(n+1,m,1)}]\}$$

$$- \frac{\tau g}{\ell}\{[1-\frac{\rho 1}{\rho 2}][\zeta^{t+\tau}_{(n,m,2)} - \zeta^{t+\tau}_{(n+1,m,2)}]\}$$

The computation of $\bar{U}$ and U^{*} is done as in the single-layer model

$$\bar{U}^{t}_{(n,m)} = \alpha\, U^{t}_{(n,m)} + \frac{1-\alpha}{4}\{U^{t}_{(n-1,m)} + U^{t}_{(n+1,m)} + U^{t}_{(n,m+1)}$$

$$+ U^{t}_{(n,m-1)}\}$$

$$U^{*t}_{(n,m)} = \frac{1}{4}\{U^{t}_{(n,m-1)} + U^{t}_{(n+1,m-1)} + U^{t}_{(n,m)} + U^{t}_{(n+1,m)}\}$$

The computation of $\bar{V}$ and V^* are analogous to the corresponding U computations above. The actual depth (and thickness of the layer) is computed with the following equations:

$$H^{t+2\tau}_{u(n,m,1)} + h_{u(n,m,1)} + \frac{1}{2}\{\zeta^{t+\tau}_{(n,m,1)} + \zeta^{t+\tau}_{(n,m+1,1)}\}$$

$$H^{t+2\tau}_{v(n,m,1)} = h_{v(n,m,1)} + \frac{1}{2}\{\zeta^{t+\tau}_{(n,m,1)} + \zeta^{t+\tau}_{(n+1,m,1)}\}$$

The following symbols were used in the finite difference formulas above:

x,y	space coordinates
t	time
U,V	components of velocity
u,v	indicators of U and V point (location) in the grid
h	initial depth (when $\zeta = 0$)
ζ	surface elevation (for the second layer, it indicates the deviation of the depth of the layer from its prescribed mean value)
H	total depth ($H = h + \zeta$)
H_u, H_v	depths at u and v points respectively
X,Y	components of external forces
g	acceleration of gravity
f	Coriolis parameter
r	friction coefficient (bottom stress for lower layer)
α	coefficient of horizontal eddy viscosity (also acts as a smoothing coefficient)
n,m	coordinates of the grid point, 1 and 2 indicate the first (surface) or second (deep) layer
τ	half time step
ℓ	half grid length
ρ_1, ρ_2	densities of first and second layer

As the HN model provides a current vector at each grid point at each time step, one can solve the interacting advection and diffusion problem using a time-stepping finite difference method. In the frontal model the distribution of surface layer temperature will be advected and diffused to obtain the changes in position and intensity of the surface front as affected by wind-induced current components. The following restraints and considerations apply to the advection/diffusion computations:

(a) Vertical diffusion between layers is neglected

(b) A Fickian type diffusion with basic Lagrangian approach, and with constant diffusivity is used since the advection and diffusion equations are solved separately in short, interlocking time-steps.

(c) The Austausch (eddy diffusion) coefficient is related to time-step and grid size used. The advection is computed linearly in the following finite difference form:

$$S^{t+\tau}_{n,m} = S^{t}_{n,m} - \tau \left| U^{t+\tau}_{n,m} \right| \frac{\left(S^{t}_{n,m} - S^{t}_{n,m\pm1}\right)}{\ell} - \tau \left| V^{t+\tau}_{n,m} \right| \frac{\left(S^{t}_{n,m} - S^{t}_{n\pm1,m}\right)}{\ell}$$

where: Sn,m-1 or n,m+1 (respectively n-1, n+1) are used, depending on the direction (sign) of U and V.

The following diffusion formula for temperature has been used; heat is conserved provided no decay or heat exchange formula is applied and the correct Austausch coefficient is chosen.

$$S^{t+\tau}_{n,m} = S^{t}_{n,m} - \frac{4\tau A}{\ell^2} S^{t}_{n,m} + \frac{\tau A}{\ell^2}\left(S^{t}_{n-1,m} + S^{t}_{n,m-1} + S^{t}_{n+1,m} + S^{t}_{n,m+1} - 4S^{t}_{n,m}\right) + \frac{\tau A}{\ell^2}\left(S^{t}_{n-1,m-1} + S^{t}_{n-1,m+1} + S^{t}_{(n+1,m-1)} + S^{t}_{(n+1,m+1)}\right)$$

This scheme requires that

$$\frac{U\Delta t}{\Delta l} < 1$$

The Austausch coefficient A is taken from the graph on Figure 1:

$$A = \frac{1000}{\Delta t} A_{(graph)}$$

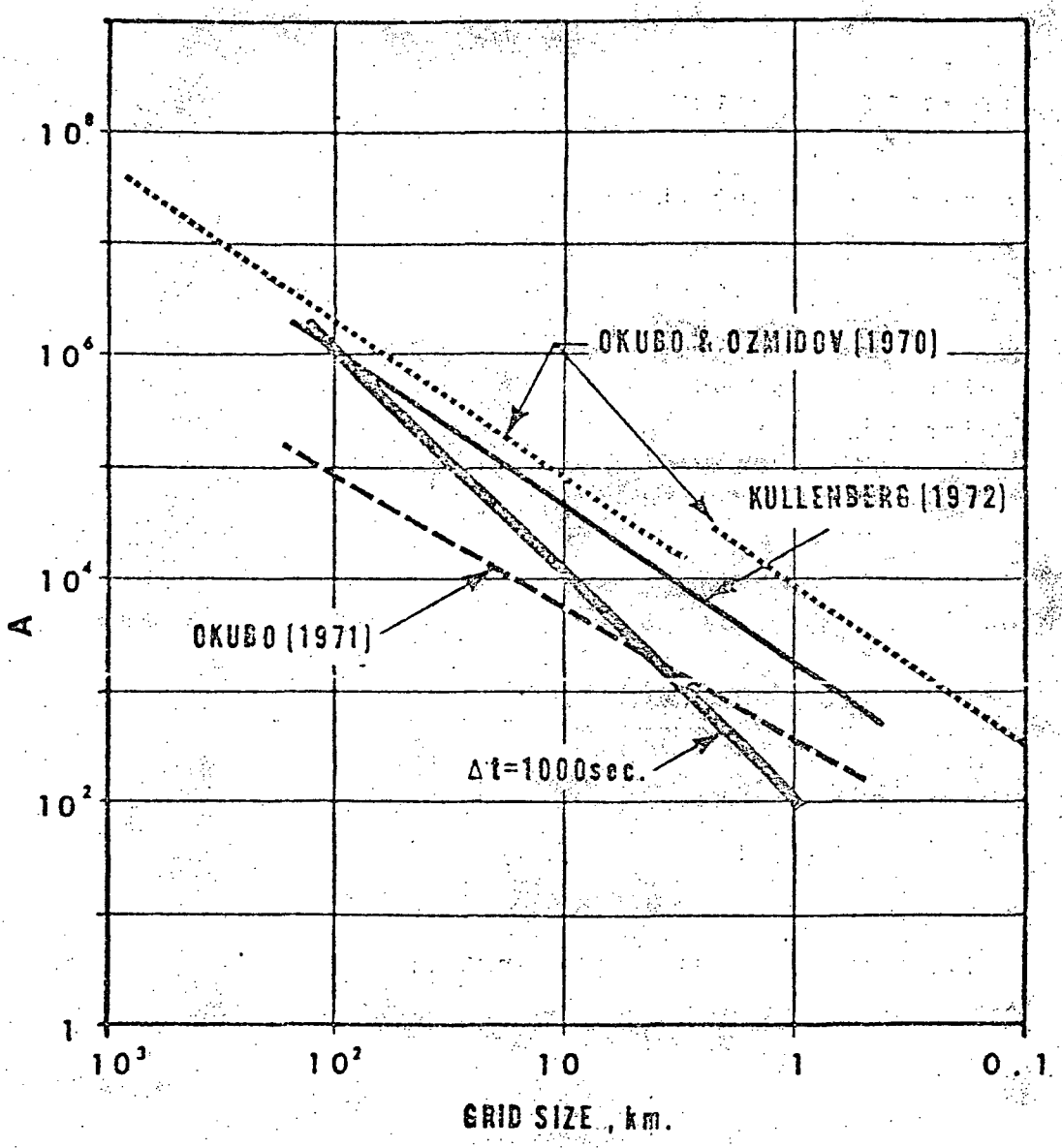

FIGURE 1: DEPENDENCE OF AUSTAUSCH COEFFICIENT (A) ON GRID SIZE (Δt=1000 sec)

Figure 1 also shows some other horizontal dimension (grid size) - Austausch coefficient relations found experimentally by different researchers.

The maximum length of the time step in the numerical model is determined by the grid length and maximum depth according to the Courant-Friedrichs-Lewy criterion:

$$0.5\Delta t \leq \frac{0.5\ell}{\sqrt{2gH_{max}}}$$

where Δt is time step (sec); ℓ is grid length (cm); g is acceleration of gravity; and H_{max} is the maximum depth in the area of computation (cm). Any attempt to increase the time step above this criterion results in "blow up" or computational instability.

The selection of the size of the area and the distance between grid points is usually based on requirements concerning topography, accuracy, and availability of computer core memory. A 10 km grid size was used in the present model.

The grid net (staggered grid) is shown in Figure 2. It consists of three different sets of grid points: (1) the water elevation points (Z) at the intersection of the grid; (2) the point for U-velocity component to the right and (3) the V-velocity component below the corresponding Z point. Each of these three points has the same coordinate designation (n,m).

As this model has been specially adapted

for the frontal study, no rotation of the grid from a normal position is permitted.

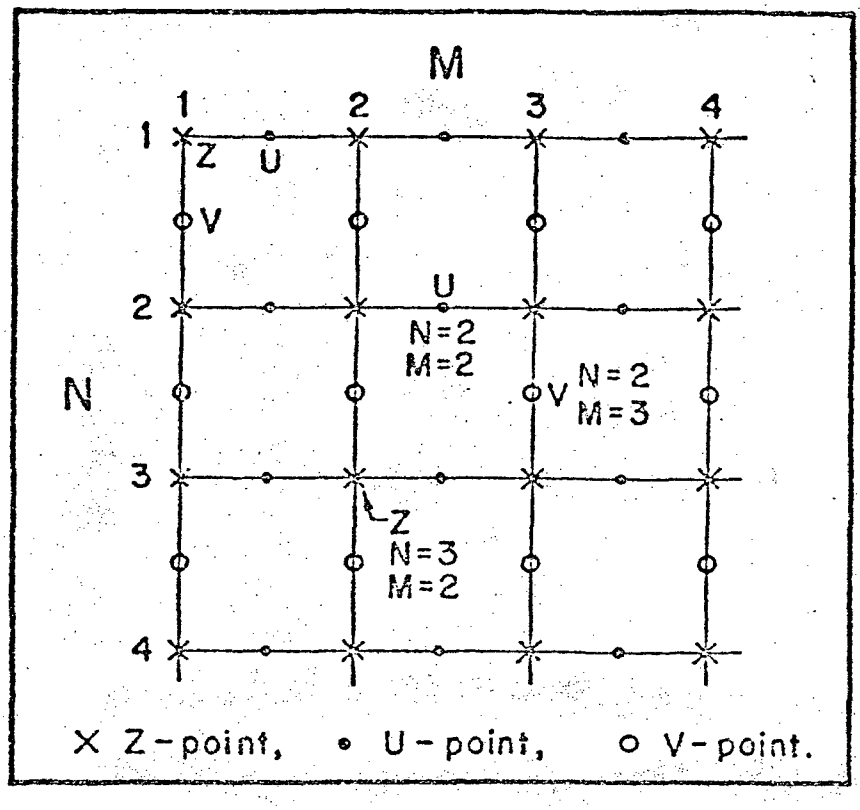

FIGURE 2: SCHEME OF THE GRID NET

The solution to the hydrodynamical equations is uniquely determined if all boundaries are either closed or prescribed. In the present study, the boundaries must be, however, left open for in- and out-flow. Much effort has been spent in the past to find theoretically and practically (from computational point of view) satisfactory solutions to open boundary treatment. Two relatively simple approaches have proven most useful. In one approach, the variables (U,V and Z) are computed out to one row or column from the

boundary and these next-to-boundary values are transferred to the boundary at each time step. The second approach, which has verified somewhat better, is to compute the variables up to the open boundaries and then replace the one missing parameter (which can be either U, V or Z) with its value at the boundary. This method is commonly referred to as the "leaky boundary" method.

2. Model Inputs and Other Parameters and Program Organization

The smoothing coefficient (ALPHA in the program) acts as a horizontal viscosity coefficient. Normal value for ALPHA in surface layers is between 0.985 and 0.99. For the second layer a somewhat lower value (0.92) is used to suppress some computationally caused gravity waves.

The bottom friction is a non-linear (quadratic) quantity with a coefficient r of 0.003. The value for the internal friction coefficient is somewhat uncertain. Numerical experimentations have shown that 0.0015 gives verifiable results.

If the model is applied in real conditions, depth values, as well as initial layer thickness values must be digitized at U and V points. A sea/land table is read in at Z points. The coast must pass through U and V points and no flow into or out from the coast is allowed. This condition is not pertinent to the frontal model, as it has four open boundaries.

In the present model the permanent current (e.g. thermohaline current), the wind and surface temperature are prescribed at each grid point. The wind speed is given on an input card (or in a data statement in present model) in m sec^{-1}. The wind direction must be given in grid coordinates and in the direction toward which the wind is blowing. Thus, a west wind is coming from -x toward +x and should be given an angle of 0°; a north wind has an angle of 270°; east wind, 180°, and south wind, 90°.

The FORTRAN program is organized into eight subroutines. The common blocks are identical in all subroutines. The main program calls the major subroutines and counts the time. Subroutine JO2 is for initialization of the fields; it inputs and computes a number of derived parameters used in other subroutines. It is called only once.

Subroutine VECTOR is called by subroutine JO4 and computes the resultant direction of the current from U and V components during output times. Subroutine JO4 is for output and is called at any desired time interval (T1). The latter is given in the data statement. This subroutine also writes parameter values for special (selected) points on a tape for output at the end of computations (using subroutine JO8).

Subroutine JO5 is the main computational subroutine and is called each time step. This subroutine also calls

wind subroutine SO1 and the current and temperature initialization subroutine (CURRENT and TEMPS). Subroutine SO1 calls the wind subroutine (WINDS) and computes the wind current component.

Subroutine WINDS contains various (different) frontal wind generation sections, different types of initial frontal surface current generation sections and the initial surface temperature distribution section.

References

OCEANOGR. DEPT. EPRF, 1974. A vertically integrated Hydrodynamical-Numerical Model (W. Hansen type). ENVPREDRSCHFAC Tech. Note 1-74.

LAEVASTU, T., 1974. A multi-layer Hydrodynamical-Numerical Model (W. Hansen type). ENVPREDRSCHFAC Tech. Note. 2-74.

3. System Variables

3.1 Description of Input Parameters

The following parameters are set internally in subroutine JO2 in DATA statements:

AGFN	NOT USED
*ALPHA	Velocity field smoothing parameter or pseudo eddy vescosity for top layer; ALPHA = .998
*C	Drag coefficient for computation of wind stress $C = 3.2 \times 10^{-6}$
C1	Flag to indicate whether or not wind stress is imposed; C1 = 1 for wind stress, C1 = 0 for no wind stress
DEBUG	Flag used to print and initial current, wind and temperature fields; DEBUG = 1 prints these fields at beginning of the program, DEBUG = 0 suppresses the print
DL	1/2 distance between nodes on the computational grid; $DL = 10^5$ cm
D+	1/2 the tine between iterations of the integration scheme; DT = 60 sec
F	Coriolis parameter; $F = 2\omega\sin\phi$ ω = angular rotation of the earth; ϕ = latitude; ($F = 1.0312 \times 10^{-4}$ at Card 29 of JO2)
G	Acceleration due to gravity; G = 970. cm sec^{-2}
HTL1	Initial depth (thickness) of the top layer; HTL1 = 7500.0 cm
IUE	NOT USED
IZE	NOT USED
JA	Should be zero always
KKE	NOT USED

LI	Reset at Card 341 of JO5 to LI = 1 as temperature advection is calculated (may be removed from data statement)
ME	Number of columns in the computational grid; ME = 30
NG	NOT USED
NE	Number of rows in the computational grid; NE = 25
NS	NOT USED
NURU	DUMMY variable; leave at NURU = 6
*R	Bottom friction coefficient; $R = 3 \times 10^{-3}$
RBETA	Used only in PRINT statement in subroutine JO2 (card 63) which may be removed
ROL	NOT USED
SI	Time (sec) at which wind field is set to zero; $SI = 36 \times 10^{4}$ (SI must be greater than TE for wind input throughout run)
SIGMA	NOT USED
T	Time index - always set at zero initially
TE	Total time for integration of equations (Simulated real time); TE = 43200. sec
TW	Time (sec) at which wind field is first imposed; TW = 100.0 sec
T1	Output (printer) interval in seconds; T = 3600 implies output parameters will be printed at 1-hour intervals
T2	Leave at zero always
T3	NOT USED

The following are set in DATA statements in JO5:

*ALP	Velocity field smoothing parameter or pseudo eddy - viscosity for bottom layer; ALP = 0.92
IFLG	Flag used to initialize current filed on first iteration; IFLG ≠ 0 results in bypassing this initialization
IFLG2	Flag used to set up temperature field on first iteration; IFLG2 = 0 results in bypassing the temperature field initialization
*RHO1	Density of the top layer; RHO = 1.025 g cm^{-3}
*RHO2	Density of the lower layer; RHO2 = 1.027 g cm^{-3}

The following is defined in JO5 at card 350:

AUS	Eddy diffusion coefficient; AUS = 5.0 x 10^{-3}

*The range of these variables is given in Table A-1.

3.2 Initialization Options

The following are used to select an option in the initialization of the current, temperature and wind fields.

In JO5:

Card 109 selects current (cm sec^{-1}) field initialization

KEY=1 Currents parallel to the front, but in opposing directions from one side of the front to the other. (Case I and III Current Field)

KEY=2 Currents converging and decreasing toward front (not used to date)

KEY=3 Uniform east west currents at 2.5 cm sec^{-1} (Case II)

KEY=4 Currents converging and increasing toward front (not used to date)

KEY=5 Currents diverging from front (not used to date)

In JO5:

Card 332 is used to select the temperature field initialization

KEY=1 This is the only option at present for the initialization of the temperature field. The temperature field is homogenous in the east west direction.

In JO1:

Card 20 is used to select the wind field initialization

KEY=1 Case I wind field divergent south of front, convergent north of front

KEY=2 (has not been used to date)

KEY=3 Call to subroutine HURRW for the generation of a moving wind field

3.3 Description of Output Parameters

The normal output (DEBUG=0) consists of initial printout of the values of: DT, DL, ALPHA, R, F, SIGMA, RBETA, LAMDA.

SIGMA (NOT USED)

RBETA (NOT USED)

LAMDA is the variable C described in 3.1 of this appendix

Following the printout of the above, these fields are printed at the interval specified by T1:

Z Height of the free surface above the initial position in CM. This field is entitled, "WATER LEVEL (CM) AFTER T=__"

Z2L The height of the interface above the inital position in CM. This field is entitled, "MLD DEPTH (CM) AFTER T=__"

RAD,ANG The top layer resultant current speed (RAD) in CM sec^{-1} and the direction (ANG) toward which the current is flowing in degrees true (North is 0°, East is 90°). This field is entitled, "RESULTANT CURRENT SPEED (CM/SEC) AND DIRECTION (DEG.) AFTER T=__". Note that the field consists of numbers of the form RR.DDD. where RR is the Current Speed and DDD is the Direction.

RAD2,ANG2 The bottom layer resultant current speed (RAD2) and direction (ANG2) in CM sec^{-1} and degrees true. The same conventions are sued for RAD2 and ANG2 as for RAD and ANG. The fiedl is entitled, "DEEP LAY. CURRENT SPEED (CM/SEC) AND DIRECTION (DEG.) AFTER T=__".

S The temperature of the top layer in degrees Centigrade. The field is labeled "TEMPERATURE OF SURFACE LAYER (DEGREES) AFTER T=__". It should be noted that these 30 by 25 fields are printed in two sections of 15 by 25 each. They are indexed properly with row and column indicated so there should be no problem with interpretation.

For DEBUG=1 (debug print desired), the following are printed as the first ten columns of the 25 by 30 array upon initialization:

The components of the wind field (in $msec^{-1}$) and the value of KEY which was used to select the option. The first twenty-five lines are those of the XW array (the east-west component of the wind). The next twenty-five lines are those of the YW array (the north-south component of the wind). The print commands are located in subroutine SOl, cards 26,27.

The components of the initial current field ($CM\ sec^{-1}$) and the value of KEY which was used to select the option. The first twenty-five lines of the array are those of U (the east-west component of the top layer of the current). The next twenty-five lines are those of the V array (north-south) component of the current in the top layer). Note that the bottom layer is initially at rest.

The temperature field in degrees Centigrade. As only one option is available at present, no value of KEY is printed.

TABLE A-1

	RANGE OF TYPICAL VALUES	
PARAMETER	MIN	MAX
ALPHA	.995	.999
ALP	.90	.99
AUS	5.0×10^{-4}	5.0×10^{-3}
C	1.8×10^{-6}	3.6×10^{-6}
R	2.0×10^{-3}	4.0×10^{-3}
RHO1	1.023	1.028
RHO2	1.024	1.029

APPENDIX B

SPECTRO-ANGULAR WAVE MODEL FOR THE STUDY OF THE MODIFICATIONS OF SURFACE WAVES AT OCEANIC FRONTS

CONTENTS

Program listing separately submitted

1. The Basic Spectro-Angular Wave Analysis/ Forecasting Model (The French Model)

The spectro-angular wave analysis/forecasting model used in the present study has been developed in Meteorologie Nationale, Paris, France (Gelei and Devillaz, 1969 - Devillaz, 1965,a,b). It has been, however, considerably modified by the present authors and adapted for the specific purpose of this study. This French spectro-angular wave model (DSA5) is considered to be one of the best available numerical wave forecasting models. The method of propagation and spreading of wave energy makes this model attractive for this particular study.

The basic formula for computation of spectro-angular energy density is:

$$\frac{de}{dt} = T^{\nu}\left[W, |\theta - w|, T \right] - \frac{Ae}{T^4} m_o - \vec{V}(T,\theta)\nabla e(T,\theta)$$

with:

$$m_o = \Sigma_T \Sigma_\theta \, e(T,\theta)$$

where:

e = the spectro-angular density

$\vec{V}(T,\theta)$ = the "unit speed" of the component, i.e.,

$V(T,\theta) = \frac{gT}{4\pi}$, g being gravity

W = surface wind speed in knots

θ = a component azimuth

w = a surface wind azimuth

T = the wave period in seconds

$T^{\vee}$ = the spectro-angular increase

A = the empirical dampening coefficient

The form of the spectro-angular increase is:

$$T^{\vee}\left[T,|\theta-w|,W\right] = P(T,W,)\ S(\theta-w)$$

where:

P = the spectral increase

S = the function for angular dispersion, such that:

$$\int_{-\frac{\pi}{2}}^{+\frac{\pi}{2}} S(\theta-w)d(\theta-w) = 1$$

From μ, the decay coefficient of a component is given by:

$$\frac{1}{e}\frac{de}{dt} = \frac{64\mu\pi^4}{g^4 dedu}\ \frac{1}{T^4} = \frac{A}{T^4}\ m_o$$

where:

edTdθ = the energy density due to that component

dedu = the specific water mass

g = gravity

$A = 18 \times 10^{-9}$ CGS

leaving:

$$\frac{Am_o}{T^4}\ e$$

The energy density is computed for 6 different periods and 16 directions. The growth and decay constants are pre-computed into a look-up table in the program.

2. Model Inputs and Outputs

The wind speed and direction at each grid point is prescribed every 3 to 12 hours, depending upon the availability of surface wind analysis/forecasts. In the present program, the wind speed and direction is printed out for checking in a code as used in the program (speed in 5-knot intervals; direction, in 16 compass points), as well as in conventional form.

A special subroutine in the program permits the introduction of a cyclone. The radius of maximum winds, the maximum wind speed and the direction and speed of movement of the cyclone is determined by internal parameters, set in the main program.

As the energy propagation is related to grid size, the coefficients AMUL and AMUL1 in the subroutine CONST must be calculated with the following formula:

AMUL = 4.5/grid size in nautical miles.

Grid sizes smaller than 30 nautical miles should not be used if wind speed is introduced each 3 hours or longer time interval, as "holes" in energy propagation will occur in the program.

Various outputs of wave parameters are provided for in the program. First the $H_{1/10}$ (average height of the "tenth

highest wave") can be printed at each grid point. The wave period and direction of maximum energy are also printed out in field form. In order to display and study the energy spectrum, a special subroutine IMPDENS prints the distribution of energy by compass directions and by different periods at desired output points.

3. The Organization of the Numerical Model

The main program, TYWAVE, reads the input cards, calls all other subroutines and counts the time. It also stores the energy densities from previous time steps.

The second subroutine, AJUST, is for adjustment (and smoothing) the energy spectrum.

Subroutine ECRI computes and prints the height ($H_{1/10}$), period and direction of maximum energy and prints out these fields.

The subroutine CALCUL computes the actual spectro-angular density fields (RO) considering decay (using proper decay constants from AMOR table) and growth corresponding to new wind fields and time (using proper growth constants from table CROIS).

Subroutine VENTOS calls the wind fields, puts the speed and directions into codes used in the program and prints out the wind fields.

Subroutine CONST contains the growth (CROIS) and decay (AMOR) tables and other constants required by the program.

Subroutine ADVEC simulates the movement of the "swell" (waves from previous time step). The "spreading counters" AM, BN and CP are generated by subroutines AVANCX and AVANCY, which are called before calling ADVEC.

Subroutine HURRW creates a moving cyclone. The parameters of the cyclone (grid size, speed and radius of maximum winds and direction and speed of the movement of the cyclone) are given in this subroutine. Subroutine PPAGE, called in HURRW subroutine, outputs the wind fields created by it.

The constants needed for output of wave spectra are created with subroutine SELCPT. The energy density table is created in subroutine IMPDENS, which calls a compass language subroutine DECRIPC which packs the data into the array TABLEAU. The array is printed when the final pass through the subroutine IMPDENS is made.

4. Symbols Used in the Program

Card Input

The following parameters are read with the data cards:

IHIND	0/1	0=forecast, 1=hindcast (set to 0, usually)
IRO	0/1	0=new start, 1=use old sea state
IMER3	0/1	1=fields read in for every 3 hours
IMER6	0/1	1=fields read in for every 6 hours

A zero in the latter two positions means that the fields will be read in every 12 hours; since the wind fields are internally generated every three hours, the current convention is IMER3=1 and IMER6=0.

ISTOCK	0/1	1=stacking of fields for the special points output - not used currently
NSTEP	Blank/Value	The number of hours of computation
IDENS3	0/1	Densities for the special points are taken every 3 hours, if IDENS3 = 1
IDENS6	0/1	1 = special points densities taken every 6 hours

Other arrays and variables in the program are:

AM	The longitudinal spreading
AMOR	The decay constants
AMUL	Coefficient of advection velocity
AMUL1	A decay coefficient relative to grid, used to compute the the overall decay
BACK	Background wind speed (not used in this model)
BN	The later spreading counters (odd)
COST	Cosine table for advection computations
CP	The lateral spreading counters (even)
CROIS	The growth constants
EX	Spreading counter in the x direction
EY	Spreading counter in the y direction

F	Incrementation value for the three spreading counters; AM, BN, CP
IALT	A counter, with the value of either +1 or -1, which is used by the program to consult the IDIFM tables
JAN	Year
ICHART	A counter which triggers output of the sea-state graph
ICOMPM	Longitudinal spreading reference cycle constant
ICOMPN	Lateral spreading reference cycle constant (odd)
IDE	Same as IDENS
IDIFM	The longitudinal spreading constants
IDIFN	The lateral spreading constants (odd)
IDIFP	The lateral spreading constants (even)
IHED	Time counter
IHER	Hour
INDRFT	Indrift component of the cyclone
INTEN	Maximum wind speed, knots
IRANGE (IRAN)	A counter used to load the fields as a safety factor
IRESUL	The array containing the height of the 1/10 highest waves, $H_{1/10}$

ISTEP	Step counter
IT	Index counter for the 6 period loop
ITETA	Index counter for the 16 direction loop
ITETMA	The array containing the "maximum wave direction"
IVEN	A counter which causes the next set of wind fields to be read
IVENT (IV2)	The two arrays which contain the input wind data, the first being wind speed and the second the wind direction
JOUR	Day
MESH	Grid size (nautical miles)
MOIS	Month
NR, NW	Counters
P	Grid step constant, used in AVANCX
Q	Grid step constant, used in AVANCY
SINT	Sine table used for advection computations
RCIRC	Radius of cyclone (max. winds) (nautical miles)
REYE	Radius of the eye
RO	The spectro-angular density field generated for a given time interval
ROCUM	The summation of the spectro-angular densities for the run in progress
ROCUM1	The summation of the spectro-angular densities from the previous run

ROPRIM	The summation field of the spectro-angular densities used to add the advection effects to RO
ROTECU	The summation of the spectral directions, used to find the direction of maximum energy
ROTETA	The "maximum direction" retained
ROTM (IROTM)	The maximum period field
ROTT	The six period arrays from which the ROTM value is chosen
UCNTR, VCNTER	U and V components for the movement of cyclone center (knots)
VMAX	Maximum wind speed of the cyclone (m/sec)
XORIG, YORIG	X and Y for the original center of the cyclone
XBACK, YBACK	X and Y components of the background wind speed (knots)

5. REFERENCES

GELCÍ, R. and E. DEVILLAZ, 1969. Numerical computation of sea state. Dept of Transp., Gen. Secr. Civ. Aviation, Bureau of Nat. Met., Office of Mar. Met. Study. Report 268 (Transl.)

DEVILLAZ, E., 1965. Traitement numérique de l'état de la Mer. Le modéle polyvalent, DSA-5-M. Min. Trav. Publ. Transp., Secr. Gen. l'Aviation Civ., Dir. Mét. Nat. L'Etab. d'Etud. Rech. Mét., Notes 201.

DEVILLAZ, E., 1965. Traitement numérique de l'état de la Mer. Dispersion artificielle et premiers résultats du mode DSA-5-M. Min. Trav. Publ. Transp., Secr. Gen. l'Aviation Civ., Dir. Mét. Nat., L'Etab. d'Etud. Rech. Mét., Notes 211.

HUBERT, W.E., and W. YOGI, 1974. Modification to wind profile subroutine of EPRF typhoon wave model, Ocean Data Systems, Inc. Technical Report.

APPENDIX C

WAVE REFRACTION MODEL

CONTENTS

Program listing separately submitted

1. The Dobson Wave Refraction Model

Dobson utilized the theory of Munk and Arthur as the basis of his model. Figure 1 gives the definition sketch for the wave ray equations. Application of Huygen's principle for monochromatic wave propagation yields the following relationships:

$$S = c\delta t$$

$$\delta\alpha = \frac{\delta n}{s}$$

$$\delta\alpha = -\frac{\delta c \delta t}{n}$$

$$\delta\alpha = n\frac{\delta\alpha}{\delta n}$$

$$\delta n = s\delta\alpha$$

Thus, as $t \to 0$, $n \to \delta n \to 0$ and

$$\frac{\delta\alpha}{\delta t} = \frac{Dc}{Dn}$$

Also

$$K = \frac{D\alpha}{Ds} = \frac{-1}{c}\frac{Dc}{Dn}$$

From this it follows

$$n = n_0 B \quad \text{where } B = \frac{b}{b_0}$$

$$\delta n = n_0 \delta B$$

$$\delta\alpha = n_0 B \frac{D\alpha}{Dn} = \frac{n_0 \delta B}{s}$$

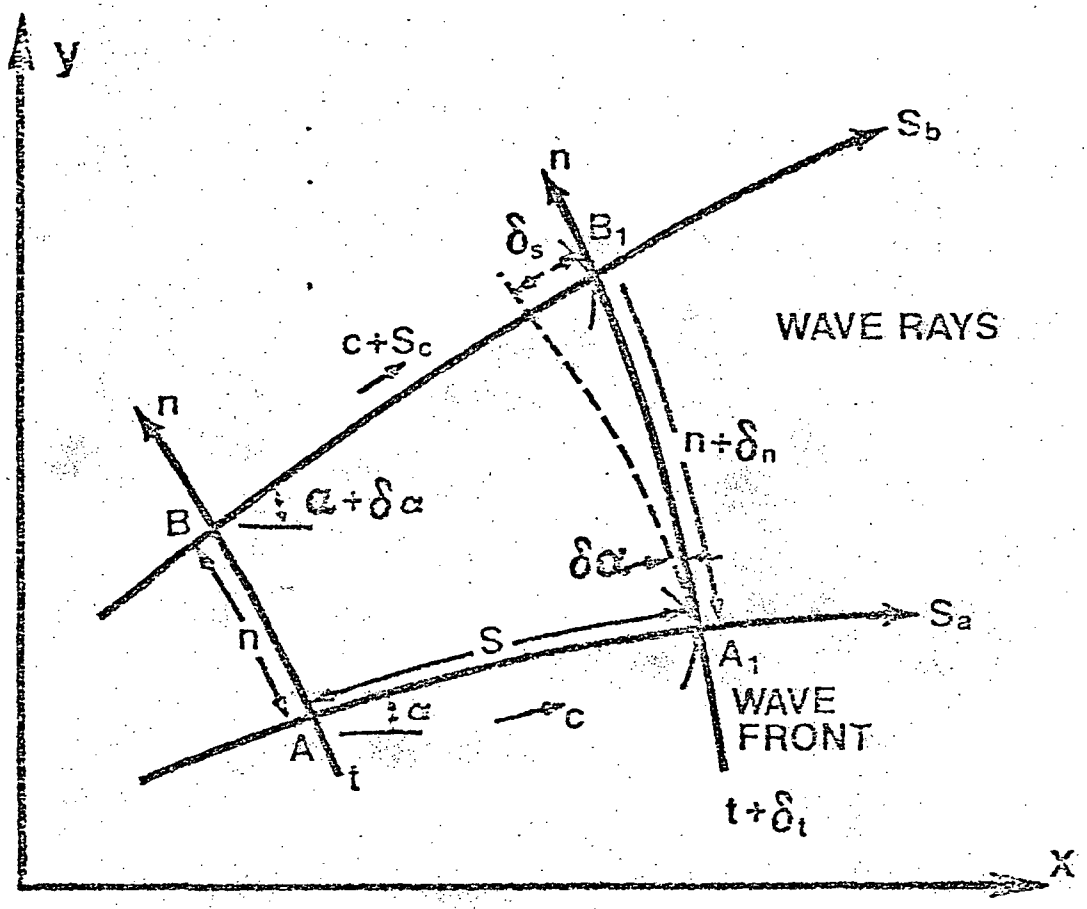

Figure 1. Graphic definition of wave ray equation

Using Gauss's integral theories this yields,

$$\frac{D\alpha}{Dn} = \frac{1}{B}\frac{dB}{ds}$$

which in turn, after applying operators and combinations, results in the equation for ray separation as a function of time:

$$\frac{D}{Dn}\left(\frac{D\alpha}{Dt}\right) = -\frac{D^2c}{Dn^2}$$

After further manipulation, this equation can be converted to the form

$$\frac{d^2B}{dt^2} + p(t)\frac{dB}{dt} + q(t)B = 0$$

where:

$$p(t) = -2\left(\cos(\alpha)\frac{\partial c}{\partial x} + \sin(\alpha)\frac{\partial c}{\partial y}\right)$$

and

$$q(t) = c\left(\sin^2(\alpha)\frac{\partial^2 c}{\partial x^2} + 2\sin(\alpha)\cos(\alpha)\frac{\partial^2 c}{\partial x \partial y} + \cos^2(\alpha)\frac{\partial^2 c}{\partial y^2}\right)$$

The equation for the curvature of wave rays is then;

$$K = \frac{1}{C}\sin(\alpha)\frac{\partial c}{\partial x} - \cos(\alpha)\frac{\partial c}{\partial y}$$

The iterative equations which result in the summarized solution are as follows:

$$\Delta\alpha = \bar{K}_s \Delta s$$

$$\bar{K}_s = \left[(K_s)_i + (K_s)_{i+1} \right]^{1/2}$$

$$\alpha_{i+1} = \alpha_i + \Delta\alpha$$

$$\bar{\alpha} = (\alpha_i + \alpha_{i+1})^{1/2} = \alpha_i + \frac{\Delta\alpha}{2}$$

$$X_{i+1} = X_i + \Delta s \cos(\bar{\alpha})$$

$$Y_{i+1} = Y_i + \Delta s \sin(\bar{\alpha})$$

If further operations and the chain rule are applied, the governing equations can be expressed as functions at the mean water depth, h(s,y), as follows:

$$\frac{\partial c}{\partial X} = \frac{\partial h}{\partial x} \frac{\partial c}{\partial h}$$

$$\frac{\partial^2 c}{\partial x^2} = \frac{\partial^2 h}{\partial x^2} \frac{\partial c}{\partial h} + \left(\frac{\partial h}{\partial x}\right)^2 \frac{\partial^2 C}{\partial h^2}$$

with corresponding expressions for the y - direction terms.

The wave celerity has previously been given as:

$$c = C_0 \tanh \left(\frac{\sigma h}{c}\right)$$

This form can be readily converted to

$$\frac{dc}{dh} = \frac{\sigma c \ (1-R_c^2)}{cR_c + \sigma h \ (1-R_c^2)}$$

where:

$$R_c = \frac{c}{x_0}$$

Applying the chain rule to this equation yields:

$$\frac{d^2c}{dh^2} = U \frac{dc}{dh}$$

where:

$$U = \frac{-2\sigma c \, R_c}{[cR_c + \sigma h \, (1-R_c^2)]^2}$$

Substituting into the governing equation, yields the final form of these equations:

$$\frac{\partial^2 c}{\partial x^2} = \frac{dc}{dh} \left[\frac{\partial^2 h}{\partial x^2} + U \left(\frac{dh}{\partial x}\right)^2\right]$$

$$\frac{\partial^2 c}{\partial y^2} = \frac{dc}{dh} \left[\frac{\partial^2 h}{\partial y^2} + U \left(\frac{\partial h}{\partial y}\right)^2\right]$$

$$\frac{\partial^2 c}{\partial x \partial y} = \frac{dc}{dh} \left[\frac{\partial^2 h}{\partial x \partial y} + U \frac{\partial h}{\partial x} \frac{\partial h}{\partial y}\right]$$

Dobson uses the least squares method and a second degree equation to describe the depth from the trend surface

$$h_t = e_i + e_2 x + e_3 y + e_4 x^2 + e_5 xy + e_6 y^2$$

The deviation at that grid point is given by:

$$\Delta h = H_{ij} - h_t$$

His method utilizes twelve points and coefficients chosen to minimize the squared deviations. With the least squares criterion that:

$$F\ (e_1,\ e_2,\ e_3,\ e_4,\ e_5,\ e_6) \ = \ \Sigma(\Delta h)^2$$

then there will be a minimum when:

$$\frac{\partial F}{e_1} \ = \ \frac{\partial F}{e_1} \ = \ \ldots . \ = \ \frac{\partial F}{e_6} \ = \ 0$$

Dobson uses a matrix approach to this problem and finds polynomial solutions from:

$$[E] \ = \ [sxy] \ \cdot \ [H]$$

where [E] is the coefficient matrix (e_1 --- e_6)

$$[sxy] \ = \ [xy]^{-1} \ \cdot \ [uxy]$$

[uxy] is a constant, special unit matrix

[H] is the depth matrix

This yields the derivatives of h with respect to x and y as shown:

$$\frac{\partial h}{\partial x} \ = \ e_2 + 2e_4x + e_5y$$

$$\frac{\partial^2 h}{\partial x^2} \ = \ 2e_4$$

$$\frac{\partial h}{\partial x \partial y} \ = \ e_5$$

with similar expressions for the y terms.

The curvature and wave separation are now representable in terms of depth using these coefficients. The equations become

$$K = \frac{\sigma(1-R_c^2)}{cR_c + \sigma h\ (1-R_c^2)}\ [\sin(\alpha)$$

$$(e_2 + 2e_4 + e_5 y) - \cos(\alpha)\ (e_3 + e_5 x + 2e_6 y)]$$

$$p(t) = \frac{-2\sigma c\ (1-R_c^2)}{cR_c + \sigma h(1-R_c^2)}$$

$$[\cos(\alpha)\ (e_2 + 2e_4 x + e_5 y) + \sin(\alpha)\ (e_3 + e_5 x + 2e_6 y)]$$

$$q(t) = \frac{\sigma c^2\ (1-R_c^2)}{cR_c + \sigma h\ (1-R_c^2)}$$

$$\{\sin^2(\alpha)\ [2e_4 + U(e_2 + 2e_4 x + e_5 y)^2] +$$

$$2\sin(\alpha)\cos(\alpha)\ [e_5 + U(e_2 + 2e_4 x + e_5 y)(e_3 + e_5 x + 2e_6 y)]$$

$$+ \cos^2(\alpha)\ [2e_6 + U(e_3 + e_5 x + 2e_6 y)^2]\}$$

where x and y are local coordinate values. The p(t) and q(t) solutions can then be used to find β by:

$$B_{i+1}^{(n)} = \frac{[(tp_i - 2)B_{i-1}^{(n)} + 2(2 - t^2 q_i)B_i^{(n)}]}{(2 + tp_i)} + \frac{2\varepsilon_{i+1}^{(N-1)}}{(2+tp_i)}$$

where t is the constant increment of time between points, ε is an error term, and n is the order of approximation. B is then used to find the refraction coefficient.

To the above equations, the formulae devised by Johnson (1948) have been included in order to simulate the refraction at wave fronts by currents. His method is based on a version of Snell's Law:

$$\frac{C_0}{\sin(\alpha)} = \frac{u + c}{\sin(\beta)}$$

These relationships are displayed in Figure 2.

Solving for $\sin(\beta)$ we have

$$\sin(\beta) = \sin(\alpha)/(1-m \sin(\alpha))^2$$

where $m = \frac{u}{c_0}$

There results, dependent upon the angle of interception, changes in the wave length, height and steepness:

$$L = \frac{L_0}{(1-m \sin(\alpha))^2}$$

$$\frac{H}{L} = M \left(\frac{H_0}{L_0}\right)$$

where

$$M = [(\cos(\alpha)/\cos(\beta) \{ (1-m \sin(\alpha))^6/(1+m \sin(\alpha)) \}]^{1/2}$$

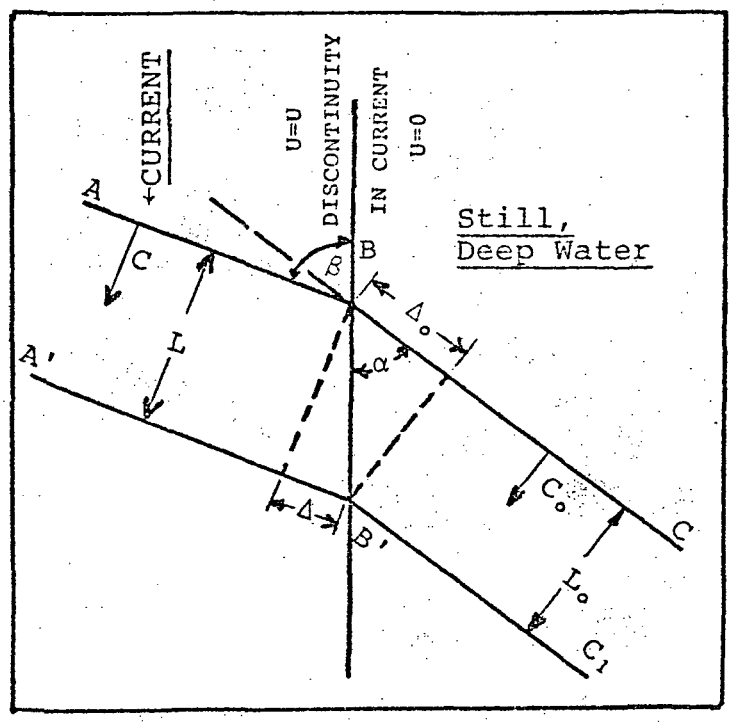

C_o = Initial Wave Velocity

C = Final Wave Velocity Relative to Moving Water

Figure 2. Refraction of Surface Waves by Currents (After Johnson).

2. Model Inputs and Outputs

DATA CARD SETUP

Card 1	(5I5, 4F10.5,I2,F10.5)
MI, MJ	The maximum values of I and J which define the grid. Note: I = X + 1, J = Y + 1. Maximum 50 by 50.
IGRCON	Grid unit identifier: 1=feet 2=nautical miles 3=meters
LIMNPT	Maximum number of points to be computed for each ray.
NPRINT	Frequency for printed output
GRID	Number of grid units per grid division
DCON	Conversion factors for depth units
DELTAS	Minimum length of increment along ray (grid units)
GRINC	Length of increment for ray in deep water (grid units)
ITEST	If = 0, depth field (Card Two) is read, If = 1, artificial deep water depth field generated
Card 2, etc	(16F5.1)
DEP (I, J)	Depth data at grid points. More than one card
XCONST	Value of deep water depth field (in units identified by IGRCON)
Card 3,	(I5)
NOSETS	Number of sets of rays of different periods
Card 4	(18A4)
TITL	Identifying title for each set

Card 5	(I3, 1X, 2F6.1)
NORAYS	Number of rays in each set
T	Wave period (seconds)
HO	Wave height on deep water (feet)
Card 6	(3F7.2)
X, Y	Coordinates of the starting point for each ray
A	Initial direction of wave ray, measured anti-clockwise from positive X direction (degrees)

OUTPUT VARIABLES (not previously defined)

NPT	The number of the point on the ray
WLO	Deep water wave length (feet)
CO	Deep water wave speed

LISTING OF INPUT CARDS FOR AN ACTUAL DEPTH GRID (Example)

```
  37   36    1  300    51650,00000   1,00000    ,00500    ,20000    1
120.0115,0101.0 96.0 91.0 88.0 84.0 80.0 44.0 72.0 69.0 65.0 65.0 62.0 55.0 52.0
 46.0 36.0 30.0 15.0    0 -1.0-10.0-10.0-10.0-10.0-10.0-10.0-10.0-10.0-10.0-10.0
-10.0-10.0-10.0-10.0123.0118.0110.0108.0 94.0 87.0 84.0 81.0 74.0 72.0 69.0 64.0
 63.0 60.0 55.0 54.0 43.0 36.0 20.0  5.0    0 -1.0-10.0-10.0-10.0-10.0-10.0-10.0
-10.0-10.0-10.0-10.0-10.0-10.0-10.0-10.0125.0115.0108.0102.0 96.0 90.0 87.0 84.0
 81.0 77.0 40.0 64.0 60.0 58.0 53.0 49.0 43.5 32.5  6.0  5.0    0 -1.0-10.0-10.0
-10.0-10.0-10.0-10.0-10.0-10.0-10.0-10.0-10.0-10.0-10.0-10.0129.0115.0101.0 99.0
 96.0 93.0 90.0 78.0 75.0 73.5 71.0 63.0 57.5 56.0 54.0 44.5 39.0 30.0 17.0  5.0
    0 -1.0-10.0-10.0-10.0-10.0-10.0-10.0-10.0-10.0-10.0-10.0-10.0-10.0-10.0-10.0
133.0126.0118.0108.0 98.0 94.0 90.0 85.0 75.0 41.0 68.0 60.0 55.0 51.0 48.0 40.5
 35.5 32.0 14.0  8.0 -1.0-10.0-10.0-10.0-10.0-10.0 -1.0 -0.5 -0.5 -1.0 -0.5    0
 -1.0-10.0-10.0-10.0135.0124.0114.0109.0104.0 96.0 91.0 86.0 74.0 68.0 64.0 59.5
 55.0 49.0 41.5 39.5 36.0 30.0  9.0    0 -1.0-10.0-10.0-10.0-10.0 -1.0   -0   -0
    0    0    0    0 -1.0 -1.0-10.0-10.0138.0125.0116.0109.0 98.0 94.0 89.0 84.0
 80.0 72.0 64.0 57.0 50.0 44.0 40.0 39.0 34.0 24.0 10.0    0-10.0-10.0-10.0-10.0
 -1.0 -0.5    0   .5  1.0  1.5  1.0    0    0 -0.5 -1.0 -1.0136.0132.0122.0108.0
102.0 97.0 94.0 86.0 78.0 66.0 60.0 55.0 49.0 43.0 40.0 39.0 34.0 22.0    0 -1.0
-10.0-10.0-10.0    0    0    0    0   .5   .5  1.0  1.0  1.0    0 -0.5 -0.5 -0.5
137.0130.0126.0115.0107.0102.0 92.0 76.0 70.0 68.0 56.0 50.0 44.0 41.0 37.5 35.0
 31.0 16.0  8.0 -1.0-10.0-10.0    0    0   .5   .5  1.5  2.0  2.0  1.5  1.5  1.0
    0    0    0 -1.0128.0125.0114.0109.0101.0 96.0 91.0 82.0 69.0 60.0 57.0 49.0
 43.0 41.0 37.0 34.5 29.0 15.0    0 -1.0-10.0-10.0    0  1.0  1.0  1.0    0    0
  1.0  1.5  1.5  1.8  2.0  1.5    0 -1.0132.0122.0114.0109.0104.0 99.0 89.0 79.0
 72.0 63.0 53.0 48.0 44.0 39.0 35.0 34.0 30.0  5.0 -1.0-10.0-10.0 -1.0    0    0
  1.0    0    0    0  6.0  1.0  1.5  1.0  2.0  4.0    0    0138.0129.0120.0110.0
106.0 98.0 84.0 77.0 68.0 53.0 49.0 30.0 17.5 17.0 26.0 24.0 13.0 -1.0-10.0-10.0
-10.0    0    0    0    0    0-10.0    0    0  5.0  2.0  1.5  1.0   .5  1.0  1.0
134.0132.0120.0113.0106.0 96.0 77.0 60.0 52.0 43.0 31.0 28.5 20.0 17.5 23.5 19.0
 12.0 -1.0 -1.0    0    0    0    0    0    0    0    0-10.0    0  7.0  6.0  2.0
  2.0  1.0   .5   .5138.0132.0123.0118.0105.0 93.0 61.0 48.0 35.0 32.0 29.0 26.0
 25.5 24.5 21.0 20.0 10.0-10.0    0    0 30.0 30.0 20.0    0    0    0    0    0
    0    0  7.0  2.5  1.0  2.0  2.0  1.5141.0132.0120.0114.0106.0 82.0 59.0 36.0
 34.0 31.0 29.0 29.0 27.0 24.0 21.0 18.0 15.0    0    0 31.0 26.5 22.5 21.0    0
    0 10.0  5.0    0    0    0    0    0    0    0    0    0144.0135.0126.0108.0
 95.0 60.0 40.0 36.0 32.0 30.0 33.0 32.0 30.0 29.0 28.0 18.0 20.0 45.0 32.0 33.0
 31.0 35.0 37.0 42.0 69.0 50.0 47.0 43.0    0    0    0    0    0    0-10.0    0
144.0136.0129.0115.0 96.0 53.0 44.0 33.0 33.0 34.0 34.0 35.0 33.0 37.0 40.0 45.0
 51.5 52.0 45.0 45.0 45.0 45.0 45.0 45.0 45.0 45.0 45.0 71.0 71.0 68.0 43.0 34.0
 15.0    0    0 0148.0136.0129.0125.0 89.0 46.0 37.0 36.0 36.5 36.5 37.0 69.0
 40.0 47.0 56.0 63.0 65.0 45.0 45.0 45.0 45.0 45.0 47.0 53.0 43.0 45.0 48.0 72.0
 83.0 81.0 67.0 49.0 37.0 26.0 13.0 15.0150.0146.0138.0127.0104.0 59.0 43.0 39.0
```

LISTING OF INPUT CARDS FOR AN ACTUAL DEPTH GRID (Continued)

```
 37.0 37.0 41.0 42.0 47.0 54.0 53.0 55.0 45.0 45.0 36.0 34.0 34.0 36.0 30.0 28.0
 31.0 31.0 18.0 29.0 45.0 63.0 65.0 60.0 54.0 39.0 35.0 23.0153.0147.0143.0132.0
107.0 73.0 46.0 41.0 39.0 39.0 40.0 43.0 50.0 54.5 54.0 51.0 51.0 38.0 32.0 24.0
 19.0 19.0 16.0 14.0 13.0 12.0 10.0  7.0  7.0  3.0 42.0 58.0 63.0 56.0 53.0 45.0
156.0152.0144.0124.0113.0 97.0 52.0 44.5 43.0 42.0 41.0 47.0 49.0 52.0 51.0 51.0
 50.0 39.0 30.0 23.0 20.0 17.0 14.0 13.0  8.0  8.0  9.0    0    0    0    0 48.0
 33.0 30.0 40.0 51.0160.0154.0147.0132.0116.0 93.0 71.0 52.0 45.0 43.0 44.0 49.0
 49.0 51.0 51.0 53.0 52.0 53.0 29.0  6.0  6.0  6.0  6.0  6.0  6.0  6.0  6.0    0
 -1.0-10.0    0    0 42.0 35.0 22.0 21.0168.0159.0150.0139.0122.0107.0 95.0 60.0
 50.0 50.5 50.0 51.0 51.0 51.0 45.0 41.0 48.0 45.5 48.0    0    0    0    0    0
    0    0    0 -1.0-10.0-10.0-10.0    0    0 42.0 36.0 21.0177.0168.0111.0137.0
129.0114.0103.0 72.0 61.0 59.0 55.0 54.5 53.5 46.0 41.5 41.5 44.0 43.0 65.0 42.0
 38.0 36.0 32.0 29.5 24.0 20.0 15.0  9.0    0-10.0-10.0 -1.0    0 22.0 42.0 47.0
180.0177.0162.0147.0137.0123.0111.0 92.0 75.0 65.0 64.0 61.0 57.5 52.5 48.5 47.5
 46.5 46.0 44.0 42.0 39.0 39.0 37.0 34.0 31.5 26.0 19.0 14.0  5.0    0 -1.0 -1.0
    0 11.5 23.5 41.0179.0174.0162.0143.0137.0121.0118.0113.0 97.0 85.0 77.0 64.0
 59.5 56.0 49.0 50.0 52.0 48.5 47.0 43.0 40.0 39.5 38.5 37.0 34.0 30.0 25.0 18.0
 11.0    0-10.0 -1.0    0    0    0 20.0183.0176.0171.0158.0143.0133.0129.0121.0
107.0 91.0 88.0 84.0 71.0 58.0 57.0 57.5 57.5 55.0 51.0 47.0 43.0 41.0 39.5 39.0
 37.0 34.0 29.0 23.5 16.0  5.0    0 -1.0 -1.0 -1.0    0    0185.0183.0178.0174.0
163.0149.0133.0107.0110.0104.0 99.0 88.0 78.0 76.0 71.0 65.0 57.0 56.5 56.0 50.5
 46.0 42.0 40.0 39.5  9.0 38.0 31.0 27.0 21.0 11.0  3.0 -1.0-10.0-10.0-10.0-10.0
200.0192.0179.0168.0154.0146.0132.0132.0122.0110.0109.0 92.0 87.0 79.0 73.0 70.0
 65.0 60.0 54.0 52.0 51.0 47.0 44.0 43.0 41.0 39.0 65.0 30.0 24.0 17.0  5.0    0
 -1.0-10.0-10.0-10.0201.0200.0195.0184.0168.0144.0135.0126.0121.0121.0116.0108.0
 98.0 96.0 82.0 79.0 68.0 66.0 59.0 55.0 63.0 50.0 47.0 46.0 44.0 42.0 39.0 38.0
 27.0 24.0 11.0    0 -1.0-10.0-10.0-10.0202.0200.0193.0179.0174.0156.0151.0145.0
132.0125.0119.0108.0 99.0 94.0 89.0 82.0 78.0 68.0 60.0 59.0 57.0 51.0 50.0 49.0
 47.0 45.0 41.0 39.0 31.0 23.0 17.0  3.0    0 -1.0-10.0-10.0203.0201.0199.0185.0
179.0168.0154.0150.0132.0125.0119.0115.0109.0 92.0 89.0 83.0 76.0 71.0 68.0 60.0
 58.0 54.0 51.0 50.0 48.0 46.0 41.0 38.0 34.0 28.0 19.0 11.0    0 -1.0-10.0-10.0
206.0202.0198.0183.0178.0161.0155.0144.0136.0133.0124.0115.0110.0 97.0 91.0 86.0
 79.0 72.0 63.0 61.0 59.0 54.0 52.0 50.0 49.0 45.0 43.5 42.0 40.0 31.0 23.0 19.0
  2.0 -1.0-10.0-10.0208.0203.0200.0194.0182.0173.0164.0150.0147.0135.0127.0116.0
108.0105.0102.0 96.0 65.0 79.0 78.0 73.0 66.0 63.0 58.5 56.0 52.5 50.0 48.0 46.0
 40.0 34.0 29.0 22.0 12.0    0 -1.0-10.0212.0204.0196.0189.0183.0178.0163.0160.0
159.0153.0149.0126.0125.5121.0111.0104.0 91.0 82.0 78.0 77.0 74.0 67.0 62.0 59.0
 56.0 54.0 51.0 48.0 44.0 39.0 30.0 25.0 14.0  2.0 -1.0-10.0216.0208.0204.0194.0
192.0180.0172.0165.0160.0154.0149.0131.0129.0123.0115.0101.0 96.0 91.0 87.0 81.0
 76.0 72.0 65.0 61.0 57.0 55.0 54.0 49.0 47.0 41.0 33.0 28.0 20.0  5.0 -1.0-10.0
220.0212.0200.0196.0192.0181.0170.0167.0163.0151.0147.0134.0127.0122.0118.0112.0
104.0100.0 97.0 87.0 48.0 72.0 71.0 65.0 60.0 58.0 55.0 52.0 47.0 42.0 35.0 30.0
 22.0 20.0 -1.0-10.0
   3
  COLUMBIA R,  PERIOD  8 SECCS,  DEEP WATER DIRECTION, E,S,E,
  3    8,00 10,00
  10,0    3,5  110,0
  12,0    3,5  110,0
  27,0    3,5  110,0
  COLUMBIA R, PERIOD 10 SECS, DEEP WATER DIRECTION, E,S,E,
  3   10,00 10,00
  10,0    3,5   90,0
  15,0    3,5   90,0
  25,0    3,5   90,0
  COLUMBIA R, PERIOD 12 SECS, DEEP WATER DIRECTION . E,S,E,
  3   12,00 10,00
  10,0    3,5   25,0
  15,0    3,5   25,0
  25,0    3,5   25,0
```

3. Organization of the Numerical Model

The main program is written in FORTRAN IV and is easily adaptable to any operating system with a FORTRAN compiler.

The main program is largely a bookkeeping routine, it reads in the depth and wave data, initializes many of the necessary parameters and keeps track of which ray is being computed. It also sets the size of the common block being utilized, a description of which follows.

Variables in Common

IPT (200)	Intermediate storage array
D (12)	Depth at grid points used for surface fitting computations, D (K). (in depth units)
E (6)	Coefficients for the equation of surface of best fit, E (L)
B1, B2	Values of Beta at the points NPT and (NPT-1)
CXY	Wave speed at a point on the ray (ft/sec)
DCDH	The differential coefficient of speed with respect to depth (dc/dh)
DCON	Conversion factor for depth units
DELTAS	Minimum length of increment along ray (grid units)
DRC	Depth at which refraction commences (0 . 6 x WLO)
DTGR	Time interval between calculation points on the ray

DXY	The calculated depth at the point X, Y
GRINC	Length of increment for ray in deep water
HO	Wave height in deep water (feet)
IGO,JGO,KGO	Branching identifiers
LIMNPT	Maximum number of points to be computed for each ray
NPRINT	Frequency for printed output
NPT	The number of the point on the ray
PHX, PHY	Partial differential coefficients of depth with respect to X and Y ($\partial h/\partial x$, $\partial h/\partial y$)
RCCO	Ratio of actual wave speed to deep water wave speed, (CXY/CO)
RHS	Maximum limit for X on a ray
RK	Refraction coefficient
SIG	Angular frequency of the wave (σ)
SK	Shoaling coefficient
TOP	Maximum limit for Y on a ray
WL	Wave length at a point on the ray (feet)
WLO	Deep water wave length (feet)
SLOP	The slope at frequency of output
DS	Incremental distance along ray
DY2	The depth at the new point
DYB1, DYB2	The depths at the breaking point and reforming point, respectively
ILGO	Intermediate identifier
V	Intermediate value in computing the curvature
WLB	Wavelength at breaking (feet)

SUBROUTINE RAYCON

This routine controls each individual ray as it progresses across the grid. Initially it assumes that the wave is still in deep water and calculates the second point on the ray. The subroutine DEPTH is called and the depth at this point is found.

If this depth is greater than the refraction depths, then the subroutine WRITER is called and the details are printed out for that point. If the wave has reached shallow waters CURVE is called to calculate the initial value of ray curvature.

With the initial point found, the subroutine REFRAC is called to find the next point on the wave ray. HEIGHT is then called to compute the wave height at that point. If the breaking height criterion is not exceeded, the wave details will be printed, depending on the frequency of output, or the next point will be computed.

If breaking is evident, the routines SLOPE and BREAK are called. If certain program limitations are met, RAYCON also acts to stop the computation of that ray; for instance, if the ray has reached the boundary or there is no convergence.

Local Variables

ANG	The ray angle with respect to the X axis (degrees)
A	The ray angle (in radians)

SUBROUTINE REFRAC

This routine solves the refraction equations:

$$\Delta\alpha = K_s \Delta S$$

$$\overline{Ks} = [(Ks)_i + (Ks)_{i+1}]^{1/2}$$

$$\alpha_{i+1} = \alpha_i + \Delta\alpha$$

$$\overline{\alpha} = (\alpha_i + \alpha_{i+1})^{1/2}$$

$$X_{i+1} = X_i + s \cos(\overline{\alpha})$$

$$Y_{i+1} = Y_i + s \sin(\overline{\alpha})$$

iteratively, to find the next point on the ray.

Local Variables

FK	Curvature at the point NPT.
FKK	Curvature at the point (NPT + 1).
XX, YY	Coordinates at the point (NPT + 1).
AA	Angle of ray at the point (NPT + 1).
DS	Incremental distance along ray (in grid points)
RESMAX	Limiting difference between successive approximations for the new curvature.
NCUR	Identifier, controlling the stability of the solution.

SUBROUTINE CURVE

This routine first tests for whether the wave is in deep or shallow water and then computes the local speed using the appropriate equation. It then computes the local differential coefficients and finds the curvature at the point by the equation

$$K = \frac{\sigma\,(1-R_c^2)}{cR_c + \sigma h\,(1-R_c^2)\,\sin(\alpha)\,[(e_2+2e_4x+e_5y) - \cos(\alpha)\,(e_3 + e_5x + 2e_6y)]}$$

where $R = c/co$ and e_2 through e_6 are computed fitting coefficients.

Local Variables

CI	Intermediate value of wave speed used to solve for the intermediate water wave speed.
FK	Curvature at the point X, Y.

SUBROUTINE DEPTH

This routine determines the local origin for the point on the ray and then calculates the local coordinates. A test is made to see whether the point lies within the same mesh square as the previous point. If it does, the new depth is calculated using the new local coordinates with the coefficients computed when the ray first entered the square. Otherwise, new coefficients for the surface equation are calculated and the depth is found.

Local Variables

SXY	The special unit matrix for use with a square grid.
I, J	The grid coordinator at the local origin for the point at the ray.

SUBROUTINE HEIGHT

This routine calculates the shoaling coefficient and refraction coefficient using the value of Beta calculated at the previous point. These two coefficients are then used to calculate the local height of the wave.

A test is made to see if the breaking wave criterion has been reached. If so, the subroutine BREAK is called by RAYCON which uses the reforming height and wavelength to calculate subsequent wave heights. If the wave has not broken, it computes the finite difference form of the equation of wave intensity to find the value of Beta at the next point.

Local Variables

H	The wave height at a point on the ray.
CG	The group speed of the wave.
P, Q	Variables used in the calculation of Beta.

SUBROUTINE SLOPE

This routine calculates the slope of the surface using the depths at each point and then taking a mean slope over the frequency output. It thus gives the contour over which the ray traverses.

Local Variables

SLOP1	The slope of the bottom contour at each point.
SLOP	The slope at frequency of output.

SUBROUTINE BREAK

This subroutine initialites the wave height to the breaking wave height and then calculates the length of the breaking zone. It then determines the coordinates and calls the routine DEPTH to determine the depth at the reforming point.

The slope is calculated and from this the reforming wave height and length are determined. If the slope is non-reforming, the routine will continue to evaluate heights until either a reforming slope is encountered or the boundary conditions are reached.

Local Variables

RUN	The slope over the breaker zone.
HA	The reforming wave height.
HP	Wave height prior to reforming.
LA	Reforming wavelength.
WLB	Length over the breaker zone.

SUBROUTINE ERROR

This routine estimates a measure of the error by using a least squares surface to calculate the depth at the point X, Y. It finds the maximum difference between the depths at the grid points calculated, using the surface polynomial, and the actual data depths, and then computes the standard deviation of these differences. The maximum difference is expressed as a percent of depth at the point X, Y.

Local Variables

DP	The computed depth at the four grid points surrounding the point X, Y.
DIFMAX	The maximum difference between the actual depth at a grid point and the computed depth.
FIT	The standard deviation of the least squares surface.

SUBROUTINE WRITER

This routine controls the printed output of the program. It also includes various error messages which are printed when the error conditions have occured. Also, all intermediate stops are handled by this routine.

Local Variables

NWRITE	Branching identifier to control output.

SUBROUTINE BAR

This routine calculates the amount of deformation to the wave front crossing an oceanic velocity discontinuity, including wavelength and height changes, based on the equations described in Section 1.

Local Variables

XM	Defined as u/cxy
U	A current velocity
STP	Resulting steepness
XMM	The steepness factor

Note:

U is set internally in BAR, slight alterations would allow it to be read from a data card.

4. References

Dobson, R.S., 1967: Some applications of a digital computer to hydraulic engineering problems. Department of Civil Engineering, Stanford University, 182 pp.

Johnson, J.W., 1947: The refraction of surface waves by currents, Trans., Amer. Geophysical Union, V. 28, No. 6, pp. 867-874.

Rabe, K., 1975: An evaluation of available wave refraction models for use on the CDC 3100 computer. Environmental Prediction Research Facility, Technical Note.

Smith, B.S.L. and F.E. Camfield, 1972: A refraction study and program for periodic waves approaching a shoreline, and extending beyond the breaking point. College of Marine Studies, Technical Report No. 16, University of Delaware, 128 pp.

APPENDIX D

COMPUTATION OF HEAT AND MOISTURE EXCHANGE AT THE OCEANIC FRONTS

CONTENTS

1. The Formulas Used in the Model

The heat and moisture exchange program computes the latent heat exchange with the following formula (Laevastu, 1960):

$$Q_e = (0.26 + 0.077V)\ (0.98e_w - e_a)\ L_t \qquad [1]$$

where Q_e is latent heat exchange (g cal cm^{-2}, 24h), V is wind speed (m sec^{-1}), e_w is saturation vapor pressure of the sea surface, e_a is vapor pressure of the air at the height of 10m, and L_t is latent heat of vaporization.

The sensible heat exchange is computed with the following formula (Laevastu, 1960):

$$Q_h = 39\ (0.26 + 0.077V)\ (T_w - T_a) \qquad [2]$$

where Q_h is sensible heat (g cal cm^{-2}, 24h), T_w is sea surface temperature (°C) and T_a is air temperature at the height of 10 m.

For computation of saturation vapor pressure of the sea surface the Goff-Gratch (1946) formula is used:

$$\begin{aligned} \log_{10} e_w = {} & -7.90298\ (T_s/T_{wa} - 1) + 5.02808\ \log_{10}(T_s/T_{wa}) \\ & - 1.3816 \times 10^{-7}\,(10^{11.344(1-T_{wa}/T_s)} - 1) \\ & + 8.1328 \times 10^{-3}\,(10^{-3.49149(T_s/T_{wa} - 1)} - 1) + \log_{10} e_{ws} \end{aligned} \qquad [3]$$

where e_w is saturation water vapor pressure, e_{ws} is saturation vapor pressure at steam point temperature, T_s is steam point temperature (373.16°K) and T_{wa} is absolute temperature of the sea surface (°K).

The sea surface temperature and surface wind are prescribed (and/or available from other programs). Changes in surface air temperature and water vapor pressure differential are computed with the Åmot-Mosby formula with Laevastu-Harding (1974) constants.

$$\Delta T = \Delta T_o e^{-Kt} + \left(\frac{C}{K} + \frac{1}{K} V_r \frac{\partial T_w}{\partial r}\right) (1 - e^{Kt}) \qquad [5]$$

The same formula is used both for air temperature (T_a) and water vapor pressure (e_a) computation, whereby ΔT and T_w in the above formula are replaced with Δe and e_w. The symbols used in formula [5] are: ΔT is $T_w - T_a$, ΔT_o is ΔT at time 0, t is time (hours), C and K are empirical constants (for T_a: C = 0.10 and K = 0.35 and for e_a: C = 0.40 and K = 0.50) and $V_r \partial T_w/\partial r$ is the rate of change of sea surface temperature under the trajectory of the surface wind.

2. Model Inputs and Outputs

In addition to the necessary constants (grid size, time step, etc.), the main inputs required by the model are sea surface temperature and surface winds. Synoptic observations of surface air temperature and water vapor pressure of the air are too inaccurate and too sparce in space and time to use for direct computation. Thus, these are computed with the well verified Åmot-Mosby formula (Laevastu and Harding, 1974).

The model computes (and prints out) sensible and latent heat exchange in terms of g cal cm^{-2} in 24 h. Furthermore, the resulting changes of sea surface temperature as well as the sea surface temperature changes due to advection and eddy diffusion can be computed with this model.

3. Organization of the Numerical Model

The main program THERMAL reads the constants and other data, calls other subroutines, keeps time and prints out the surface temperature field.

The first subroutine called is SETFLD. It initializes the sea surface temperature, currents, surface wind, and an initial guess for the surface air temperature.

The next subroutine WATER computes the saturation vapor pressure of the sea surface and vapor pressure and temperature of the surface air.

The subroutine ANOMALY computes the advection and diffusion of sea surface temperature. The final subroutine CALC computes the convective transfer of sensible heat and the transfer of latent heat by evaporation.

4. Symbols Used in the Program

A	Eddy diffusion coefficient
AA	Absolute temperature of sea surface (°K)
AK	TS/AA
AZA	Output interval (sec) (data)
AZZ	Time counter for output (initialized 0)
C	Constant in air temperature computation (data)
DT	Time step (sec) (data) (also TTT)
EA	Vapor pressure of the air (mb)
EC	Constant C in vapor pressure computation (data)
EK	Constant K in vapor pressure computation (data)
EW	Saturation vapor pressure of sea surface (mb)
EWEA	$(e_w - e_a)$
EWS	Saturation pressure of water at steam point temperature (data)
H	Time in hours
K	Constant K in air temperature computation (data)
LG	Grid size (cm) (data)
NE	Number of grid points in y direction
ME	Number of grid points in x direction
QE	Latent heat exchange (g cal cm^{-2}, 24h)
QH	Sensible heat exchange (g cal cm^{-2}, 24h)

T	Time counter (sec)
TA	Air temperature (°C)
TE	End of computation (sec) (data)
TS	Steam point temperature (data)
TW	Sea surface temperature (°C)
TWTA	$(T_w - T_a)$
U	Surface current, u component
UU	Relative humidity
UW	Surface wind, u component
V	Surface current, v component
VW	Surface wind, v component

5. References

GOFF, J.A. and S. Gratch, 1946.
Trans. Amer. Soc. Heat and Vent. Eng., Vol. 52, p. 95.

LAEVASTU, T., 1960.
Soc. Scient. Fenica, Comm. Phys. - Mathem., Vol. 25, No. 1.

LAEVASTU, T and J.M. Harding, 1974.
J. Geophys. Res., Vol. 79, No. 30.